MODULATION OF AQUEOUS HUMOR INFLOW AND OUTFLOW IN MAMMALIAN EYES

LI KA LOK STANLEY

Ph.D

The Hong Kong Polytechnic University

2017

The Hong Kong Polytechnic University

School of Optometry

Modulation of Aqueous Humor Inflow and Outflow in Mammalian Eyes

Li Ka Lok Stanley

A thesis submitted in partial fulfillment of the requirements

for the degree of Doctor of Philosophy

August 2016

CERTIFICATE OF ORIGINALITY

I hereby declare that this thesis is my own work and that, to the best of my knowledge and belief, it reproduces no material previously published or written, nor material that has been accepted for the award of any other degree or diploma, except where due acknowledgement has been made in the text.

_____ (Signed)

Stanley Ka-lok, Li (Name of Student)

Abstract

Glaucoma is the leading cause of irreversible blindness worldwide. In principle, glaucoma could be treated by interrupting the pathogenesis of the disease or by neuroprotection of the retinal ganglion cells. However, currently, lowering intraocular pressure (IOP) remains the only effective intervention to slow the onset and progression of glaucomatous blindness. IOP can be lowered by reducing the rate of aqueous humor inflow, by reducing the flow resistance (increasing outflow facility) through the conventional (trabecular) outflow pathway, or by shunting outflow through the relatively pressure-insensitive uveoscleral outflow pathway.

Diurnal variation of aqueous humor inflow has been well documented, with the rate falling by about a half in the early morning hours. In contrast, IOP does not display a proportional diurnal drop, which has been found to partly reflect a reduction in outflow facility. One major regulator of outflow facility is thought to be matrix metalloproteinase-9 and -2 (MMP-9 and MMP-2) secreted by the human trabecular meshwork (TM) cells. Since TM cells are subject to diurnal temperature oscillations arising from variations in core body temperature and eyelid closure during sleep, the effects of temperature oscillations on the activity of secreted MMP-9 and MMP-2 were investigated. The zymography results showed that the activity of MMP-9 and MMP-2 was increased with a temperature rise of 4°C. The changes were in the opposite direction when the temperature was lowered. Temperature cycling did not entrain clock gene expression, indicating that the MMP-release oscillations did not result from a circadian rhythm with a peripheral clock located in the TM cells. Heat shock transcription factor 1 (HSF1) inhibitor KNK437 reduced the MMP-9, but not MMP-2 temperature cycling-driven oscillations. In contrast, inhibition of TRPV1 or TRPM8 channels had no effects on temperature-driven MMP-9 and MMP-2 oscillations. Our results suggest that temperature cycling may alter MMP-9 and MMP-2

activity in the TM cells, potentially leading to extracellular matrix (ECM) remodeling and alteration of outflow resistance.

Aqueous humor inflow is produced by the secretion of fluid and solutes across the bilayered ciliary epithelium. The solutes and fluid taken from the extracellular fluid by the pigmented ciliary epithelium (PE) is transferred to the non-pigmented ciliary epithelium (NPE). This fluid transfer is facilitated by intercellular gap junctions, where inflow can be inhibited by interrupting gap junctional communication. Various gap junction isoforms are expressed in the ciliary epithelium of different species, and their functional significance has not been completely elucidated. Gap junction connexins in the ciliary epithelium of pig, which is considered to be a good animal model for studying aqueous humor formation, have been characterized, using RT-PCR and Western blot (WB). Our results showed the presence of Cx43, Cx45, Cx47, Cx50 and Cx60 in porcine ciliary epithelium. Cx43 was found to be located primarily at the interface between PE and NPE cells by immunohistochemistry. The expression level of Cx43 was shown to be over 200-fold higher than that of the other connexins by qPCR. siRNA knockdown of Cx43 significantly reduced both mRNA and protein expression, as well as dye diffusion rate across isolated PE-NPE cell couplets. The results indicate that Cx43 provides a major conduit for fluid transfer between PE and NPE cells.

Additionally, the effects of temperature and melatonin on the regulation of aqueous inflow were studied. Increasing the temperature by 4°C inhibited the short-circuit current (Isc) across porcine ciliary epithelium by half. The temperature-induced effect on Isc was reversible and repeatable. Increasing the incubation temperature by 4°C for 30 mins caused a reduction of Cx43 protein expression, while decreasing the temperature had an opposite effect in porcine ciliary epithelial cells. However, no changes were detected in the dye transfer rate across isolated PE-NPE cell couplets when the temperature was increased. The

findings suggest that temperature alteration may have a direct effect on Cx43 expression without influencing gap junction permeability. In addition, melatonin was found to stimulate the transepithelial electrical measurements and facilitate the dye transfer across PE-NPE cell couplets. A pretreatment with MT_1/MT_2 antagonist luzindole did not inhibit melatonin-induced Isc stimulation, and MT_3 antagonist prazosin blocked its stimulation completely. The findings suggest that melatonin may facilitate the solute and fluid movement from PE to NPE cells, leading to an increase in transepithelial secretion, potentially via a putative MT_3 receptor. Whether or not it contributes to the observed diurnal changes in aqueous humor flow and IOP awaits further investigation.

Publication, presentations and award arising from the thesis

Publication

1. Li, S.K., Banerjee, J., Jang, C., Sehgal, A., Stone, R.A., Civan, M.M., 2015. Temperature oscillations drive cycles in the activity of MMP-2,9 secreted by a human trabecular meshwork cell line. Invest Ophthalmol Vis Sci. 56, 1396-1405.

Presentations

1. Li SK, Banerjee J, Jang C, Sehgal A, Stone RA, Civan MM. Physiological temperature oscillations alter matrix metalloproteinase MMP-2,9 secretion by TM5 human trabecular meshwork cells independent of clock genes *Per2* and *Cry2*. [ARVO Abstract]. Invest Ophthalmol Vis Sci 2014;55:ARVO E-Abstract 2903

2. Li SK, Shan SW, Cheng AK, Civan MM, To CH, & Do CW. Gap Junctions – their characterization and basis in porcine ciliary epithelium. [ARVO Abstract]. Invest Ophthalmol Vis Sci 2016;57:ARVO E-Abstract 6405

3. Li SK, Shan SW, Yip SP, Civan MM, To CH & Do CW. Characterization of gap junctions in porcine ciliary body epithelium. International Conference of Vision and Eye Research 2017, Hong Hong

Award

1. Best paper Award (2nd Prize)
   International Conference of Vision and Eye Research 2017 held in Hong Kong on 26-27 May 2017 for the paper titled “Characterization of gap junctions in porcine ciliary body epithelium”

Acknowledgements

The work presented here represents not only my efforts, but reflects the collaborative effort of the whole team of researchers and collaborators, the schools and the universities and the Hong Kong and the US societies. Here, I would like to give my sincere thanks to Dr Chi-wai Do, my chief supervisor. His guidance, advice, patience, concerns and support were major contributions to the completion of the thesis. I would also like to thank my co-supervisors Prof. Chi-ho To and Prof. Mortimer M. Civan for their guidance, advices and encouragement. Prof Civan also gave me a valuable and joyful experience in working at a renowned university in the US. Also, I wish to give thanks to Prof. Stone and collaborators for the inspiration, advice and efforts on the paper published. During my study, Dr. Juni Banerjee and Dr. Samantha Shan have helped me to tackle many of the difficulties encountered in the experiments. They, together with Dr. Maureen Boost and Dr. Lily Chan, have also helped me with the preparation of this thesis. I would like to thank all of them. Lastly, I would like to give my sincere thanks to my labmates and family members as they have helped and tolerated me during my years of study. Without all of your support, this thesis would not have been born.

Stanley Ka-lok Li

Table of contents

List of figures

List of tables

List of abbreviations

5-MCA-NAT	5-Methoxycarbonylamino-N-acetyltryptamine
AHF	aqueous humor formation
AsODN	antisense oligodeoxynucleotide
cAMP	cyclic adenosine monophosphate
CBE	ciliary body epithelium
CE	ciliary epithelium
Cx	connexin
DMEM	Dulbecco's Modified Eagle Medium
DMSO	dimethyl sulfoxide
ECM	extracellular matrix
FBS	fetal bovine serum
GAPDH	glyceraldehyde 3-phosphate dehydrogenase
Hept	heptanol
HSF1	heat shock factor 1
IOP	intraocular pressure
Isc	short-circuit current
LY	Lucifer yellow
MMP	matrix metalloproteinase
NFA	niflumic acid
NPE	non-pigmented ciliary epithelium
PBS	phosphate-buffered saline
PBST	phosphate-buffered saline plus 0.05% Tween-20
PCR	polymerase chain reaction
PD	potential difference
PE	pigmented ciliary epithelium
POAG	primary open angle glaucoma
PS	Penicillin-Streptomycin

qPCR	quantitative polymerase chain reaction
Rt	transmural resistance
TIMP	tissue inhibitor of matrix metalloproteinases
TBST	0.1 M Tris-HCl, pH 8.0, 0.5M NaCl, 0.05% Tween-20
TM	trabecular meshwork
WB	Western blot/blotting

CHAPTER 1 Introduction

1.1 Background

Glaucoma is the leading cause of irreversible blindness worldwide (World Health Organization, 2014). In 2014, around 57 million people suffered from the disease. If left untreated, glaucoma causes progressive loss of retinal ganglion cells, leading to permanent loss of vision. As yet, there is no cure for the disease, but the progression of glaucomatous vision loss can be retarded by reducing intraocular pressure (IOP). Currently, lowering IOP remains the only clinically proven intervention for slowing glaucomatous blindness, irrespective of baseline IOP level (Collaborative Normal-Tension Glaucoma Study Group, 1998a; Collaborative Normal-Tension Glaucoma Study Group, 1998b; The AGIS Investigators, 2000; Quigley, 2011). The first line of treatment for glaucoma is life-long instillation of ocular hypotensive eye drops. However, various local and systemic side effects from these agents limit the choices of IOP control strategy for the patients (Bartlett and Jaanus, 2008). Moreover, prolonged use of these drugs may reduce the efficacy in lowering IOP (Gehr et al., 2006). In this case, multiple drugs may be required to maintain the reduced IOP level. In view of this, it is crucial to develop more potent and long lasting IOP-lowering medications in order to overcome these limitations.

Although glaucoma is a common, yet serious, disease, its pathogenesis is not yet clearly understood. Primary open angle glaucoma (POAG) is the most common form of glaucoma in which the elevated IOP is believed to be resulted from an increased resistance in the aqueous humor drainage (Grieshaber et al., 2010). However, the precise mechanism of how the resistance is generated is still elusive.

In addition, most of the clinically-available anti-glaucoma agents act by reducing the rate of aqueous humor formation. However, the precise mechanisms of their actions remain unclear. Therefore, it is important to understand the regulatory mechanism of both aqueous inflow and outflow with a view to developing novel agents for glaucoma therapy.

1.2 Mechanism of aqueous humor formation

The aqueous humor is formed from the blood with the following steps (Bill, 1975; Brubaker, 1991): First, blood flows into the vascular bed of the ciliary processes. Second, blood leaves from the fenestrated capillaries of the ciliary processes into the interstitial space of the ciliary stroma by ultrafiltration. Third, certain ions and solutes are selectively transferred from the interstitial space across the ciliary epithelium (CE) into the posterior chamber, establishing an osmotic gradient. Fourth, due to the presence of the blood-aqueous barrier, the osmotic gradient drives the water flow across the CE transcellularly; thereby forming the aqueous humor. Transferring ions and solutes across the CE is an important step for aqueous inflow. It is an active process, accounting for ~80% of aqueous humor production, while the remaining ~20% is achieved by ultrafiltration (Bill, 1975; Cole, 1977; Civan, 1998).

1.2.1 Ion transport across the ciliary epithelium

The active transport of ions from the ciliary stroma across the CE to the posterior chamber establishes an osmotic gradient and provides the driving force for aqueous humor formation (AHF). The ions are transferred across the CE by the following

steps (Civan, 2008): 1) Uptake of ions from the ciliary stroma into the pigmented ciliary epithelial (PE) cell; 2) ion transfer from the PE cells, via gap junctions, to non-pigmented ciliary epithelial (NPE) cells; and 3) release of ions from the NPE into the posterior chamber. The key ions (i.e. Na^+, Cl^- and, to a lesser extent, HCO_3^-) involved in trans-CE secretion are briefly summarized below.

1.2.1.1 Transepithelial ion transport

It was initially suggested that there was a net Na^+ transport across the CE establishing the osmotic gradient for AHF (Cole, 1962; Diamond and Bossert, 1967). However, the negative transepithelial potential difference observed in various species suggested that anions, such as HCO_3^- and Cl^-, rather than cations, might be the major driving force of AHF (Chu and Candia, 1987; Do and To, 2000; Kong et al., 2006; Wu et al., 2013). Moreover, net Na^+ flow across the CE was not detected in many species including cat (Holland and Gipson, 1970), rabbit (Kishida et al., 1982) or ox (To et al., 1998a), indicating that Na^+ is unlikely to be the major ion involved in AHF.

HCO_3^- has long been considered to be an important ion for AHF. Carbonic anhydrase in the CE has been identified to catalyze the conversion of dissolved CO_2 and H_2O into H^+ and HCO_3^-, resulting in the production of HCO_3^-. HCO_3^- was then thought to be transferred to the posterior chamber, establishing the osmotic gradient for AHF (Friedenwald, 1949). Carbonic anhydrase inhibitor has been demonstrated to reduce the HCO_3^- concentration in the aqueous humor (Maren, 1976) and the AHF rate (Dailey et al., 1982). However, opposing evidence across different species has indicated that HCO_3^- might not be the only ion responsible for AHF. For

example, HCO_3^--depleted bathing solution was shown to reverse the polarity of electrical potential in the CE of rabbit (Krupin et al., 1984), but not of ox (Do and To, 2000) and pig (Kong et al., 2006). These findings suggest that the contribution of HCO_3^- to AHF may differ between species. In addition, no net HCO_3^- transport has been reported across bovine CE (To et al., 2001). Based on these results, it is thought that HCO_3^- may play an indirect role in facilitating Cl^- transport across the CE (To et al., 2001).

It is generally accepted that Cl^- plays a central role in mediating AHF (Civan, 2003). This notion was supported by the presence of net Cl^- transport across the CE in many species including cat (Holland and Gipson, 1970), rabbit (Crook et al., 2000), ox (Do and To, 2000), pig (Kong et al., 2006) and human (Wu et al., 2013). In addition, the transepithelial parameters are significantly inhibited by Cl^- channel blockers (Do and To, 2000; Shahidullah et al., 2003; Law et al., 2009). All these findings strongly suggested that Cl^- ion could be important to the secretion of aqueous humor. It has been suggested that Cl^- release to the aqueous humor was coupled to Na^+ movement mediated by Na^+,K^+-ATPase (Civan, 2008; Shahidullah et al., 2011). This notion helps to explain why the calculated short-circuit current (Isc) based on net Cl^- secretion was much higher than the Isc measured across the CE (Do and To, 2000; Kong et al., 2006).

1.2.1.2 Uptake of NaCl by pigmented ciliary epithelium

The uptake of NaCl is primarily achieved by the Na^+-K^+-$2Cl^-$ co-transporter and the parallel Na^+/H^+ and Cl^-/HCO_3^- antiporters.

It has been shown that the Na^+-K^+-$2Cl^-$ co-transporter is primarily localized at the basolateral membrane of the PE cells (Dunn et al., 2001). It is an electroneutral transport as 1 Na^+, 1 K^+ and 2 Cl^- are transported across the plasma membrane simultaneously. Inhibition of this co-transporter has been found to reduce Na^+ and Cl^- uptake into bovine PE cells (Helbig et al., 1989). Bumetanide, a specific inhibitor of the Na^+-K^+-$2Cl^-$ co-transporter, has been shown to reduce Cl^- secretion across the CE in rabbit (Crook et al., 2000), ox (Do and To, 2000) and pig (Kong et al., 2006). Similarly, the AHF rates was found to be inhibited with bumetanide treatment in an *ex vivo* perfused eye study (Shahidullah et al., 2003). All these findings indicate the significance of the Na^+-K^+-$2Cl^-$ co-transporter in stimulating Cl^- secretion across the CE.

Na^+/H^+ and Cl^-/HCO_3^- antiporters provide an additional pathway for transferring NaCl into the PE cells (Helbig et al., 1989). The conversion of H^+ and HCO_3^- from CO_2 and H_2O in PE cells is catalyzed by carbonic anhydrase, providing the source of H^+ and HCO_3^- in exchange for Na^+ and Cl^- at the basolateral membrane of PE cells (Civan, 2008). Sodium-hydrogen antiporter 1 (NHE-1) and anion exchanger 2 (AE2) were found to be the major ion antiporters for this uptake (Counillon et al., 2000). In the presence of HCO_3^- in the bathing solution, Cl^- uptake in PE cells is enhanced by the parallel coupled Na^+/H^+ and Cl^-/HCO_3^- antiporters (Bowler et al., 1996; McLaughlin et al., 1998). Moreover, 4'-Diisothiocyano-2,2'-stilbenedisulfonic acid (DIDS), an anion exchanger inhibitor, has been found to inhibit the Isc across the CE of rabbit and bovine eyes (Crook et al., 2000; Do and To, 2000). In addition, the AHF rate of arterially-perfused bovine eye is reduced with DIDS administration (Shahidullah et al., 2003). Nevertheless, DIDS and 5-(N,N-dimethyl)-amiloride (DMA), an inhibitor of Na^+/H^+ antiporter, has no effect

on Isc and fluid flow in porcine CE, suggesting the possibility of species variations in mediating Cl^- uptake (Kong et al., 2006; Law et al., 2009).

1.2.1.3 Ion transfer from pigmented ciliary epithelium to non-pigmented ciliary epithelium

Gap junctions linking the PE and NPE cell layers provide conduits for ions to transfer from PE to NPE cells. The presence of gap junctions in CE is supported by both histological and biochemical studies (Raviola and Raviola, 1978; Coca-Prados et al., 1992; Wolosin et al., 1997b). Functionally, down-regulation of gap junction protein has been found to inhibit fluid transfer from PE to NPE cells (Wang et al., 2010). Pharmacological intervention by gap junction blockers, such as heptanol and octanol, was shown to inhibit the Isc across the CE in different species (Wolosin et al., 1997a; Do and To, 2000; Kong et al., 2006). Apart from *in vitro* studies, inactivation of gap junction protein has been found to reduce mouse IOP *in vivo* (Calera et al., 2009). All these findings support the crucial role of gap junctions in driving AHF.

1.2.1.4 Ion release from non-pigmented ciliary epithelium

In NPE cells, Na^+ is pumped out to the posterior chamber by Na^+,K^+-ATPase at the basolateral membrane of the NPE cells (Shahidullah et al., 2013). It is believed that Cl^- is coupled with Na^+ movement and released through Cl^- channels to the posterior chamber, thereby facilitating electroneutral NaCl secretion.

The Na^+,K^+-ATPase hydrolyzes ATP to ADP to pump out Na^+ and take in K^+. For

each ATP molecule hydrolyzed, three Na^+ are pumped out of and two K^+ are taken into the cell (Glynn, 2002). The ATPase on the both sides of the CE bilayer has been documented by autoradiography (Usukura et al., 1988) and immunohistochemistry (Mori et al., 1991). However, Na^+,K^+-ATPase was found to be more abundant in NPE cells than in PE cells (Usukura et al., 1988). In addition, the expression of Na^+,K^+-ATPase isoforms differs between PE and NPE cells, suggesting that it may have different functional characteristics (Crambert et al., 2000). Moreover, regional differences of Na^+,K^+-ATPase in the CE have been observed. For example, Na^+,K^+-ATPase isoforms have been found to be expressed more abundantly in the anterior pars plicata than in the posterior pars plana (Ghosh et al., 1991). This suggests the presence of regional differences in forming the aqueous humor.

Ouabain is a cardiac glycoside that can selectively inhibit the activity of Na^+,K^+-ATPase. It has been demonstrated that ouabain can inhibit the Isc across CE of different species (Iizuka et al., 1984; Krupin et al., 1984; Chu and Candia, 1987; To et al., 1998a; Kong et al., 2006; Law et al., 2009). Blocking Na^+,K^+-ATPase with ouabain has been shown to reduce the AHF in isolated perfused eye models of rabbit (Kodama et al., 1985) and ox (Shahidullah et al., 2003). Furthermore, ouabain has been demonstrated to decrease the IOP in experimental animals (Becker, 1963; Waitzman and Jackson, 1965).

Cl^- release is believed to be the rate-limiting step in the process of AHF under normal physiological conditions due to the following reasons (Do and Civan, 2004): First, the Cl^- concentration in PE cells has been found to be 4-fold higher than the value calculated from the electrochemical equilibrium (Bowler et al., 1996; Civan, 1998). This suggests that Cl^- uptake by the PE cells is not rate-limiting. Second, the

intracellular ion contents and electrical potentials are similar between PE and NPE cells (Bowler et al., 1996; McLaughlin et al., 2007), indicating an unimpeded flow of ions between the two cell layers. Third, the baseline activity of the Na^+-K^+-ATPase on the basolateral membrane of the NPE cells is high (Krupin et al., 1984), implying that the Na^+ pump is not the rate-limiting step.

This explanation is supported by the significant inhibition of net Cl^- secretion, Isc (Do and To, 2000) and AHF rate (Shahidullah et al., 2003) in the bovine eye by 5-nitro-2-(3-phenylpropylamino) benzoic acid (NPPB), a Cl^- channel blocker. Similar inhibitions of Cl^- secretion and Isc have also been shown in porcine CE with niflumic acid (NFA) (Kong et al., 2006), providing further evidence to support the importance of Cl^- release by NPE cells in the process of AHF. The simplified model of aqueous humor secretion is summarized in Fig. 1.1.

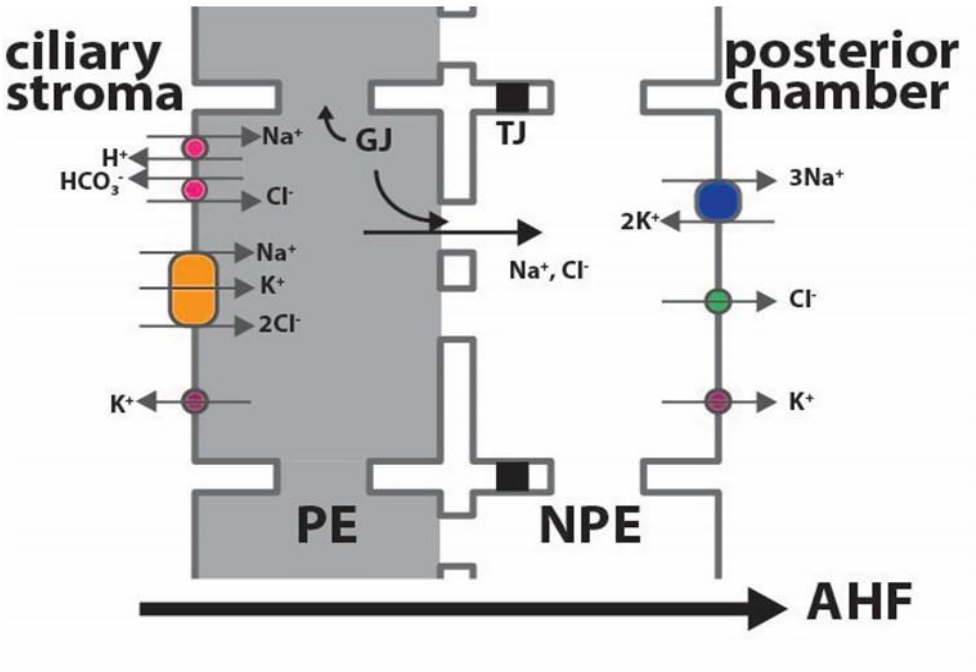

Fig. 1.1 A cellular model of aqueous humor formation. GJ: gap junction; TJ: tight junction; PE: pigmented ciliary epithelial cell; NPE: non-pigmented ciliary epithelial cell; AHF: aqueous humor formation.

1.3 Overview of aqueous humor outflow pathways

After its production in the CE, the aqueous humor flows from the posterior chamber, through the pupil, into the anterior chamber. It then leaves the eye through the conventional trabecular pathway and the unconventional uveoscleral pathway.

The majority of aqueous humor leaves the eye through the pressure-dependent trabecular pathway (Pang and Clark, 2008). In this case, the aqueous humor passes through the trabecular meshwork (TM), entering the Schlemm's canal and collector channels, and leaves the eye through episcleral veins. It has been shown that the

outflow resistance of TM is usually elevated in POAG patients (Rohen et al., 1989), and the increase in outflow resistance has been suggested to be the major cause of IOP elevation.

A small portion of the aqueous humor leaves the eyes through the relatively pressure-independent uveoscleral pathway. In this case, the aqueous humor enters the root of the iris, passing through the interstitial spaces of the ciliary muscles, the uvea, and then enters the suprachoroidal space for drainage (Bill, 1966; Inomata et al., 1972; Inomata and Bill, 1977; Johnson et al., 2017). It was estimated that the uveoscleral pathway accounted for 10-30% of aqueous drainage in humans (Bill and Phillips, 1971; Townsend and Brubaker, 1980). However, the magnitude of outflow through this pathway may reduce with age (Toris et al., 1999). It was speculated that the accumulation of extracellular materials and thickening of the collagen and elastic fibers could account for this reduction (Toris et al., 1999). In addition, the reduction might help explain why aging is one of the risk factors for ocular hypertension or glaucoma (Toris and Camras, 1998).

1.4 Trabecular meshwork

1.4.1 Structure

The TM consists of 3 layers, namely uveal meshwork, corneoscleral meshwork, and juxtacanalicular or cribriform meshwork (Llobet et al., 2003). The uveal meshwork is made of connective tissues that are totally covered by endothelial cells. This layer contributes negligible resistance to outflow facility. The corneoscleral meshwork consists of a more organized network of collagen lamellae covered by endothelial-

like cells (Gong et al., 1996). Due to the decrease in intercellular space, the outflow resistance gradually builds up in this layer. The last layer, the juxtacanalicular meshwork or cribriform meshwork, comprises trabecular meshwork cells embedded in an extracellular matrix (ECM). As the intercellular spaces become smaller, this layer provides the majority of the outflow resistance. After the TM, the endothelial cells (inner wall) of the Schlemm's canal form the last barrier before the aqueous humor leaves the eye. It had been estimated that this thin layer of cells contributed less than 10% of the outflow resistance to the trabecular outflow pathway (Bill, 1975). However, more recent findings have showed that the process of fixation affected the pore number and outflow resistance; therefore, the contribution of the inner wall of the Schlemm's canal might have been underestimated (Sit et al., 1997; Tamm, 2009).

1.4.2 Extracellular matrix (ECM) in trabecular meshwork (TM)

The ECM components in the TM are similar to those found in other parts of the body (Acott and Kelley, 2008). They include various types of collagens, fibronectin, laminin, elastin, gelatin, thrombospondin-1, myocilin, versican, hyaluronic acid and other glycosaminoglycans (Acott and Kelley, 2008; Roy Chowdhury et al., 2015).

In glaucomatous eyes, excessive amounts of ECM components have been found in the TM (Rohen, 1983; Lutjen-Drecoll et al., 1989). For example, there is an increase in the ECM protein fibronectin (Babizhayev and Brodskaya, 1989), cross-linking enzyme (Tovar-Vidales et al., 2008), materials that resist chondroitin sulfate and glycosaminoglycan degradation enzymes (Knepper et al., 1996), protease inhibitors

(Dan et al., 2005), and transforming growth factor-β2 (TGF-β2) (Inatani et al., 2001). The cross-linked actin networks (CLANs) have also been found to be elevated in the TM of glaucoma patients (Hoare et al., 2009). Additionally, the activity of ECM degrading enzymes matrix metalloproteinases (MMPs) have been found to be inhibited in the TM of ocular hypertensive eyes (De Groef et al., 2013). The above evidence supports the notion of an increase in outflow resistance and elevated IOP in glaucoma patients.

1.4.3 Matrix metalloproteinases (MMPs)

The ECM of TM cells contributes to the outflow resistance at the anterior chamber angle. The regulation of ECM turnover can help alter the outflow drainage and thus IOP (Bradley et al., 2001). One of the major regulators of ECM is the MMP family. MMPs are endopeptidases which hydrolyze macro-biomolecules and are characterized by the presence of Zn^{2+} in their active sites (Stawikowski and Fields, 2015). Around 200 family members have been identified in mammals (Puente et al., 2003). Collectively, MMPs can digest a wide range of components found in the ECM, including collagen, gelatin, fibronectin, elastin, proteoglycans and laminin. MMPs are involved in bone remodeling, cell migration, inflammation, immunity, and apoptosis (Crawford and Stack, 2015).

1.4.3.1 ECM regulation by MMPs in the TM

MMPs and tissue inhibitors of matrix metalloproteinases (TIMPs) have been detected in the aqueous humor and in the TM cells (De Groef et al., 2013). The ECM of the TM is continuously remodeled by MMPs.

The expression of both MMPs and TIMPs has been found to be related to glaucoma. It has been reported that the MMP to TIMP ratio is lower than the norm of 1:1 in patients with POAG due to a relative increase in TIMPs compared to MMPs (Schlotzer-Schrehardt et al., 2003; Maatta et al., 2005). Similarly, the expression of TIMP-2 has been found to be elevated in the aqueous humor in pseudoexfoliative glaucoma patients (Schlotzer-Schrehardt et al., 2003; Maatta et al., 2005).

In addition, changes in the compositions of ECM in the TM and aqueous humor are altered with respect to MMP inhibition in POAG patients. A higher hyaluronic acid level has been found to increase both MMP-9 and MMP-2 levels in human TM cells (Guo et al., 2012). However, it has been shown that the hyaluronic acid level in the TM is lower in POAG patients (Knepper et al., 1996). This suggests that the reduction of MMP-9 and MMP-2 in the anterior angle of POAG patients could result from a reduced level of hyaluronic acid, leading to an increase in outflow resistance (De Groef et al., 2013). Moreover, the level of transforming growth factor (TGF)-β2 is elevated in the aqueous humor of POAG patients (Tripathi et al., 1994; Picht et al., 2001). As TGF-β2 has been shown to decrease the activity of MMP-2 in cultured human TM cells (Tripathi et al., 1994), this indicates that the decreased MMP-2 activity may be associated with POAG. Furthermore, TGF-β2 can promote the expression of fibrillar substances, such as fibronectin and tissue transglutaminase, which increase fibrous cross-linkage in the ECM, thereby increasing outflow resistance.

Laser trabeculoplasty is a common surgical intervention to lower IOP in glaucoma therapy. The mechanism of IOP reduction is not due to shrinkage of the TM at the burnt treatment site (Johnson, 2007) nor the holes created in TM (Pang and Clark,

2008), but is possibly related to profound structural remodeling of the ECM. This modification may be associated with the increased MMP level (Johnson, 2007). It has been proposed that laser trabeculoplasty increases the expression of cytokines interleukin-1 (IL-1) and tumor necrosis factor α (TNF-α), which subsequently up-regulates MMP-3, MMP-9 and MMP-12 in human TM culture (Bradley et al., 2000; Fleenor et al., 2003; Pang et al., 2003; Hosseini et al., 2006; Kelley et al., 2007).

The role of MMPs in outflow facility has been shown experimentally (Bradley et al., 1998). In perfused human anterior segment culture, MMP-2, MMP-3, and MMP-9 were demonstrated to reversibly increase the outflow facility, while inhibition of endogenous MMPs could reduce the outflow facility. Moreover, IOP has been found to be elevated in MMP-9-deficient mice (Robertson et al., 2013), further supporting the important role of MMPs in regulating outflow facility.

The important role of MMPs in ECM remodeling of TM cells makes them a promising target in glaucoma therapy (De Groef et al., 2013). In fact, it has been demonstrated that an MMP-1 cDNA-carrying virus vector could reverse the steroid-induced down-regulation of MMP-1 in human TM cells (Spiga and Borras, 2010). A similar study has also showed that the above gene therapy could prevent and lower the elevated IOP induced by steroids in sheep (Gerometta et al., 2010). This evidence supports the therapeutic potential of MMPs as cellular targets for the alteration of outflow facility and IOP.

1.4.4 Other aspects of outflow resistance in TM

TM cells have been found to have the properties of smooth muscle cells (Lepple-

Wienhues et al., 1991). Disassembly of the actin cytoskeleton of TM cells by Rho-kinase inhibitors, cytochalasins D and latrunculins has been shown to increase the outflow facility in enucleated porcine and human eyes (Johnson, 1997; Rao et al., 2001; Park et al., 2016), and monkey eyes *in vivo* (Peterson et al., 1999; Peterson et al., 2000). Clinically, a selective Rho-kinase inhibitor ripasudil is being used for ocular hypertension and glaucoma treatment (Garnock-Jones, 2014). It was also found that the TM stiffness was increased in POAG patients (Last et al., 2011). The activation of cyclic guanosine monophosphate/nitrogen oxide (cGMP/NO) system was demonstrated to trigger TM cell relaxation (Stumpff et al., 1997) and decrease both the outflow resistance and IOP in various animal models (Behar-Cohen et al., 1996).

Abnormal structures in cross-linked actin networks (CLANs) have been found to be more abundant in the TM of glaucoma patients than those of normal subjects (Clark et al., 1995; Clark et al., 2005; Hoare et al., 2009). CLANs are geodesic-dome-like polygonal structure formed by re-organized F-actin microfilaments. They are believed to inhibit the actin filament remodeling, causing an increase in 1) stiffness in TM cells (Filla et al., 2009) and 2) outflow resistance in glaucomatous eyes (Fujimoto et al., 2016).

CHAPTER 2 Effects of temperature oscillations on MMP-9 and MMP-2 activity in the TM cells

2.1 Introduction

2.1.1 Circadian rhythms

2.1.1.1 Significance of circadian rhythm to human life

The circadian rhythm regulates a broad range of physiological processes in humans, such as metabolism, the sleep cycle and hormonal secretions (Liu and Chu, 2013). An offset in this rhythm can lead to physical and psychological disorders as well as social and economic risks. For example, shift workers have a higher risk of heart attacks, cancer and psychological disorders (Waterhouse and DeCoursey, 2004; Liu and Chu, 2013) with a reported worse work performance than a daytime worker (Waterhouse and DeCoursey, 2004). Also, the rate of traffic accidents is higher after midnight (Hamelin, 1987).

2.1.1.2 Properties of circadian rhythm

In general, circadian rhythm has the following characteristics (Johnson et al., 2004; Buhr and Takahashi, 2013). First, its rhythmic cycle persists without external time cue(s) with a period of approximately 24 hours. Second, it is entrainable by certain time signals (cues) which oscillate around a 24-hour period. Third, it cannot be altered by different ambient temperatures when there are no oscillating time cues

(temperature compensation). Finally, endogenous oscillations of molecular clocks governing the biological rhythm can be identified; and these clock elements are subject to specific time cues oscillating in a 24-hour period. For example, the oscillating expression of the clock elements CLOCK, PER2 and CRY2 is often found to be circadian rhythms of mammals.

A biological rhythm that lasts for approximately 30 days is classified as circalunar rather than circadian. If the observed rhythm cannot persist without an external cue, it may reflect a direct response to a stimulus, not an endogenous oscillation. If a rhythm is not entrainable, it will continue to run according to its period and phase without synchronizing to the external clock. Since the rhythm cannot adapt to any changes in the environment, it should not be considered as a circadian rhythm. If a circadian rhythm varied with ambient temperature, the rhythm would function as a temperature sensor rather than as a time-keeper.

2.1.1.3 Temperature as a circadian time cue

Although the circadian rhythm should be temperature compensated, temperature can still be the entraining agent even for homeothermic animals, including mammals (Buhr and Takahashi, 2013). In principle, the environmental temperature should not affect circadian rhythms in homeothermic species (temperature compensation) as they can maintain their own body temperature (Rensing and Ruoff, 2002). However, when the internal body temperature oscillates by a magnitude of 2°C to 4°C, it can act as an entraining cue to alter the phase of a circadian rhythm (Sandstrom et al., 2009; Buhr et al., 2010; Edery, 2010). Buhr et al. (2010) have demonstrated the entrainment of a clock element PER2 by 2.5°C

temperature oscillation in cultured mouse cells. Subsequently, they used KNK437, a HSF1 inhibitor, to inhibit the induction of heat shock proteins and inhibited the phase resetting of the circadian rhythm driven by temperature oscillation (Buhr et al., 2010). This supports the idea that temperature oscillation is involved in circadian rhythms via a heat shock pathway.

2.1.2 Diurnal variation of aqueous humor flow

The rate of aqueous humor formation (AHF) follows a circadian rhythm (Civan, 2008). It decreases by 50% from approximately 2.7 μl/min during the day to about 1.3 μl/min at night in healthy humans (Brubaker, 1998). This reduction forms an oscillation pattern over a 24-hour period. The entrainability of AHF rhythm by light has been demonstrated in rabbits, in which the AHF rate was higher in daytime and lower at night (Rowland et al., 1986; Smith and Gregory, 1989). With several cycles of 12-hour light and 12-hour dark (12L:12D), the phase of AHF rhythm could be shifted. The rhythm persisted in phase with the entraining light-dark cycles for several loops when the external time cue was removed (i.e. the ambient environment was changed into complete darkness), indicating that the rate of AHF displays a circadian rhythm.

Accompanying IOP was not reduced proportionately, despite this 50% reduction of aqueous humor inflow in humans (Liu, 1998; Asejczyk-Widlicka and Pierscionek, 2007; Liu et al., 2011). Therefore, we speculated that there was a periodic alternation in outflow resistance at night to counter balance the drop in AHF. Since AHF displays a circadian rhythm, we also speculated that the outflow resistance might follow such a rhythm. All in all, with the temperature fluctuation described

in Section 2.1.1.3, it may be suggestive that temperature could be a potential entraining agent for outflow resistance rhythm.

2.1.3 MMP-9 and MMP-2 as targets for study

Matrix metalloproteinase-9 (MMP-9) and MMP-2 belong to a gelatinase sub-group of the MMP family and are able to digest the extracellular matrix (ECM). As described in Section 1.4.3, both MMP-9 and MMP-2 are present in TM and aqueous humor (De Groef et al., 2013). Their activity had been found to be reduced in the TM of primary open angle glaucoma (POAG) patients (Guo et al., 2012). Both MMPs were shown to be associated with the changes in outflow facilities (Bradley et al., 1998), rendering them promising targets for outflow resistance modification. Investigation of the roles of MMP-9 and MMP-2 in the regulation of outflow resistance is technically easier than that of other MMPs. A technique termed zymography, which is derived from electrophoresis, can aid in the analysis of the activity of MMP-9 and MMP-2 based on the digestion of gelatin as a substrate (Hawkes et al., 2010). Currently, this technique is not available for all MMPs due to the technical difficulties in recovering its enzymatic function after electrophoresis.

2.1.4 Aims of the study

As there is a significant decrease in AHF (around 50%) but no proportionate reduction in IOP at night, it is suspected that there may be a change in outflow resistance at night. Since AHF rate displays a circadian rhythm, it is possible that a similar rhythm may be displayed in outflow resistance. In addition, as a small

physiological temperature change in mammals was found to be a universal time cue to synchronize circadian rhythm in mammals (Buhr et al., 2010), it is possible that temperature could be the circadian cue to regulate the diurnal rhythm of outflow resistance. We have yet to explore the underlying mechanism in alterations of outflow resistance and whether it actually follows a true circadian rhythm. To study the effect of temperature cycling on outflow resistance, the activity of secreted MMP-9 and MMP-2 was monitored. Specifically, the aims of the study were to 1) determine whether physiological temperature cycling can alter the activity of MMP-9 and MMP-2 secreted by TM cells in an oscillating manner; 2) investigate whether the oscillation patterns of the activity of MMPs display circadian rhythms by analyzing the expression of clock genes *Cry2* and *Per2*; and 3) study the signaling pathways leading to temperature cycling-driven oscillation patterns of MMP activity.

2.2 Materials and methods

2.2.1 Cell model

Transformed TM cell line (hTM5) (Alcon Research, Fort Worth, TX, USA) derived from a normal human donor, was cultured as previously described (Pang et al., 1994; Li et al., 2011). The cells (passage 30-38) were incubated at 37°C in 5% CO_2 humidified incubator with Dulbecco's Modified Eagle Medium (DMEM) supplemented with 10% fetal bovine serum (FBS).

2.2.2 Temperature cycling

hTM5 cells were placed in a 48-well plate for 12 hours at 37°C with each cell-containing well having approximately 6.25 x 10^4 or 1.2 x 10^5 cells. The cells were then washed with serum-free DMEM. Fresh 1% FBS DMEM without phenol red was supplied to the cells. A 24-hour incubation period at 37°C was allowed for adaptation until confluence. The incubation temperature was then alternated between 33°C and 37°C every 12 hours and the entire medium was collected (or removed in the clock gene analysis experiment) before altering the incubation temperature. Fresh medium, with or without drug, was replenished immediately after medium sample collection. The cycling time varied from 2.5 to 12 days.

2.2.3 Gelatin zymography

Gelatin zymography was adopted to measure the enzymatic activity of MMP-2 and MMP-9 (Hawkes et al., 2010; Hu and Beeton, 2010; Li et al., 2011). As described

in Section 2.2.2, the collected media during temperature cycling treatment were centrifuged at 13,200 rpm at 4°C for 20 min. The supernatant was removed and stored at -80°C prior to zymography. Media samples were thawed and mixed with zymogram sample buffer (Bio-Rad, Hercules, CA, USA) at a ratio of 1:2 according to the manufacturer's instruction. Aliquots of 15 or 20 µl sample-buffer mixtures, according to the comb size used, were loaded into each lane of a 10% polyacrylamide gel incorporated with gelatin [0.375M Tris-HCl, 0.1% sodium dodecyl sulfate (SDS), 10% acrylamide/bisacrylamide, 0.1% gelatin, 0.1% ammonium persulfate, 0.05% tetramethylethylenediamine (TEMED)] prior to SDS electrophoresis.

After electrophoresis, the gel was incubated with shaking for 4 hours in zymogram renaturing buffer (2.5% Triton X-100 aqueous solution) at room temperature. The zymogram renaturing buffer was then removed and the gel was incubated with zymogram developing buffer (25 mM Tris-HCl, 2.5 mM $CaCl_2$, 210 mM NaCl, and 25 µM $ZnSO_4$) in a humidified incubator at 37°C for 18 hours. Following this, the gel was stained with Coomassie Brilliant Blue R-250 Staining Solution (Bio-Rad, Hercules, CA, USA) for 22 hours and de-stained with several washes of zymogram de-staining buffer (10% acetic acid and 10% ethanol aqueous solution) until clear transparent bands representing MMPs were seen against the blue-stained gel. The gel was subsequently scanned (Scanjet 3570c, Hewlett-Packard, Palo Alto, CA, USA) and the band intensities were analyzed by software Image-J (National Institutes of Health, Bethesda, MD, USA).

2.2.4 Reverse transcription-polymerase chain reaction (RT-PCR)

2.2.4.1 RNA extraction

Total RNA of hTM5 cells was extracted with RNeasy Micro Kit (Qiagen, Valencia, CA, USA) at room temperature according to the manufacturer's manual. The cells were lysed and homogenized with 350 µl Buffer RLT Plus. The homogenized lysate was transferred to a gDNA Eliminator spin column and centrifuged at 10,000 rpm for 30 sec. The eluate was mixed with 350 µl 70% ethanol and then immediately transferred into an RNeasy MinElute spin column. The column was centrifuged at 10,000 rpm for 15 sec and the flow-through was discarded. 10 µl DNase I stock solution was mixed with 70 µl Buffer RDD and transferred onto the RNeasy spin column membrane. Following a 15 min digestion time at room temperature, the column was washed with 350 µl Buffer RW1 for 15 sec at 10,000 rpm, before an addition of 500 µl 80% ethanol and centrifugation at 10,000 rpm for 2 min. The column was then centrifuged at 13,200 rpm for 5 min to remove all the ethanol. Finally, 14 µl RNase-free water was added at the center of the spin column membrane, the column centrifuged at 13,200 rpm for 1 min, and the eluate containing the RNA collected.

2.2.4.2 Reverse transcription

Taqman Reverse-Transcription Reagents (Applied Biosystems, Foster City, CA, USA) were used for reverse transcription. Each 20 µl reaction mixture contained 2.0 µl 10X RT Buffer, 1.75 mM $MgCl_2$, 0.5 mM dNTP mix, 5.0 mM 1,4-

Dithiothreitol (DTT), 1.0 U/μl RNase inhibitor, 2.5 U/μl MultiScribe™ RT, 2.5 μM random hexamers, and 1 μg template RNA. The reaction mixture was warmed to 25°C for 10 min and then to 37°C for 30 min. Finally, it was heated to 95°C for 5 min before storage.

2.2.4.3 Polymerase chain reaction (PCR)

AccuPrime™ Taq DNA Polymerase High Fidelity (Invitrogen, Carlsbad, CA, USA) was used to amplify the TRPV1-4 cDNAs in accordance with the manufacturer's protocol. Each 50 μl reaction mixture contained 5 μl 10X AccuPrime™ PCR Buffer I, 0.2 μM forward primer, 0.2 μM reverse primer, 20 ng template DNA, and 0.2 μl AccuPrime™ Taq High Fidelity. For the negative control [RTase(-)], the reverse transcriptase was replaced by H_2O. The thermal cycling conditions were as follow: 1) 5 min initial denaturation at 95°C; 2) 40 cycles of 30 sec denaturation at 94°C, 30 sec annealing at 60°C and 60 sec extension at 72°C; and 3) 5 min final extension at 72°C.

The primer sequences used are listed in Table 2.1.

Table 2.1 The primer sequences for TRPV1-4 detected by RT-PCR

target gene	**forward strand (5'-3')**	**reverse strand (5'-3')**	**band size (bp)**
TRPV1	GCCTGGAGCTGTTCAAGTTC	TCTCCTGTGCGATCTTGTTG	177
TRPV2	CAAACCGATTTGACCGAGAT	GTTCAGCACAGCCTTCATCA	167
TRPV3	ACGAGGCAACAACATCCTTC	CCGCTTCTCCTTGATCTCAC	226
TRPV4	GACGGGGACCTATAGCATCA	AACAGGTCCAGGAGGAAGGT	228
GAPDH	CCATGGAGAAGGCTGGGG	CAAAGTTGTCATGGATGACC	194

2.2.4.4 Agarose gel electrophoresis

1% Agarose containing 0.05% ethidium bromide in TBE buffer [89 mM Tris, 89 mM boric acid, 2 mM Ethylenediaminetetraacetic acid (EDTA)] was used to separate PCR products by size. PCR products were mixed with 6X DNA loading dye (Thermo Scientific, Rockford, IL, USA) and GeneRuler 100bp DNA ladder (Thermo Scientific, Rockford, IL, USA) was used as the DNA marker. Electrophoresis was conducted at 70V for 80 min. The bands were visualized and photographed under UV light by ChemiDoc XRS System (BioRad, Hercules, CA, USA).

2.2.5 Quantitative RT-PCR (qPCR)

Quantitative RT-PCR (qPCR) was conducted to determine the gene expression changes of the two selected clock genes, *Per2* and *Cry2*. The RNA isolation procedure was described above in Section 2.2.4. The isolated RNA was reverse-

transcripted to cDNA using the kit, Superscript® II First-Strand Synthesis System (Invitrogen, Carlsbad, CA, USA).

TaqMan probes (Integrated DNA Technologies, Inc., Coralville, IA, USA) were chosen for the qPCR assay. The primers used were custom made and pre-validated and are listed in Table 2.2. Power SYBR Green Universal Master Mix (Applied Biosystems, Foster City, CA, USA) was used for the assay. Each 25 µl reaction contained 10 ng cDNA, 0.2 µM of each of the primers and 12.5 µl 2X Master Mix solution and these were loaded in a 96-well plate for thermocycling in Applied Biosystems 7300 Real-Time PCR System (Applied Biosystems, Foster City, CA, USA) using the following thermocycling program parameters [2 min Uracil-DNA Glycosylase (UDG) treatment step at 50°C, 10 min denaturing step at 95°C, 40 cycles of 15 sec denaturation at 95°C and 1 min annealing and extension at 60°C]. For no template control (NTC), template DNA was replaced by the same volume of H_2O. The results were analyzed using ΔΔCt method and β-actin was used as the internal control.

Table 2.2 The primer sequences for clock genes *Cry2* and *Per2* detected by qPCR

target gene	**corresponding protein**	**forward strand (5'-3')**	**reverse strand (5'-3')**
Per2	PER2	CCAGTGGACATGAGACCAAC	TTGCCATCATCAGGCTAAAG
Cry2	CRY2	AGGACTTGGTCCAGCTGTCT	GTTCATTCGGGGTCTCTCAT
ACTB	β-actin	CCAGTGGTACGGCCAG	GCGAGAAGATGACCCAGAT

2.2.6 Solutions and pharmacological agents

Unless otherwise specified, all media and chemicals used for cell culture were obtained from Gibco (Grand Island, NY, USA) and other biochemical agents were purchased from Sigma-Aldrich Corp. (St. Louis, MO, USA). Dulbecco's Modified Eagle Medium (DMEM) with phenol red was purchased from Cellgro (Manassas, VA, USA). Heat shock factor 1 (HSF1) inhibitor 3,4-methylenedioxy-benzylidine-γ-butyrolactam (KNK437; Calbiochem, San Diego, CA, USA), TRPV1 and TRPM8 receptor inhibitor N-(4-tertiarybutylphenyl)-4-(3-cholorphyridin-2-yl)tetrahydropyrazine-1(2H)-carboxamide (BCTC; Enzo Life Sciences, Farmingdale, NY, USA); and TRPV4 and TRPM8 inhibitor 2-methyl-1-[3-(4-morpholinyl)propyl]-5-phenyl-N-[3-(trifluoromethyl)phenyl]-1H-pyrrole-3-carboxamide (HC 067047; Santa Cruz Biotechnology, Dallas, TX, USA) were dissolved in dimethyl sulfoxide (DMSO) with the final concentration less than 0.5%.

2.2.7 Statistical analysis

All results were presented as mean ± SEM, unless otherwise specified. The notation N referred to the number of independent experiments conducted and n represented the number of measurements done in experiments. The data were analyzed by a statistics program SigmaStat (Aspire Software International, Ashburn, VA, USA). Unless otherwise specified, all data passed normality or equal variance tests. Holm-Sidak All Pairwise Multiple Comparison Procedures were performed after two-way repeated measures ANOVA. Experimental results with p-value < 0.05 in their null hypotheses were considered to be statistically significant. P-value

notations used in statistical analysis are shown below:

Symbol	***p*-value**
ns	> 0.05
*	< 0.05
**	< 0.01
***	< 0.001

2.3 Results

2.3.1 Effect of temperature cycling on MMP-9 and MMP-2 activity

The effects of temperature cycling on MMP-9 and MMP-2 activity are shown in Fig. 2.1 and Fig. 2.2, respectively. Cells were divided into 2 sets, and they were incubated at 37°C for 3 days (from Day 1 to Day 3). They were then subject to incubation temperature cycling for another 3 days (Day 4 to Day 6). The temperature cycling pattern was a loop of 33°C for 12 hours followed by 37°C for 12 hours each day. The two cell sets were subject to the same temperature cycling but in opposite phases, i.e. one set was incubated at 33°C during daytime (labeled as daytime 33°C) and the other set was at 37°C (labeled as daytime 37°C). The "daytime" label refers to the laboratory ambient time (9 AM to 9 PM) and is not related to the circadian timing terminology. After Day 7, the cells were maintained at constant temperature, i.e. 33°C for the group "daytime 37°C" and 37°C for the group "daytime 33°C". The media were collected every 12 hours (before replenishment of fresh media and change of incubation temperature, if needed) and the activity of the secreted MMP-2 and MMP-9 in the media were analyzed by zymography.

As shown in Fig. 2.1 and Fig. 2.2, it was found that there were temperature cycling-driven changes in MMP activity. For example, when the temperature was raised, the activity of both MMP-9 and MMP-2 increased; when the temperature dropped, the MMPs activity decreased. The temperature cycling-driven intensity pattern of the MMPs was conserved in both the reverse-phased sets of cells (Fig. 2.1 and Fig.

2.2). In other words, the order of temperature alternation did not affect the oscillation patterns of MMPs. Moreover, there was a gradual increase in the activity of both MMP-2 and MMP-9 over time. This might be caused by an incomplete suppression of cell division during the experimental period. The activity of both MMP-9 and MMP-2 was found to be higher at 37°C than at 33°C with two-way repeated measures ANOVA (N = 6, group daytime 33°C, $p = 0.003$; group daytime 37°C, $p < 0.002$ for MMP-9 as shown in Fig. 2.1) (N = 6, group daytime 33°C, $p < 0.001$; group daytime 37°C, $p = 0.146$ for MMP-2 as shown in Fig. 2.2). The temperature effect on MMP-9 was greater than that on MMP-2. After Day 7, when temperature cycling ceased and a constant temperature was applied, the oscillation pattern disappeared within 24 hours. When the cells were incubated at a constant temperature, both MMP-9 and MMP-2 displayed higher activity at higher temperature condition. Taken together, it could be concluded that there was a temperature cycling-driven oscillation pattern in the intensities of both MMP activity, with an elevated temperature leading to an increased activity, and *vice versa*. This oscillation pattern disappeared when the temperature cycling stopped. Combining all the temperature cycling experiments conducted at all measured time points, i.e. Day 1 to Day 13, if applicable (n = 436), the average normalized intensity differences of MMP-9 and MMP-2 between the incubation temperature of 33°C and 37°C were 0.40 ± 0.03 and 0.22 ± 0.02, respectively.

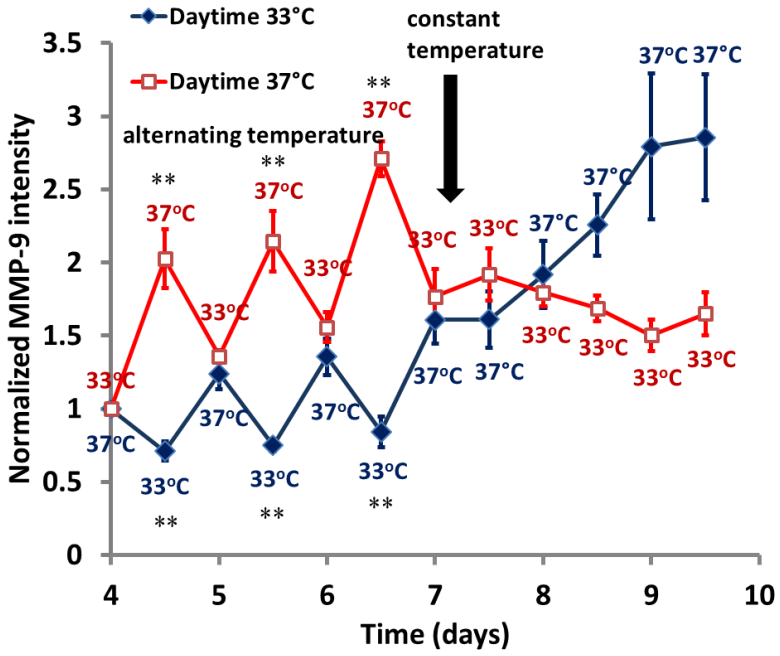

Fig. 2.1 Effect of temperature cycling on MMP-9 activity. The cultured hTM5 cells were subject to a temperature cycling pattern of 33°C for 12 hours and 37°C for 12 hours from Day 4 to Day 6. The incubation temperature was then held constant at 33°C (Daytime 37°C, open squares) or 37°C (Daytime 33°C, filled diamonds) from Day 7 to Day 9 (N = 6).

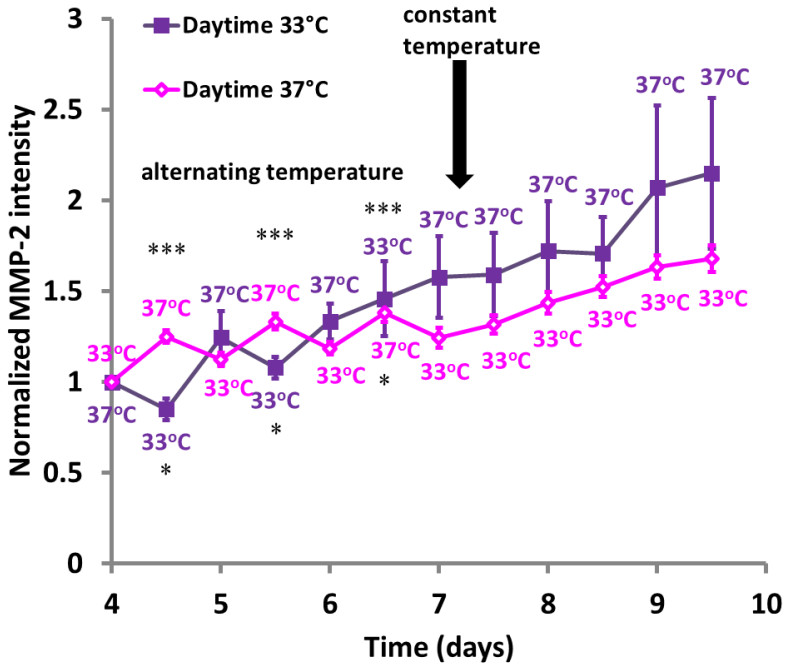

Fig. 2.2 Effect of temperature cycling on MMP-2 activity. Cultured hTM5 cells were subject to a temperature cycling pattern of 33°C for 12 hours and 37°C for 12 hours from

Day 4 to Day 6. The incubation temperature was then held constant at 33°C (Daytime 37°C, open diamonds) or 37°C (Daytime 33°C, filled squares) from Day 7 to Day 9 (N = 6).

To confirm whether MMP activity oscillations were entrainable, the experiment was repeated with an extended temperature oscillating period from 3 days to 6 days. As shown in Fig. 2.3, the results showed that the oscillation patterns of MMP-9 and MMP-2 activity could not be maintained when the temperature cycling cues were stopped.

To enhance visualization of MMP activity changes, sequential subtraction curves were plotted as shown in Fig. 2.4 and Fig. 2.5. The intensity difference indicated at any given time point (t) was the remainder of the original normalized MMP intensity at time point t minus that at the previous time point (t - 1), i.e. 12 hours before. The δ+ label indicated that the intensity difference at that time point was obtained from increasing temperature, while δ- represented the intensity change from decreasing temperature. The differences from no temperature changes were labeled as δs. Cells were incubated under temperature oscillation for 6 days and then at constant temperature for another 6 days. The MMP intensity differences labelled δ+ were significantly different from those labelled as δ- in MMP-9 (N = 4, $p < 0.001$ for Fig. 2.4, and $p = 0.022$ for Fig. 2.5, two-way repeated measures ANOVA) and in MMP-2 (N = 4, $p = 0.001$ for Fig. 2.4 and $p = 0.031$ for Fig. 2.5), respectively. The results also showed that the intensities of MMP-9 and MMP-2 increased significantly with temperature rise and decreased with temperature drop.

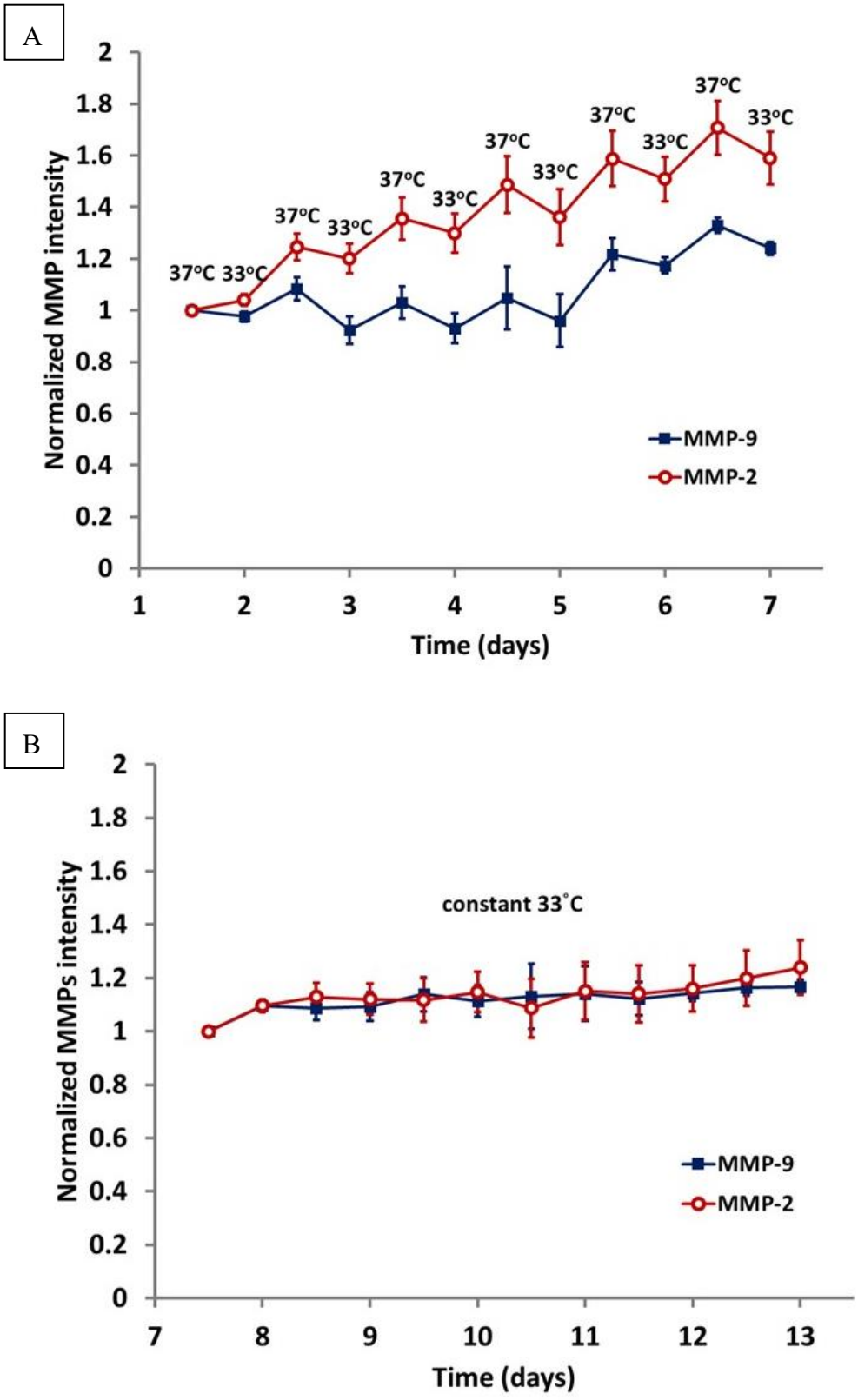

Fig. 2.3 Effect of 6-day temperature cycling on MMP-9 and MMP-2 activity. (A) The cultured hTM5 cells were subject to a 6-day temperature cycling pattern of 33°C for 12 hours and 37°C for 12 hours from Day 1 to Day 6. (B) Afterwards, the incubation temperature was held constant at 33°C (Day 7 to Day 13) (N = 6).

When the temperature oscillation stopped and the incubation temperature was held constant at either 33°C or 37°C, the MMP intensity oscillation pattern disappeared (Fig. 2.4 and Fig. 2.5). The residual fluctuations of MMP intensity differences after holding the incubation temperature at 33°C (Fig. 2.4) and 37°C (Fig. 2.5) respectively showed no significant oscillating pattern in either MMP-9 or MMP-2 by two-way repeated measures ANOVA.

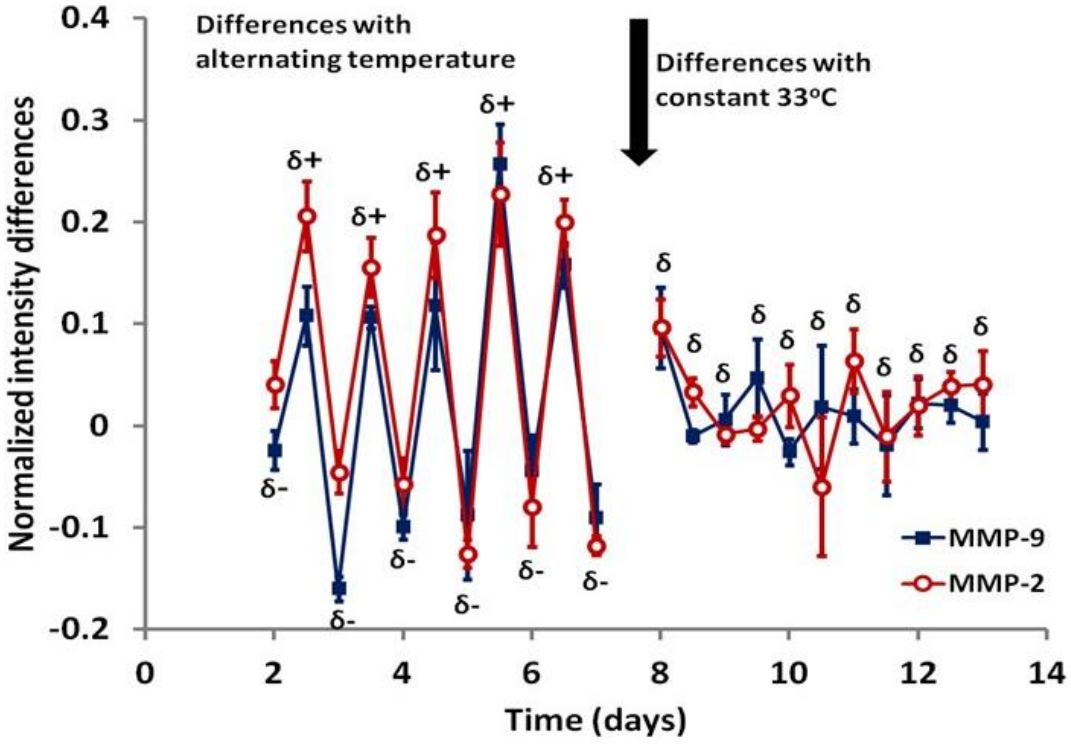

Fig. 2.4 Effect of 6-day temperature cycling on MMP-9 and MMP-2 activity (sequential subtraction, ending 33°C). Cultured hTM5 cells were subject to a temperature cycling pattern of 33°C for 12 hours and 37°C for 12 hours from Day 1 to Day 6. The incubation temperature was held constant at 33°C from Day 7. The data shown here were the remainders following subtraction of MMP activity intensities at the adjacent time point (N = 4). δ+: the intensity difference at that time point was obtained from increasing temperature, δ-: the intensity difference at that time point was obtained from decreasing temperature. δ: the intensity difference at that time point was obtained from no temperature changes.

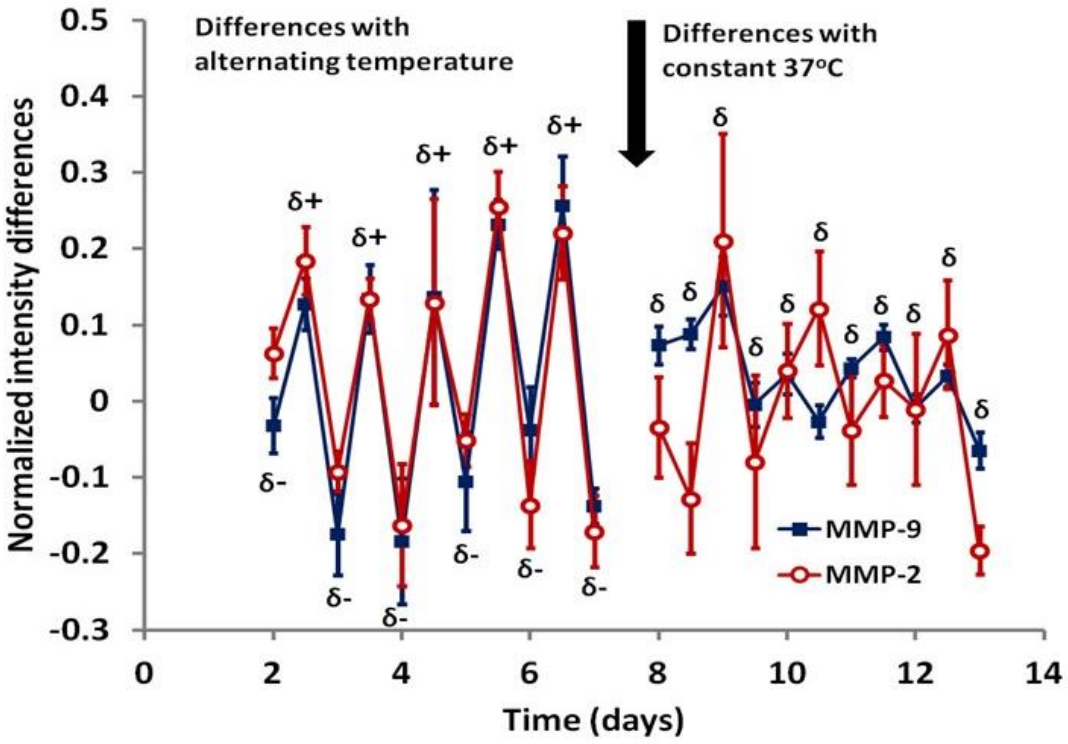

Fig. 2.5 Effect of 6-day temperature cycling on MMP-9 and MMP-2 activity (sequential subtraction, ending 37°C). Cultured hTM5 cells were subject to a temperature cycling pattern of 33°C for 12 hours and 37°C for 12 hours from Day 1 to Day 6. The incubation temperature was then held constant at 37°C. The data shown here were remainders after subtraction of MMP activity intensities at the adjacent time points (N = 4). δ+: the intensity difference at that time point was obtained from increasing temperature, δ-: the intensity difference at that time point was obtained from decreasing temperature. δ: the intensity difference at that time point was obtained from no temperature changes.

2.3.2 Effect of HSF1 inhibitor on MMP-9 and MMP-2 cycling activity patterns

Heat shock pathway has been reported to transfer temperature-induced circadian rhythm signals to the peripheral clocks of mammals. To further examine whether temperature cycling could drive the oscillation of MMP activity through the heat shock pathway, heat shock factor 1 (HSF1) inhibitor KNK437 was used during

temperature cycling experiments. Similar to the previous experiments, cells were subject to temperature oscillation for 6 days. The administration of 100 μM KNK437 or the DMSO vehicle control started on Day 3 night, after medium collection. As shown in Fig. 2.6, it was observed that KNK437 disrupted the increasing trend of MMP-9 activity compared with the DMSO (vehicle control) group. The mean normalized MMP-9 activity decreased significantly by 53 ± 8% ($p < 0.001$, one-way repeated measures ANOVA) in the presence of KNK437. Temperature cycling-driven oscillation was reduced by 68 ± 9% ($p < 0.001$).

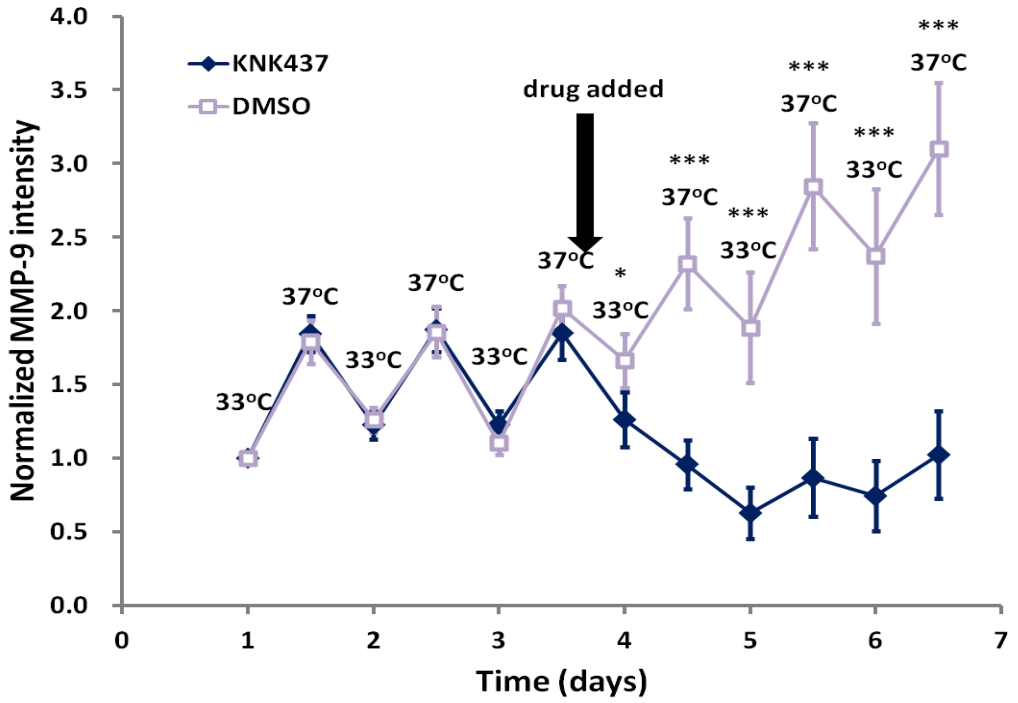

Fig. 2.6 Effect of KNK437 on MMP-9 cycling activity pattern. hTM5 cells were incubated in a temperature cycling pattern of 33°C for 12 hours and 37°C for 12 hours. At 100 μM, KNK437 inhibited an increase in MMP-9 activity over time, but not the temperature cycling-driven oscillation pattern of MMP-9 activity (N = 12, *: $p < 0.05$, ***: $p < 0.001$, Student's t-test, compared between the groups at the same time points). KNK437: heat shock factor 1 (HSF1) inhibitor; DMSO: vehicle.

In contrast, KNK437 did not inhibit the mean normalized MMP-2 activity (Fig. 2.7). Compared with the baseline value, the normalized MMP-2 intensity increased by 6 ± 4% after KNK437 treatment (N = 12, p = 0.003, one-way repeated measures ANOVA). Unlike MMP-9, the data for the temperature cycling-driven MMP-2 oscillation were not normally distributed (Shapiro-Wilk test). Therefore, they were analyzed with repeated measures ANOVA on ranks; and the result showed that the oscillation was not affected by KNK437 (p = 0.414).

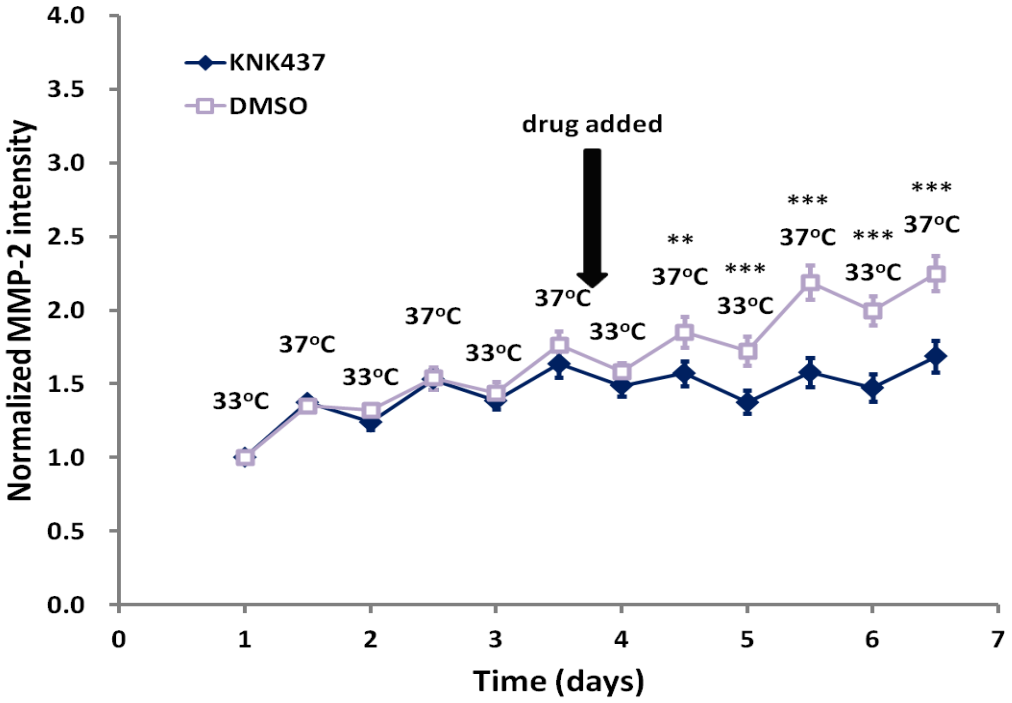

Fig. 2.7 Effect of KNK437 on MMP-2 cycling activity pattern. hTM5 cells were incubated in a temperature cycling pattern of 33°C for 12 hours and 37°C for 12 hours. At 100 μM, KNK437 inhibited the increase in MMP-2 activity over time, but not the temperature cycling-driven oscillation pattern of MMP-2 activity (N = 12, *: $p < 0.05$, **: $p < 0.01$, ***: $p < 0.001$, Student's t-test, compared between the groups at the same time points). KNK437: heat shock factor 1 (HSF1) inhibitor; DMSO: vehicle.

2.3.3 Effect of temperature cycling on expression of clock genes *Cry2* and *Per2*

The results described in Section 2.3.1 showed that the MMP activity with temperature cycling-driven oscillation pattern did not persist when the external temperature cycling stopped. This suggested that MMP intensity oscillation might not be a circadian rhythm with a peripheral clock located in the TM cells. To further examine this notion, the expression patterns of clock genes *Cry2* and *Per2* during the temperature cycling period were determined using qPCR.

The cell incubation conditions for qPCR assay were similar to previous experiments, with 10% FBS medium at 37°C for the initial 24 hours and then 1% FBS medium at 33°C/37°C cycling for 2.5 days. Fig. 2.8A shows the results of cells with the initial (and final) incubation temperature of 33°C during the temperature cycling period, while Fig. 2.8B shows those at 37°C. Cells in each condition were taken out every 3 hours during the last 12 hours of the incubation period for total mRNA extraction. There were three to four biological repeats for each condition. The assays showed that the expression levels of both clock genes *Cry2* and *Per2* increased at the 12th-hour time point, regardless of whether the incubation temperature during the last 12 hours was 33°C ($p < 0.02$, Student's t-test, Fig. 2.8A) or 37°C ($p < 0.005$, Student's t-test, Fig. 2.8B). The results suggested that these clock gene expression changes were not related to the incubation temperature cycling since both higher and lower temperatures triggered the same clock gene expression increase at the 12th-hour time point. Note that at the 6th-hour time point, there was a small but statistically significant reduction in *Per2* expression ($p < 0.005$, Student's t-test, compared with the 3rd-hour time point); however, *Cry2* did

not display a similar drop at this time point (Fig. 2.8B).

To verify the above hypothesis, a further set of qPCR experiment was conducted without cycling of incubation temperature. The incubation temperature was kept constant at 37°C for the whole experimental period. At the 12th-hour time point in the final 12-hour period, expression of both genes was increased with that of *Cry2* expression reaching statistical significance (Fig. 2.8C, $p < 0.05$, Student's t-test). The results indicated that the change of clock gene expression at the 12th-hour time point might not be due to incubation temperature cycling.

A previous study reported that change of serum concentration could alter the expression level of clock genes presumably through the change of expression levels of immediate-early genes by serum factors, mimicking a circadian rhythm (Balsalobre et al., 1998). To examine the effect of serum change, the FBS concentration and temperature were kept constant at 10% and 37°C respectively since the start of the cell culture. The clock gene expression levels were then examined. The results showed that clock genes did not demonstrate an abrupt increase in expression at the 12th-hour time point (Fig. 2.8D), although a small but statistically significant decrease of *Per2* expression was found at the 6th-hour time point ($p < 0.02$, Student's t-test). Combined with the results of Fig. 2.8C, the changes in clock gene expression were likely mediated by a serum change, not temperature cycling.

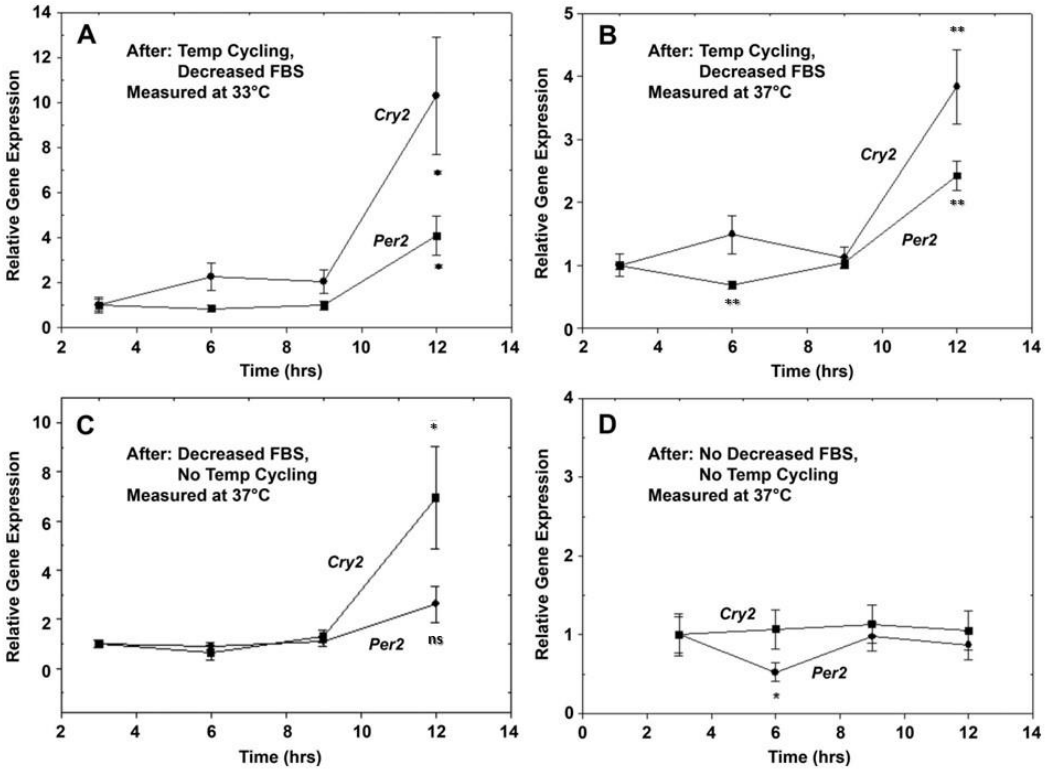

Fig. 2.8 Relative expression of clock genes *Cry2* and *Per2* in the last 12 hours under various experimental conditions. After the initial 24-hour incubation in 10% FBS medium at 37°C, hTM5 cells were incubated at 33°C/37°C temperature cycling for 60 hours in 1% FBS medium with an ending temperature of (A) 33°C and (B) 37°C, respectively. (C) After the initial 24-hour incubation in 10% FBS medium at 37°C, the cells were incubated at a constant 37°C temperature for 60 hours with 1% FBS medium. (D) The cells were incubated at a constant 37°C temperature in 10% FBS medium since the start of the culture. ns: not statistically significant, *: $p < 0.05$, **: $p < 0.01$, Student's t-test.

2.3.4 Expression of TRPV isoforms in human TM cells

It was possible that temperature cycling triggered MMP oscillation through thermo-sensitive TRP channels (see Section 2.4.4 for further discussion). Therefore, mRNA expression of TRPV1 to 4 in hTM5 cells was studied.

Their expression was verified and the results are shown in Fig. 2.9. No PCR product

was detected in the negative control [RTase(-)], suggesting that the experimental products were free from contamination. A duplicate experiment was performed and similar results were obtained.

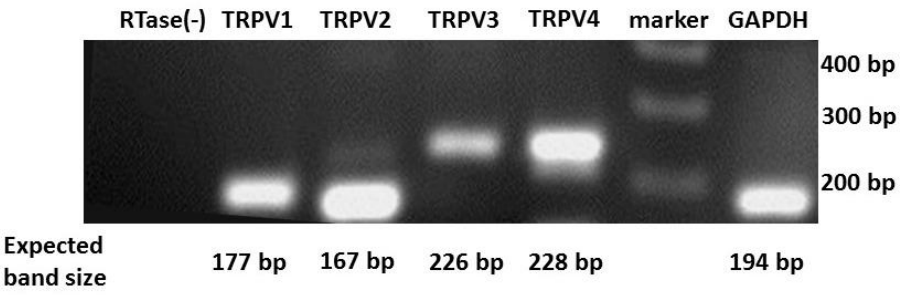

Fig. 2.9 Expression of TRPV1-4 channels in hTM5 cells by RT-PCR. TRPV1-4 channels were detected in hTM5 cells by RT-PCR. RTase(-): negative control with absence of reverse-transcriptase; GAPDH: control to show the expression of *GAPDH* gene.

2.3.5 Effects of TRP channel inhibitors on MMP-9 and MMP-2 cycling activity patterns

Since thermoTRP channels can be involved in the temperature-sensitive biological pathway and some of these channels expressed in hTM5 cells, it was speculated that they might participate in the temperature-driven oscillations of MMP activity. Their corresponding inhibitors were used to investigate the involvement of the thermoTRP channels. Similar to the experiment conducted using KNK437, the thermoTRP inhibitors were added to the media after 3 days of oscillation during a 6-day temperature-cycling incubation period.

BCTC was used as an inhibitor of TRPV1 and TRPM8. At 10 μM, BCTC was found

to disrupt the increasing trend of both MMP-9 and MMP-2 activity, compared to the control groups (Fig. 2.10 and Fig. 2.11). The mean normalized MMP-9 activity was significantly reduced by BCTC (N = 12, $p < 0.05$, one-way repeated measures ANOVA). Since the oscillation data from MMP-9 did not pass the Shapiro-Wilk normality test, Wilcoxon signed rank test was chosen for the analysis. Our results showed that MMP-9 oscillating activity was not affected by BCTC ($p = 0.063$, paired t-test). On the other hand, the data of MMP-2 passed the normality test. The analysis showed that the temperature cycling-driven oscillation of MMP-2 activity did not change significantly compared to baseline period ($p = 0.591$, paired t-test).

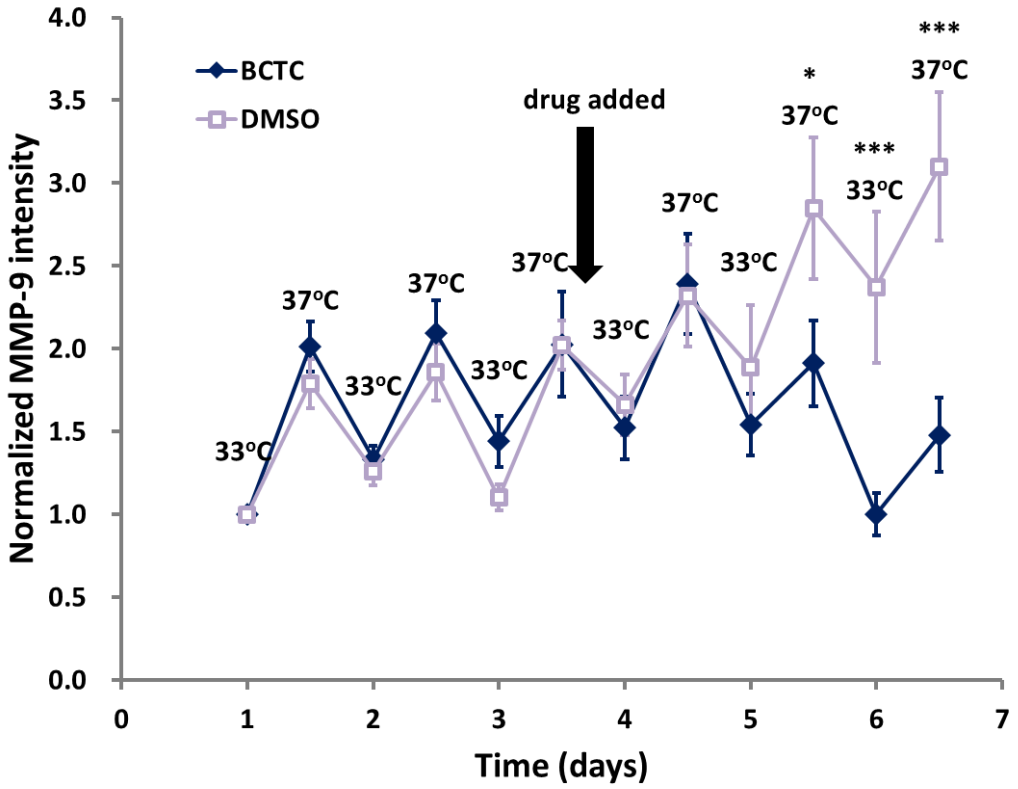

Fig. 2.10 Effect of BCTC on MMP-9 cycling activity pattern. hTM5 cells were incubated for 3 days in a temperature cycling pattern of 33°C for 12 hours and 37°C for 12 hours. At 10 μM, BCTC inhibited the upward drift of secreted MMP-9 compared with the group

treated with the DMSO vehicle, but not the temperature-driven oscillations of secreted MMP-9 activity (N = 12, *: $p < 0.05$, ***: $p < 0.001$, Student's t-test, compared between the groups at the same time points). BCTC: a TRPV1 and TRPM8 inhibitor; DMSO: vehicle.

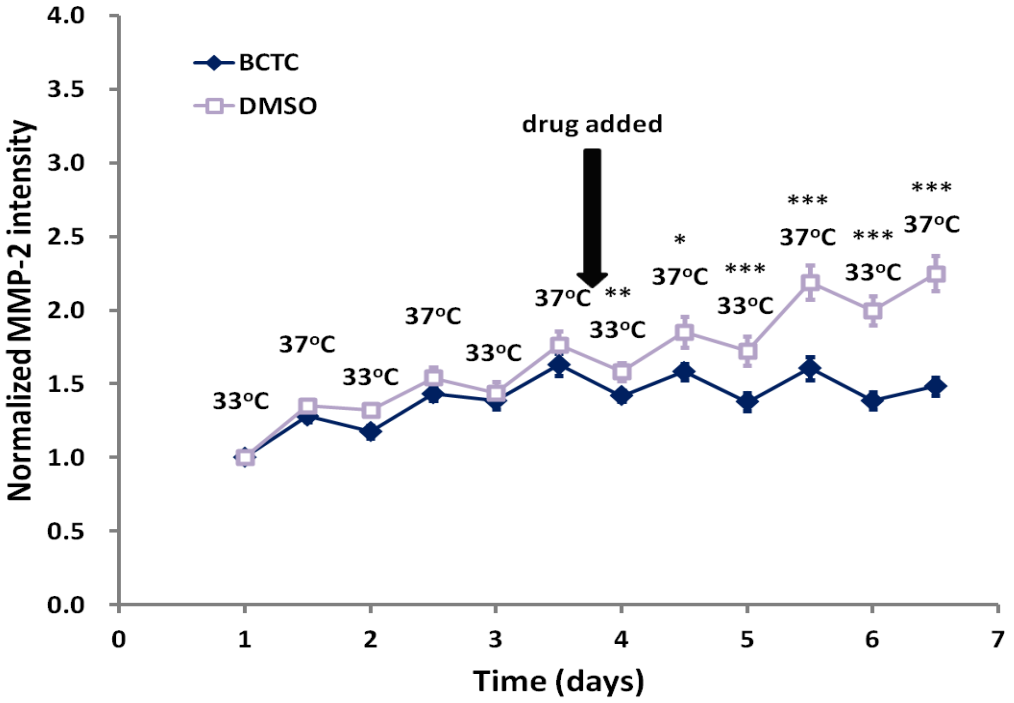

Fig. 2.11 Effect of BCTC on MMP-2 cycling activity pattern. hTM5 cells were incubated for 3 days in a temperature cycling pattern of 33°C for 12 hours and 37°C for 12 hours. At 10 µM, BCTC inhibited the upward drift of secreted MMP-2 compared with the group treated with the DMSO vehicle, but not the temperature-driven oscillations of secreted MMP-2 activity (N = 12, *: $p < 0.05$, **: $p < 0.01$, ***: $p < 0.001$, Student's t-test, compared between groups at the same time point). BCTC: a TRPV1 and TRPM8 inhibitor; DMSO: vehicle.

HC 067047 is a TRPV4 and TRPM8 inhibitor. The administration of HC 067047 at two concentrations (1 µM and 10 µM) did not show any effect on the oscillating activity of MMP-9 and MMP-2, compared with the DMSO controls (Fig. 2.12 and

Fig. 2.13) (N = 6). Combined with results of BCTC, the findings suggested TRPV1, but not TRPM8, being involved in MMP activity (see Section 2.4.5).

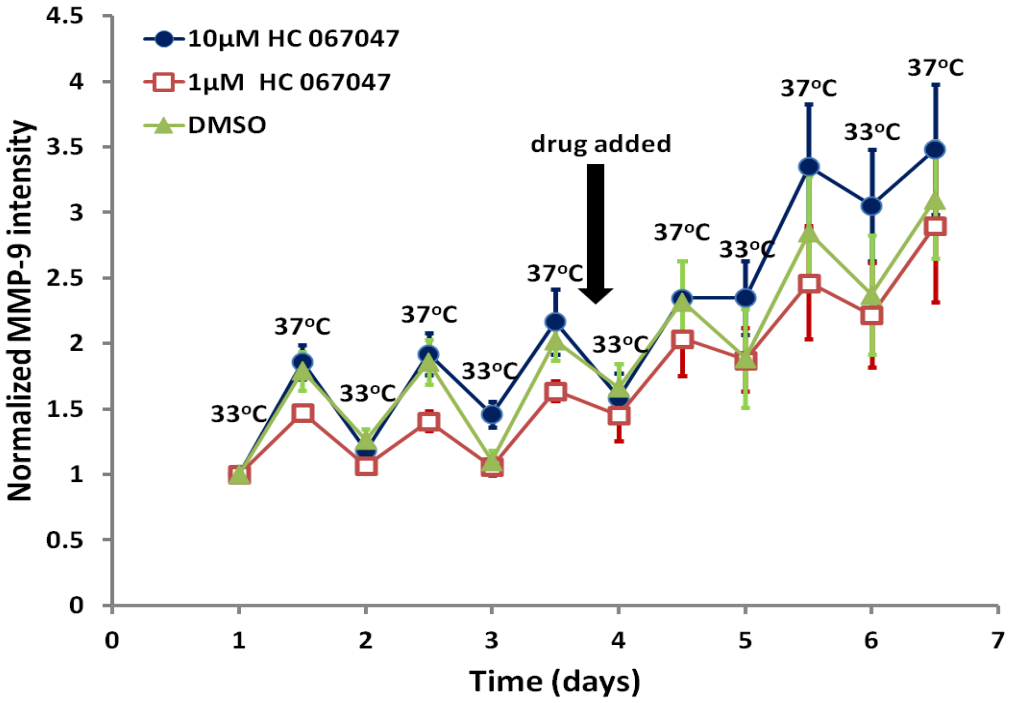

Fig. 2.12 Effect of HC 067047 on MMP-9 cycling activity pattern. hTM5 cells were incubated for 3 days in a temperature cycling pattern of 33°C for 12 hours and 37°C for 12 hours. Neither 1 nor 10 μM HC 067047 inhibited the oscillation of MMP-9 compared with the control (DMSO) (N = 6). HC 067047: a TRPV4 and TRPM8 inhibitor; DMSO: vehicle.

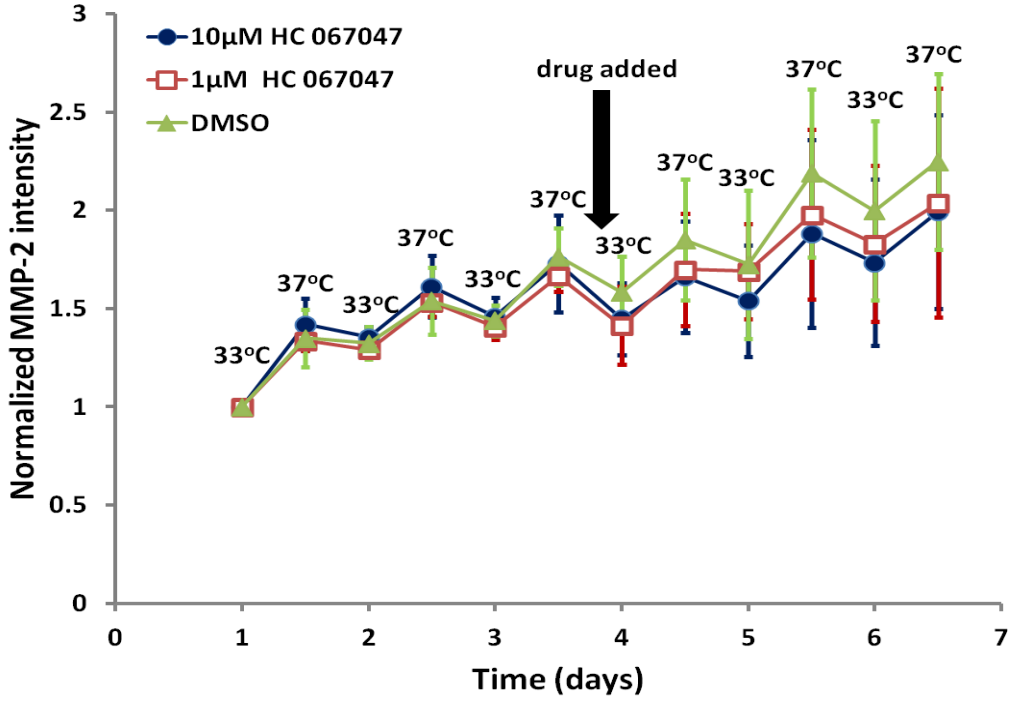

Fig. 2.13 Effect of HC 067047 on MMP-2 cycling activity pattern. hTM5 cells were incubated for 3 days in a temperature cycling pattern of 33°C for 12 hours and 37°C for 12 hours. Neither 1 nor 10 µM HC 067047 inhibited the oscillation of MMP-2 compared with the control (DMSO). HC 067047: a TRPV4 and TRPM8 inhibitor; DMSO: vehicle. (N = 6)

2.4 Discussion

Our results have shown that a small physiological temperature increase of 4°C could increase the activity of secreted MMP-9 and MMP-2 in a human TM cell line. An increase in MMP-9 activity was 40% and that of MMP-2 was 22%. The changes were found to be reversible when the incubation temperature was restored to the baseline value.

Although the incubation temperature cycling could drive the activity of secreted MMP-9 and MMP-2 to oscillate, this oscillation was not entrainable. This finding suggested that the oscillation might not be a circadian rhythm driven by the peripheral clock located in the TM cells. This notion was supported by experiments conducted using the heat shock pathway inhibitor as well as the analysis of expression of clock genes. By using inhibitors of various TRP channels, it was found that TRPV1 did not affect the oscillation of both MMP-2 and MMP-9 activity driven by temperature cycling, but might contribute to the total activity of secreted MMPs.

2.4.1 Choice of temperature for oscillation

To investigate whether the biological pattern of outflow resistance fluctuation displays a circadian rhythm linked to diurnal variation patterns in the ocular temperature, 33°C and 37°C were chosen as the temperature oscillation points. These values were thought to be within the range of physiological temperature fluctuation in the anterior chamber angle of human eye during the day. To the best of our knowledge, there is no report of direct measurement of the temperature at

the anterior chamber angle. 33°C and 37°C were chosen as oscillating temperatures because the temperature of the TM is likely to be affected by nearby structures, including the ciliary body and the iris. As the ciliary body and iris receive a rich supply of blood, their temperatures are likely to be synchronized with the core body. Since the core body temperature may fluctuate by 2°C to 4°C diurnally (Sandstrom et al., 2009; Buhr et al., 2010; Edery, 2010), the TM temperature is also likely to be subject to this oscillation. The cornea is also adjacent to the TM and can strongly influence its temperature. At room temperature, the corneal temperature in healthy humans has been reported to be 32.7 ± 0.3°C (Geiser et al., 2004) using infrared ocular thermography. This normal level can be affected by extreme conditions and the temperatures of 26.4 ± 0.9°C and 36.2 ± 0.5°C have been recorded at ambient temperatures of -20°C and 40°C, respectively (Geiser et al., 2004). Also, the reported corneal temperature might be underestimated since the infrared actually measured the temperature of the tear film, whose heat is constantly lost due to evaporation. A mathematical model suggested the temperature of the aqueous humor being about 34°C at ambient room temperature (Scott, 1988). It was deduced that the TM temperature might be around 34°C as well. Considering the continuously changing external temperature and the body temperature fluctuations, it is reasonable to consider the physiological TM temperature oscillating between 33°C and 37°C.

2.4.2 Choice of clock genes to determine if rhythm was circadian

Cry2 and *Per2* were chosen as the clock genes to be studied, because they are the core components of the circadian clock, producing negative elements for the down-regulation of observable signals during the rhythm (Dunlap, 2004). Also, they have

been studied extensively in circadian biology (Preitner et al., 2002).

2.4.3 Temperature cycling induced-oscillation of MMP activity

As demonstrated in our findings, a small temperature change induced a significant MMP activity alternation. This suggests that attention should be paid to the experimental temperature when comparing results from different outflow studies because even a small change of 4°C could induce a large difference in MMP activity. In addition, we have found that the change in MMP activity was reversible. Such a change in MMP activity was considered a biological change, not a pure physical phenomenon because Q10 values for MMP-9 and MMP-2 activity were 2.3 and 1.6, respectively. Moreover, various inhibitors suppressed MMP activity, which further suggested the change in MMP activity was a biological, not a pure physical phenomenon.

From the experimental results, it was concluded that the temperature cycling-driven oscillation of MMP-9 and MMP-2 activity was not a circadian rhythm induced by TM cells for the following three reasons: First, the oscillation pattern was not entrainable. In an entrainable biological oscillation, the oscillation pattern will continue without external stimulus (entraining agent). In this study, the MMP activity oscillated together with temperature cycles, but the oscillation stopped once the incubation temperature was held constant. Second, the interruption of HSF1 could not inhibit the overall activity or the temperature cycling-driven oscillation in MMP-2. KNK437 is a potent inhibitor against the induction of heat shock proteins (Yokota et al., 2000), effectively disrupting HSF1 trimerization, which initiates the transcription of clock genes through the heat shock protein signaling

pathway (Morimoto, 1998; Yokota et al., 2000; Buhr and Takahashi, 2013). Since the inhibitor did not disrupt MMP-2 oscillation, it indicated that MMP-2 oscillation might not be generated from HSF1-induced circadian signaling pathway. Third, temperature cycling-driven clock gene oscillation could not be recorded. As shown in Fig. 2.8, the expression of the clock genes *Per2* and *Cry2* did not show any phase relationship with the temperature cycling and the oscillation of MMP activity, but was affected by changes of serum concentration in the culture medium. Without a synchronized oscillation of clock genes, our results suggested that MMP activity oscillation might not be related to circadian rhythm induced by the peripheral clock inside TM cells. However, the possibility of MMP activity oscillation displaying a circadian rhythm could not be excluded. According to the inflow-outflow link hypothesis (Coca-Prados and Ghosh, 2008), the inflow and outflow of aqueous humor may be regulated by endocrine factors in a synchronized manner. The circadian signals from ciliary body (CB) may be carried by neuropeptides, flowing downstream to reach TM cells. This suggested CB-TM communication in an endocrine microenvironment might provide a means for MMP activity to oscillate in circadian rhythm without a peripheral clock in the TM cells.

On the other hand, there was a general increase in both MMP-9 and MMP-2 activity with time. This increase could be due to cell proliferation. As a result, more MMP molecules were secreted because of an increased number of cells. In fact, an increase in cell density with time was observed in all experimental sets, although the cells remained in a monolayer and their morphological appearance had not changed throughout the experiments. Ideally, cell numbers should be counted each time when the medium samples were collected. However, it was not practical as disturbance to the cells should be kept minimal. A compromised procedure was to

count the cell number at the end of the experiments, but we have not done it in our study.

2.4.4 MMP regulation by temperature

In rat's brain, it was reported that the expression of MMP-9 decreased under hypothermia at 33°C (Zhao et al., 2013). This result was in agreement with our findings that lowering temperature reduced MMP-9 intensity. Other studies have investigated the effect of temperature or cooling agents on MMP-2 and MMP-9 activity, with the experimental temperatures similar to those used in the current study. In rat airway smooth muscle cells, a cooling agent icilin was shown to reverse the FBS-induced up-regulation of MMP-2 activity, which was believed to have occurred through thermoTRP TRPM8/TRPA1 channels (Zhang et al., 2016). The results of lowering temperature leading to lower MMP-2 activity, were in agreement with those of the current study. Nevertheless, for studies where higher temperatures were used, the effects of temperature on MMP-2 and MMP-9 activity were diverse. For example, in human hepatocellular carcinoma cells, the N-myc downstream-regulated gene 2 (NDRG2) was up-regulated when the temperature was increased from 43°C to 45°C (Guo et al., 2013). Also, the expression of MMP-2 and MMP-9 was suppressed when the NDRG2 was overexpressed. These results implied that the expression of MMP-2 and MMP-9 was reduced with temperature increase. In human skin fibroblasts, the expression of MMP-2 was found unchanged with heat shocks at 43°C or 45°C (Park et al., 2004; Lee et al., 2012). This is different from our study where the down-regulation of MMP-2 and MMP-9 was observed at lower temperatures. The reason for the discrepancy was not clear, but the differences in temperature range and cell types used could partially account for

the differences.

Diurnal variation of MMP-9 has been studied in human tears. Markoulli et al (2012) found that the MMP-9 level in tears increased remarkably from 9.8 ng/ml at midday to 2000.7 ng/ml on awakening. Although the concentration of the inhibitor TIMP-1 also increased considerably from 74.5 ng/ml at midday to 277.8 ng/ml on awakening, the overall MMP-9/TIMP-1 ratio, nevertheless, increased by over 40-fold. It suggested that the turnover rate of ECM might increase since there was a relative increase in MMP over its inhibitor. Their results indicated that the MMP-9 activity in tears was much higher at night when the eyelids are closed than during midday. Similar to the TM, the tears are trapped under the eyelid at night and are likely subject to a higher temperature. However, whether the increase in MMP-9 in tears can be applied to TM cells has yet to be elucidated.

The temperature of anterior eye is likely to rise at night due to eyelid closure during sleep. Our results showed an increase in MMP activity at higher temperatures, suggesting a reduced outflow resistance at night, which differed from the clinical observation (Brubaker, 1998). The exact reason for this discrepancy is not apparent. Temperature clearly has the potential to influence various biological responses in the eye including outflow resistance. Since temperature is a universal cue for synchronization of the circadian rhythm, various hormonal signals originating outside the eye may also influence the physiological processes in the eye (Edery, 2010; Buhr and Takahashi, 2013). As we have only examined the activity of secreted MMP-9 and MMP-2 in TM cells, the effects of temperature change on hormonal signals and/or other MMP activity have not been determined. It is likely that the rate of ECM production may be enhanced with temperature increase, and

the production of MMP inhibitors, e.g. TIMPs, can also be increased. Their combined effects may influence the resultant changes in ECM degradation level despite the fact that both MMP-9 and MMP-2 activity increased.

2.4.5 ThermoTRP channels

Although MMP oscillation does not appear to show a circadian rhythm, it can still be a daily rhythm governed by the diurnal temperature oscillation, which involves direct temperature-sensitive channels, such as thermoTRP channels in the signaling pathway. Although all ion channels are temperature-sensitive to certain degrees, thermoTRP channels are the most sensitive ones responsive to temperature changes and are the primary temperature sensors in nerve endings (Clapham, 2003; Voets and Nilius, 2003; Voets et al., 2004; Chowdhury et al., 2014; Qin, 2014). These channels allow cations, such as Ca^{2+}, to pass through when they are open. The thermoTRPs TRPV1, TRPV4 and TRPM8 were suggested to be functioning within physiological relevant temperature (Voets et al., 2004). The heat sensation function of TRPV1 has been verified that the deletion of TRP channels disrupted the heat sensation of mice (Caterina et al., 2000). Mice with TRPM8 knocked out were found to have impaired response to cold and the cooling agent menthol (Dhaka et al., 2007; Liu and Qin, 2011). BCTC is an inhibitor of the human TRPV1 channel with a half maximal inhibitory concentration IC_{50} value of 2.6 ± 1.2 μM. It also inhibits mouse TRPM8 with an IC_{50} value of 0.8 ± 1.0 μM (Behrendt et al., 2004). In the present study, 10 μM of BCTC was used which could inhibit both TRPV1 and TRPM8. In addition, another thermoTRP inhibitor HC 067047, which can inhibit TRPV4 with IC_{50} of 48 ± 6 nM in humans was also used (Everaerts et al., 2010). It does not inhibit other TRPV channels until the concentration reaches

3.2 μM, but can inhibit TRPM8 channels with an IC_{50} value of 780 nM (Everaerts et al., 2010). Concentrations of 1 μM and 10 μM HC 067047 were used in the current study. The former concentration inhibited both TRPV4 and TRPM8, whilst the latter concentration might inhibit other TRPV channels. The results showed that BCTC, but not HC 067047, inhibited MMP activity. It indicated that TRPM8 was not involved in MMP activity and that, the effects of BCTC were mediated primarily by the inhibition of TRPV1, rather than TRPM8. It also suggested that TRPV1 contributed to the MMP activity in the TM cells. However, as neither drug affected the temperature cycling-driven oscillation of MMP-2 and MMP-9 activity, the mechanism of this oscillation is yet to be elucidated.

TRPV1 was shown to contribute to the MMP activity, which might in turn degrade the ECM and reduce outflow resistance. Therefore, it could be a potential target for IOP control. In addition to temperature manipulation, the activity of TRPV1 can be stimulated by pharmacological agents, such as capsaicin (Cordeiro et al., 2010). Such agents may enhance the MMP activity, providing a possible option for altering outflow resistance and IOP in glaucomatous patients.

2.4.6 Further study

The study of temperature effect on the activity of MMPs could be extended to other MMPs and TIMPs by investigating the effects on their expression at gene and protein levels. MMPs have not been a target for clinical anti-glaucoma drugs, but manipulating the activity of MMPs in TM cells may provide a novel and more physiological pathway for managing IOP by reducing outflow resistance in glaucoma patients. The results of this study demonstrated the changes in MMP-9

and MMP-2 activity by physiologically relevant temperature alternation and TRPV1 channel gating. Also, it provides the basis for further investigations. For example, TRPV1 agonist capsaicin can be used to examine the effect on TRPV1 on outflow resistance (Lee et al., 2012). To further evaluate the effect of various downstream heat shock pathways on MMP activity, HIF-1α inhibitor gyceollins, HSP70 inhibitor Pifithrin-μ and HSP90 inhibitor 17-AAG can be used in future studies.

In agreement with our results, a mouse perfusion model has been recently established to study aqueous outflow (Boussommier-Calleja et al., 2015). It was found that there was a 2.5-fold increase in outflow facility when the temperature changed from 20°C to 35°C. This increase was greater than the expected value of 1.4-fold induced by the change of viscosity; therefore, the authors hypothesized that there could be a contribution from a metabolic component to the trabecular outflow driven by a temperature increase. This notion was supported by the use of anti-metabolic drugs that reduced outflow facility (Boussommier-Calleja, 2013). Therefore, it is possible that an increase in temperature causes an increase in MMP activity, eliciting a metabolic alternation that results in an increased ECM turnover. Further investigations are required to establish the relationship between metabolism and the temperature-induced changes of MMPs in TM, facilitating our better understanding of the mechanism of aqueous humor outflow.

Recently, the relationship between MMPs and glaucoma has been extended to the posterior part of the eye. It has been suggested that up-regulation of MMPs, especially MMP-3 (De Groef et al., 2014) and MMP-9 (Zhang et al., 2004; Manabe et al., 2005; Santos et al., 2012), could promote ECM remodeling in the optic nerve

head and induce ganglion cell death in glaucoma. In contrast, the potential roles of MMPs, especially MMP-9 and MMP-2, in neuroprotection and axon regeneration after glaucomatous damage have also been suggested (De Groef et al., 2014). Interestingly, expression of thermoTRP channels was demonstrated in the human retina (Cordeiro et al., 2010). Therefore, manipulation of MMPs via thermoTRPs may offer a new approach to protect the ganglion cells in glaucomatous conditions.

CHAPTER 3 Characterization of gap junctions in the porcine ciliary epithelium

3.1 Introduction

As mentioned in CHAPTER 1, gap junctions provide the conduit for solutes and fluid to flow from pigmented ciliary epithelial (PE) to non-pigmented ciliary epithelial (NPE) layers in the ciliary epithelium (CE). This forms an important step to drive aqueous humor formation (AHF) (Civan, 2008).

3.1.1 Structure and function of gap junctions

Gap junction channels aggregate on the cell plasma membrane. They help exchange ions, metabolites and signaling messengers between adjacent cells and facilitate intercellular communication (Sosinsky, 2000).

The structure of a gap junction is shown in Fig. 3.1. A gap junction channel is composed of two hexagonal hemi-channels called connexons (Sosinsky, 2000). Each connexon is made of 6 connexins (Cxs). Each connexin has its N- and C-termini in the cell cytoplasm. In-between the termini are one cytoplasmic loop, two extracellular loops, and four transmembrane domains. The two extracellular loops and the four transmembrane domains are highly conserved among different connexin isoforms. Conserved polar amino acids, which are distinguished from the other transmembrane domains, have been found in the 3rd transmembrane domain (M3). It has been suggested that this domain may form the inner wall of the pore (Milks et al., 1988). The cells connected with gap junction channels are separated

by a distance of approximately 3.5 nm outside the gap junction area. The inner pore size of a connexon is about 2 nm and the outer diameter about 7 nm (Perkins et al., 1998).

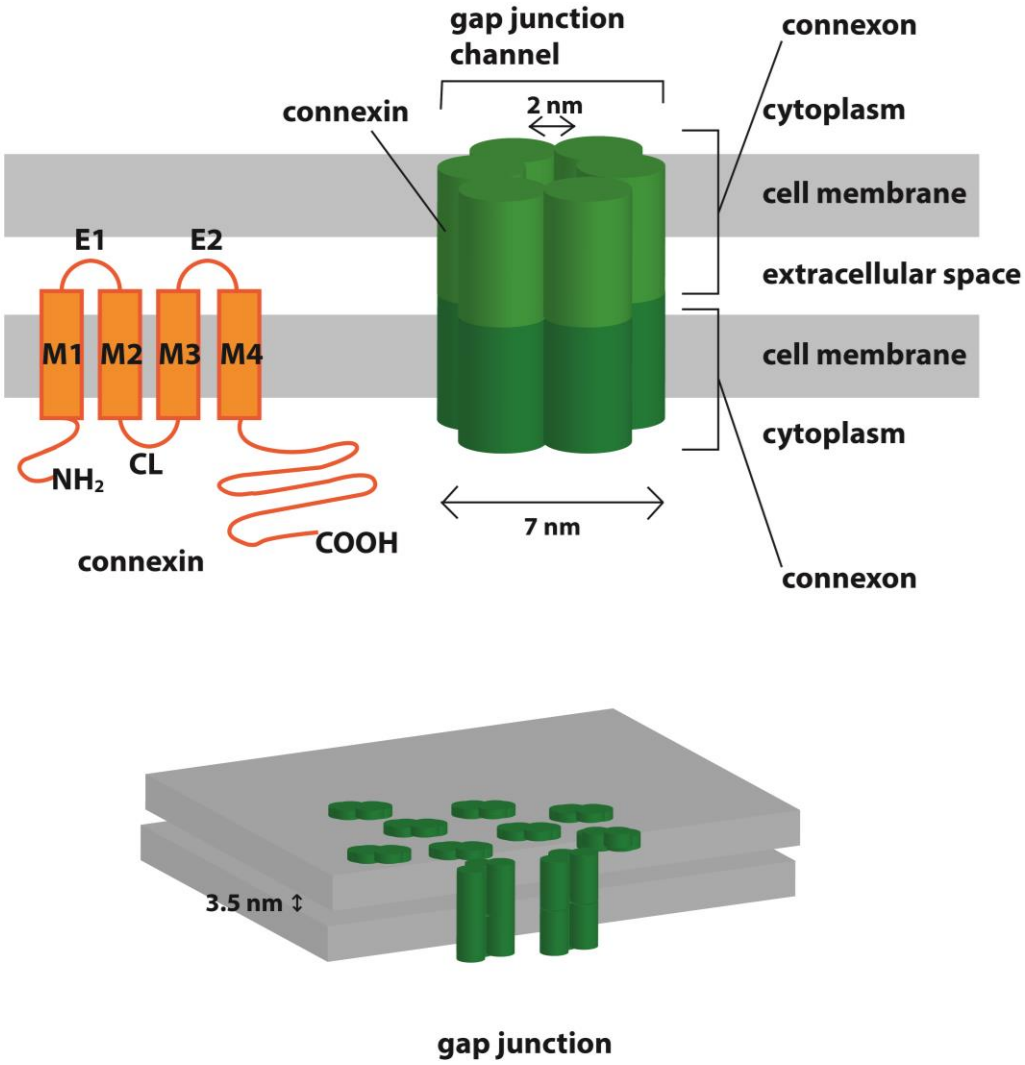

Fig. 3.1 Gap junction structure. E1, E2: extracellular loop 1, 2; M1, M2, M3, M4: transmembrane domain 1, 2, 3, 4; CL: cytoplasmic loop; NH_2: N-terminus; COOH: C-terminus.

Currently, over 20 connexin isoforms have been identified in humans and mice (Beyer and Berthoud, 2009; Hussain, 2014). As the extracellular loops among

different connexins are highly conserved, different connexins can oligomerize to form a connexon and a gap junction channel. When a connexon is composed of the same connexin isoforms, it is called a homomeric connexon; while a heteromeric connexon is composed of different connexin isoforms. When two homomeric connexons comprising the same type of connexin isoform form a gap junction channel, the channel is named homotypic; gap junction channels consisting of more than one type of connexin isoforms are termed heterotypic. Usually, tens to thousands of gap junction channels cluster together and form a gap junction.

A gap junction is responsible for cell-cell communication by synchronizing biological and electrical signals between cells (Hussain, 2014) so that the cells in a tissue can coordinate and function as a whole. As such, PE and NPE cells are connected with gap junctions and the two cell layers function as a syncytium (Krupin and Civan, 1996). Generally, gap junction channels allow molecules of up to 1000 Da to pass through its pore into the coupled cells (Salameh and Dhein, 2005). Electrical signals, including cations and anions, and biological molecules, including glucose, ATP, ADP, cAMP and IP_3, can pass through gap junctions. However, gap junctions composed of different connexins may have different permeability to various molecules (Harris and Locke, 2009). For example, Cx43 gap junctions allow glucose to pass through more readily than Cx32 isoforms.

3.1.2 Gap junctions in the body

Connexins have been found to be widely expressed in different tissues (Hussain, 2014) and are tissue-specific. For example, Cx37 and Cx43 are present in the vasculature (De Wit and Wolfle, 2009), while Cx32 and Cx47 has been identified

in the nervous system (Abrams and Rash, 2009) and Cx26 and Cx30 are expressed in the inner ear (Nickel et al., 2009). Cx43 is the most abundant connexin found in the skeletal system (Civitelli and Donahue, 2009). Genetic mutation of several connexin isoforms has been linked to detrimental diseases. Deafness was found to be related to Cx26 mutation (Severs, 2009). Mutation of Cx40 has been shown to link with atrial fibrillation (Firouzi et al., 2004; Gollob et al., 2006). Mutation of Cx43 leads to oculodentodigital dysplasia in which the characteristic clinical manifestations include small eyes, malformation of the teeth and the 4^{th} and 5^{th} fingers (Hussain, 2014). Additionally, Cx46 mutation is associated with congenital cataract, resulting from Ca^{2+} imbalance in lens fibers (Shakespeare et al., 2009).

3.1.3 Gap junctions in the eye and role of gap junctions in aqueous humor formation

In the crystalline lens, Cx43 and Cx50 have been detected on lens epithelial cells (Shakespeare et al., 2009). It has been shown that Cx43 protein is physiologically down-regulated as the lens reaches maturity and Cx46 was identified within mature lens fiber cells dedicated to Ca^{2+} homeostasis. Cx36 and Cx45 have been identified in the human retina (Massey, 2009; Sohl et al., 2010), where they coupled with photoreceptor cells, amacrine cells and ganglion cells for visual signal processing. Several connexin isoforms such as Cx26, Cx31.1 and Cx43, have also been reported in mammalian corneas (Laux-Fenton et al., 2003; Zhai et al., 2014).

Gap junctions in the CE have been identified in different species. The findings are summarized in Table 3.1:

Table 3.1 Connexins (Cxs) in ciliary epithelium of different animal species

Species	**Cx found**	**Location**
Ox (Coca-Prados et al., 1992)	Cx40 Cx43	NPE (basolateral) PE (basolateral) and PE-NPE interface
Rabbit (Wolosin et al., 1997b)	Cx43 Cx50	PE (apical and lateral) NPE (apical and basolateral)
Rat (Wolosin et al., 1997b; Coffey et al., 2002)	Cx26 Cx31 Cx40 Cx43	NPE (basolateral) NPE (basolateral) PE-NPE interface PE-NPE interface
Mouse (Calera et al., 2006; Calera et al., 2009)	Cx43	PE-NPE interface

Despite the distribution of various connexin isoforms identified in the CE of different species, the functional significance of these connexin isoforms in facilitating aqueous humor secretion has not been clearly established. Previous studies have demonstrated the significance of gap junctions in aqueous humor secretion (Do and To, 2000; Kong et al., 2006; Law et al., 2009; Wang et al., 2010). A non-specific gap junction blocker heptanol has been shown to reduce the short-circuit current (Isc) across the CE by approximately 70-80% in rabbits (Wolosin et al., 1997a), oxen (Do and To, 2000) and pigs (Kong et al., 2006). Heptanol is also found to inhibit the transepithelial fluid transport across porcine CE by 80% (Law et al., 2009). In bovine eyes, down-regulation of a gap junction protein reduced the fluid flow from PE to NPE cells by 60% (Wang et al., 2010). In addition, inactivation of a gap junction protein in mouse NPE cells has been shown to reduce

IOP (Calera et al., 2009), supporting its potential significance in glaucoma management.

3.1.4 Aims of the study

As highlighted above, gap junctions provide the major conduits for solutes and fluid transport from PE to NPE cells. It has been demonstrated that the administration of non-selective gap junction blocker significantly reduced the Isc and transepithelial Cl^- secretion across CE (Do and To, 2000; Kong et al., 2006; Law et al., 2009). Down-regulation of gap junctions has been shown to significantly reduce the fluid flow in isolated bovine PE-NPE cell couplets (Wang et al., 2010) and IOP in mouse (Calera et al., 2009). Previous biochemical and structural studies have identified the distribution of different connexins in different species (Coca-Prados et al., 1992; Wolosin et al., 1997b; Coffey et al., 2002; Calera et al., 2006; Calera et al., 2009). However, the relative abundance of these connexins and their functional significance related to aqueous humor formation (AHF) has not been investigated.

Porcine eyes are considered good models for studying AHF because of its similarities to the human eyes, such as the physical size, anatomical characteristics, electrolyte composition of the aqueous humor, as well as biocompatibility to human eyes (Beauchemin, 1974; Simoens et al., 1992; Shahidullah et al., 2005; Kong et al., 2006; Law et al., 2009). In this study, we aimed to: 1) characterize the connexin expression in porcine CE using molecular approaches; 2) determine the relative abundance of various connexins; and 3) investigate the functional significance of the most abundant connexin in mediating fluid movement from PE to NPE cells using Lucifer yellow (LY) dye transfer.

3.2 Materials and methods

3.2.1 Tissue isolation and cell culture

3.2.1.1 Porcine eye collection

Fresh porcine eyes were obtained from a local slaughterhouse. They were collected immediately after exsanguination of the pigs slaughtered for food consumption. Only the eyes satisfying the following criteria were used for experiments: 1) the eyeballs were intact without leakage of aqueous or vitreous humor; 2) the corneas, aqueous humor and crystalline lenses were clear; 3) the external ocular structures, irides and ciliary bodies were free from abnormality. The selected eyes were stored in an ice-cooled box and carried to the laboratory immediately, with the transportation time of less than 1 hour. The eyes were dissected once they were transported to the laboratory.

3.2.1.2 Ciliary body epithelium isolation

The extra-ocular connective tissues, muscles and ocular adnexa were carefully removed. The cornea was removed circumferentially by razor and the iris was excised using a pair of fine scissors. The exposed ciliary body epithelium (CBE) was cut into small pieces and collected in a microcentrifugation tube filled with phosphate-buffered saline (PBS; Affymetrix, Cleveland, OH, USA). They were then rinsed three times with PBS to remove blood and other exfoliated tissues. These CBE preparations were used for RT-PCR, Western blot (WB) and qPCR.

3.2.1.3 Ciliary epithelial cell culture

Trypsin 0.25% (Gibco, Grand Island, NY, USA) was added to the isolated CBE preparations and the mixture incubated at 37°C in a shaker set at 150 rpm for 30 min. The trypsinization was stopped by adding an equal volume of high-glucose Dulbecco's Modified Eagle Medium (DMEM; Gibco, Grand Island, NY, USA) supplemented with 1% Penicillin-Streptomycin (PS; Gibco, Grand Island, NY, USA) and 10% fetal bovine serum (FBS; Gibco, Grand Island, NY, USA). Trituration was performed to aid cell isolation. The suspension was then passed through a 40 μm nylon cell strainer (Falcon, Corning, NT, USA) and the eluate centrifuged at 1,500 rpm for 5 min. The supernatant was discarded and the pellet retained. The cells were twice re-suspended with culture medium, centrifuged at 1,500 rpm for 5 min with subsequent removal of supernatant. The cell number was counted by hematocytometry and 1.2 x 10^5 cells were transferred to each well of a 4-well plate and cultured at 37°C in a 5% CO_2 humidified incubator overnight.

3.2.1.4 Ciliary body epithelium isolation for histochemistry

Following removal of the extraocular connective tissues, muscles and fatty tissues of a porcine eye, two perpendicular incisions starting at the limbus to the equator of the eyeball were made with a sharp razor blade and the central cornea removed. The remaining peripheral cornea was lifted with forceps so as to expose the anterior chamber angle underneath. The iris base and choroid were then separated from the sclera using a pair of fine scissors to cut along the trabecular meshwork and then down to the equator. The separated sclera was flipped over, and the CBE segment were isolated with minimal vitreous attached. The segment was then transferred to

a 50 ml test tube containing PBS.

3.2.2 RT-PCR and agarose gel electrophoresis

3.2.2.1 Total RNA extraction and quantification

The total RNA of the isolated porcine CE tissue was extracted with TaKaRa MiniBEST Universal RNA Extraction Kit (TaKaRa, Otsu, Shiga, Japan) following the manufacturer's protocol. In brief, lysis Buffer RL was used to lyse the native CE cells. The samples were then centrifuged at 13,200 rpm for 5 min, the supernatant collected, and transferred to gDNA Spin Column and centrifuged at 13,200 rpm for 2 min. The eluate was mixed with 300 µl 70% ethanol and transferred to an RNA Spin Column for 1 min centrifugation at 13,200 rpm. The column was washed with 500 µl Buffer RWA for 1 min centrifugation at 13,200 rpm, followed by washing with 600 µl working Buffer RWB for centrifugation at 13,200 rpm for 1 min and further washing with fresh working Buffer RWB for 2 min. 20 µl RNase-free H_2O was added and the total RNA concentration measured by NanoDrop 2000 Spectrophotometer (Thermo Fisher Scientific, Wilmington, DE, USA).

3.2.2.2 Reverse transcription

Reverse transcription of mRNA to cDNA was performed using High Capacity cDNA Reverse Transcription Kit (Applied Biosystems, Foster City, CA, USA). Each 20 µl reaction mixture contained 2.0 µl 10X RT Buffer, 0.8 µl 25X dNTP,

2.0 µl 10X RT random primers, 1.0 µl Reverse Transcriptase (50 U), 1.0 µl RNase Inhibitor and 1.0 µg mRNA. The mixture was heated to 25°C for 10 min, followed by 37°C for 120 min, and a final 5 min at 85°C.

3.2.2.3 Primer design

The primers used are listed in Table 3.2. The inclusion criteria of the connexin isoforms for screening were as follows: 1) isoforms already reported to be present in the pig; 2) isoforms already identified in the CE of other species; 3) isoforms co-exist in humans, rats and mice, as they are considered to be more likely to express in pigs. If the primers were reported in the literature, they were adopted in the study. If the mRNA sequence of the connexin isoform was available in the database of the National Center for Biotechnology Information (NCBI, http://www.ncbi.nlm.nih.gov), the primers were designed using primer-BLAST online tool. If the mRNA sequence was not yet available for the pig, the sequences of that isoform in human, rat and mouse were compared and the common sequences were used to design the primers. Connexin isoforms showing positive PCR results were shortlisted for further investigation.

Table 3.2 RT-PCR primers for characterization of connexins (Cxs)

target gene	Cx primer code	forward strand (5'-3')	reverse strand (5'-3')	band size (bp)
GJB2	Cx26-1	CGGAAGTTCATGAAGGGAGAGAT	GGTCTTTTGGACTTCCCTGAGCA	399
	Cx26-M	CAGCATCTTCTTCCGGGTCATCTT	AGCAGGATGCAAATTCCAGACAC	201
GJB4	Cx30.3-1	GTGGTCTTCATCTTCCGGGT	GATAGGCCACATGCATGACC	214
	Cx30.3-2	CACGTCCACGTGAGGCACC	AGAGGCGCACGTGGGACACGG	263
GJB3	Cx31-1	CCTGCAGCTCATCTTCGTC	ATGATGAGCTTGAAGATGAG	169
	Cx31-q2	GGGCTCCAACCTTCACTTCA	ACTTGTTCACACCGCTCAGT	112
	Cx31-q3	GGAGTGTGTCAGGTGGAAGC	ACCTGGTGGGAGTTCACAAG	103
	Cx31-q4	GCCCACGGAGAAGAAAGTCT	GCCTCGCATAATCCTGTGGA	112
	Cx31-q5	TTCTACACACGCTCTGGCAT	CCGAGCGATGTAGCAATCCA	98
	Cx31-q6	CCACCAATGCCCCCATTCC	GCGCTGACTAGGGAACAGC	73
GJB1	Cx32-1	GGCTGTAAAAATGTCTGCTATGAC	GCAGGCTGAGCATCGGTC	647
	Cx32-2	CTGCTCTACCCGGGCTATGC	CAGGCTGAGCATCGGTCGCTCTT	386
	Cx32-3	ATCTCAGGGACACTGTGGTG	CTCAGCAGCTTGTTGATCTC	379
	Cx32-L	AAGGGCAAGCAGCAGCCAGA	GCGGCCAGCATGAAGACGGT	756
	Cx32-4	ATCCCTTCCTCTTCCCTCCC	AGAGGCCTTGGGGACTAGAG	357
	Cx32-5	TTTCCCCATCTCCCATGTGC	GGGAGGGAAGAGGAAGGGAT	908
GJA4	Cx37(B)	GACTGGGGCTTCCTGGAGAAG	GCCACCGAGATCTTGGCCATC	413
GJA5	Cx40-1	ATGCACACKGTGCGCATGCAGGA	CAGGTGGTAGAGTTCAGCCAG	399
GJA1	Cx43-3	AGGCGTGCCTACTTCACTTC	AAAGGACTGACAGCCACACC	138
GJC1	Cx45-S1	GGTGTGACAGGCCTTTGCCTACTG	AGGTCCGCGGGGAGGGTCTC	296
GJC2	Cx47-q1	GCCTGGACTCAGCTCTCTTG	CACAAGAACCACCACCCAGA	121
GJA8	Cx50-q5	GCCTCTTTCGTGCCCTAGAA	CTGCCACAGTCGTGGTGTAA	75
GJA10	Cx60-1	GCACTTTATAGACTCAGGGCCTTTG	AGCAGACATCCTTTCAGAGGGAC	176
GAPDH	GAPDH-1	CTGAGACACGATGGTGAAGG	CAAGCAGTTGGTGGTACAGG	475
	GAPDH-2	GACCAGGTTGTGTCCTGTGA	TGAGCTTGACGAAGTGGTCG	97

3.2.2.4 Polymerase chain reaction (PCR)

HotStarTaq Plus Master mix kit (Qiagen, Germantown, MD, USA) was used according to the manufacturer's instruction. Each 10 µl reaction mixture contained 0.5 U HotStarTaq Plus DNA Polymerase, 1X PCR buffer, 1.5 mM $MgCl_2$, 200 µM of each dNTP, 0.5 µM of each forward and reverse primer (Invitrogen, Hong Kong) and 0.25 µg template DNA. For no template control (NTC), template DNA was replaced by the same volume of H_2O. *GAPDH* gene was used as an internal control. The thermal cycling was performed as follow: 1) 5 min initial denaturation at 95°C; 2) 40 cycles of 30 sec denaturation at 94°C, 30 sec annealing at 55°C to 65°C and 1 min extension at 72°C; and 3) 5 min final extension at 72°C.

3.2.2.5 Agarose gel electrophoresis

Agarose was dissolved in TBE buffer [89 mM Tris, 89 mM boric acid, 2 mM ethylenediaminetetraacetic acid (EDTA)] to form 1.0% to 2.0% agarose gel with incorporation of 1X Gel Red (Biotium, Hayward, CA, USA) as a staining agent. The PCR products were mixed with 6X DNA loading dye (Thermo Scientific, Rockford, IL, USA) and GeneRuler 100bp DNA ladder (Thermo Scientific, Rockford, IL, USA) was used as the DNA marker.

Electrophoresis was conducted in the TBE buffer at 60 V for 60 to 90 min, depending on the product sizes and agarose concentrations. The separated PCR products were visualized and photographed under UV light by ChemiDoc XRS System (BioRad, Hercules, CA, USA).

3.2.3 Quantitative RT-PCR (qPCR)

Quantitative RT-PCR (qPCR) was conducted to quantify the relative abundance of the connexin isoform mRNAs in porcine CE. RNA extraction, quantification and reverse transcription were performed as described in Section 3.2.2.

The primers used for qPCR are listed in Table 3.3. They were designed by primer-BLAST online tool available on the website of the National Center for Biotechnology Information (NCBI, http://www.ncbi.nlm.nih.gov). Some of the primers were redesigned and differed from those used for RT-PCR due to qPCR optimization.

Fast SYBR® Green Master Mix (Applied Biosystems, Foster City, CA, USA) was used for amplification and detection. Each 10 µl reaction mixture contained 5 µl of the Master Mix (containing SYBR® Green I Dye, AmpliTaq® Fast DNA Polymerase, Uracil-DNA Glycosylase (UDG), ROX™ dye Passive Reference, dNTPs and optimized buffer components), 0.5 µM of each forward and reverse primer (Invitrogen, Hong Kong) and 0.125 µg template DNA. For no template control (NTC), template DNA was replaced by the same volume of H_2O. Triplication for each biological sample was done to ensure repeatability and averaging of results. The thermal cycles were as follow: 1) 2 min UDG treatment step at 50°C; 2) 10 min denaturing step at 95°C; 3) 40 cycles of 15 sec denaturation step at 95°C and 1 min annealing and extension step at 60°C; and 4) a dissociation stage. The signal was recorded by Applied Biosystems 7500 Fast Real-Time PCR System together with SDS software (Applied Biosystems, Waltham, MA, USA).

ΔΔCt method was used to calculate the relative mRNA expression of the connexins in the native porcine CE. *GAPDH* gene was used as the reference gene for the

calculation. Dissociation-curve and subsequent agarose gel analyses were performed to ensure that no non-specific product was formed during the experiment.

Table 3.3 qPCR primers for quantification of connexins (Cxs)

target gene	**corresponding protein**	**forward strand (5'-3')**	**reverse strand (5'-3')**	**band size (bp)**
GJA1	Cx43	AGGCGTGCCTACTTCACTTC	AAAGGACTGACAGCCACACC	138
GJC1	Cx45	TGACAGGCCTTTGCCTACTG	GCGAGTCTCGAATTGTCCCA	72
GJC2	Cx47	GCCTGGACTCAGCTCTCTTG	CACAAGAACCACCACCCAGA	121
GJA8	Cx50	GCCTCTTTCGTGCCCTAGAA	CTGCCACAGTCGTGGTGTAA	75
GJA10	Cx60	GCACTTTATAGACTCAGGGCCTTTG	AGCAGACATCCTTTCAGAGGGAC	176
GAPDH	Glyceraldehyde 3-phosphate dehydrogenase	GACCAGGTTGTGTCCTGTGA	TGAGCTTGACGAAGTGGTCG	97

3.2.4 Western blot

3.2.4.1 Protein extraction for qualitative analysis

The protein lysis buffer used was RIPA-cOmplete buffer (Abcam, Cambridge, MA, USA), containing 0.22% β-glycerophosphate, 10% Tergitol®-NP40, 0.18% sodium orthovanadate, 5% sodium deoxycholate, 0.38% (ethylene glycol-bis(β-aminoethyl ether)-N,N,N',N'-tetraacetic acid (EGTA), 1% sodium dodecyl sulfate (SDS), 6.1% Tris, 0.29% ethylenediaminetetraacetic acid (EDTA), 8.8% sodium chloride and 1.12% sodium pyrophosphate decahydrate, with addition of one tablet of cOmplete ULTRA Tablets, Mini, EASYpack (Roche, Mannheim, Germany) dissolved in its

10 ml preparation mix for protease inhibition. The preparation was then homogenized by sonication. Subsequently, it was incubated on ice for an hour and centrifuged at 4°C at 13,200 rpm for 30 min. The supernatant was collected and the pellet was discarded.

3.2.4.2 Protein quantification

The concentrations of protein samples were measured with Protein Assay Dye Reagent Concentrate (Bio-Rad, Hercules, CA, USA) using the Bradford principle. The extracted protein was diluted in water at a ratio of 1:5 or 1:10 to give a 20 µl solution, and was then mixed with 1 ml diluted assay solution. The mixed solution was incubated at room temperature for 5 min. The samples were then loaded into a 96-well microplate in triplication and the absorbance measured with a microplate reader (Model 680, Bio-Rad, Hercules, CA, USA) at 595 nm. The protein concentration of the samples was obtained by comparing the absorbance of the samples to that of the standards with known protein concentrations.

3.2.4.3 Sodium dodecyl sulfate-polyacrylamide gel electrophoresis (SDS-PAGE)

The samples were mixed with β-mercaptoethanol and Laemmli Sample Buffer (BioRad, Hercules, CA, USA). Depending on the connexin isoforms, the samples were heated at various temperatures between 37°C to 100°C for 5 min and then loaded into 8% to 12% polyacrylamide gel [8% to 12% acrylamide, 0.21% to 0.26% bisacrylamide, 120 µM HCl, 375 mM Tris, 0.058% tetramethylethylenediamine (TEMED), 3.5 mM sodium dodecyl sulfate (SDS), 5.3 mM ammonium persulfate]

for electrophoresis. PageRuler Retained Protein Ladder (Thermo Scientific, Waltham, MA, USA) was used to determine the size of the proteins. Electrophoresis was performed at 70V to 90V for 120 to 180 min in SDS-PAGE buffer (Tris 25 mM, glycine 192 mM, SDS 3.5 mM) with Mini-Protean II Cell Gel System (Bio-Rad, Hercules, CA, USA).

3.2.4.4 Protein transfer and blocking

After PAGE, the separated proteins were electroblotted to a polyvinylidene difluoride (PVDF) membrane (BioRad, Hercules, CA, USA) with Mini Trans-Blot® Electrophoretic Transfer Cell (BioRad, Hercules, CA, USA). The gel and the membrane were sandwiched in the middle of filter paper and filter pads, and then placed in the cassette of the system. The electroblotting was conducted in transfer buffer (25 mM Tris, 192 mM glycine, 20% methanol, pH 8.3) with an ice-cooling pack at 90V for 90 min. After electroblotting, the non-specific background bindings were blocked using blocking buffer [5% non-fat dry milk Blotto (Santa Cruz Biotechnology, Dallas, TX, USA) and TBST (0.1 M Tris-HCl, pH 8.0, 0.5M NaCl, 0.05% Tween-20)] for 1 hour at room temperature.

3.2.4.5 Antibody probing and imaging

The blocking buffer was decanted off and the membrane incubated in primary antibody diluted in 5% Blotto TBST at 4°C overnight. It was then washed three times with TBST for 10 min. The membrane was incubated in a corresponding horseradish peroxidase-conjugated secondary antibody, diluted in 5% Blotto TBST, at room temperature for 1 hour. It was then washed three times with TBST for 10

min each. Table 3.4 and Table 3.5 list the primary and secondary antibodies used in the study, respectively.

Table 3.4 Primary antibodies for characterization of connexins (Cxs)

target protein	**dilution**	**clonality**	**species**	**manufacturer**
GAPDH	1:8000	monoclonal	mouse	Calbiochem, San Diego, CA, USA
Cx37	1:500	polyclonal	rabbit	Abcam, Cambridge, MA, USA
Cx43	1:400	polyclonal	rabbit	Cell Signaling, Danvers, MA, USA
Cx45	1:1000	polyclonal	goat	Santa Cruz Biotechnology, Dallas, TX, USA
Cx47	1:500	monoclonal	mouse	Abgent, San Diego, CA, USA
Cx50	2 μg/ml	monoclonal	mouse	Invitrogen, Camarillo, CA, USA
Cx60	1:250	polyclonal	goat	Santa Cruz Biotechnology, Dallas, TX, USA

Table 3.5 Secondary antibodies for characterization of connexins

target antigen	**dilution**	**clonality**	**species**	**manufacturer**
mouse	1:2000	polyclonal	goat	Zymax, Rockford, IL, USA
rabbit	1:2000	polyclonal	goat	Invitrogen, Camarillo, CA, USA
goat	1:2000	polyclonal	rabbit	Invitrogen, Camarillo, CA, USA

SuperSignal™ West Pico Chemiluminescent Substrate (Thermo Fisher Scientific, Waltham, MA, USA) was used to provide the chemiluminescent signal for protein visualization. The peroxide and luminol/enhancer solutions from the kit were mixed in a ratio of 1:1. The PVDF membrane was then incubated in the mixed working solution at room temperature for 5 min. After incubation, the membrane was removed and covered with plastic wrap. The visual light signal was captured using ChemiDoc XRS System (BioRad, Hercules, CA, USA) or Azure c600 (Azure Biosystems, Dublin, CA, USA) detection system's CCD camera. The signal

intensity was analyzed using software Image-J (National Institutes of Health, Bethesda, MD, USA).

3.2.5 Histochemistry

3.2.5.1 Fixation/dehydration/paraffin embedding

The isolated porcine ciliary CBE segments were rinsed twice with PBS and then fixed using fresh 4% paraformaldehyde (PFA; Sigma-Aldrich St. Louis, MO, USA)/PBS at 4°C for 20 hours. The segments were dehydrated in increasing concentrations of ethanol from 70% to 100%. Next, the segments were immersed three times in xylene (Anaqua Co., Ltd, Hong Kong) for 15 min each, followed by two-time immersions in melting paraffin at 65°C for 1 hour each and a final immersion for 2 hours. Next, the segments were embedded in paraffin and were stored at 4°C overnight before sectioning.

3.2.5.2 Sectioning

The tissue blocks were sliced into 10 μm thick sections using a microtome (Model HM 310, Microm, Ramsey, MN, USA) at a cutting angle of 5°. The sections were mounted onto positively charged adhesion slides (Menzel Gläser, SuperFrost® Plus, Thermo Scientific, Braunschweig, Germany) and were then air-dried overnight at room temperature.

3.2.5.3 Deparaffinization/rehydration

After drying, the slides were heated in a 60°C oven for 30 min to melt the paraffin wax. They were then immersed twice in fresh xylene for 10 min followed by rehydration in decreasing concentrations of ethanol from 100% to 70%. Afterwards, the slides were rinsed with water.

3.2.5.4 Immunofluorescence

The hydrated sections on the slides were permeated with PBS plus 0.1% Triton X-100 (Bio-rad, Hercules, CA, USA) for 10 min. The sections were washed three times with PBS for 5 min. To block the reaction of endogenous peroxidases and reduce the background noise, the sections were then immersed in 3% H_2O_2 (Sigma-Aldrich, St. Louis, MO, USA)/methanol (Anaqua Co., Ltd, Hong Kong). The antigens on the sections were blocked with 5% normal goat serum (Vector Laboratories, Burlingame, CA, USA)/PBS for 1 hour. Next, the sections were incubated with diluted primary antibody against Cx43 (1:100; Cell Signaling, Danvers, MA, USA) at 4°C overnight. For negative controls, the primary antibody was replaced with 5% normal goat serum. On the following day, specimens were washed three times with PBST [PBS plus 0.05% Tween-20 (USB corporation, Cleveland, OH, USA)] for 10 min each. They were then incubated with FITC-conjugated secondary antibody (anti-rabbit in 1:100 dilution, Thermo Scientific, Rockford, IL, USA) at room temperature for 1 hour in the dark. On completion, they were washed three times with PBST for 5 min in the dark. The slides were mounted with VECTASHIELD Antifade Mounting Medium (Vector Laboratories, Burlingame, CA, USA) and a cover slip for microscopy. An inverted microscope

system Model Eclipse Ti-S (Nikon, Otawara, Tochigi, Japan) with an excitation filter (465 – 495 nm) and a digital camera (SPOT idea CMOS 5.0MP; Diagnostic Instruments Inc, Sterling Heights, MI, USA) were used for imaging.

3.2.5.5 Hematoxylin and eosin staining

The hydrated CBE sections described in Section 3.2.5.3 were stained with hematoxylin solution, Gill No. 1 (Sigma-Aldrich St. Louis, MO, USA). The stained nuclei were differentiated from the background by washing with 0.3% acid alcohol (0.5% HCl in 70% ethanol). The staining was enhanced with a wash of Scott's tap water substitute (Sigma-Aldrich, St. Louis, MO, USA). The tissues were then stained with eosin Y solution, alcoholic (Sigma-Aldrich, St. Louis, MO, USA). The tissues were dehydrated again by immersing in a sequence of increasing concentrations of ethanol from 80% to 100%. After that, the slides were immersed three times in xylene for 15 min each. The slides were then mounted with a cover slip and Richard-Allan Scientific™ Mounting Medium (ThermoFisher, Fair Lawn, NJ, USA). Finally, the stained tissues were visualized and photographed by an inverted microscope system Model Eclipse Ti-S (Nikon, Otawara, Tochigi, Japan) and a digital camera (SPOT idea CMOS 5.0MP; Diagnostic Instruments Inc, Sterling Heights, MI, USA).

3.2.6 siRNA knockdown

3.2.6.1 siRNA transfection

The porcine CE cells were cultured on a 4-well plate, with 1.2 x 10^5 cells in each well. Cells were incubated with 500 µl complete culture DMEM (1% PS 10% FBS) in a humidified 5% CO_2 incubator at 37°C before siRNA transfection. Prior to transfection, the culture medium was replaced with 400 µl fresh medium. The siRNA sequence was purchased from Molecular Informatrix Laboratory (Hong Kong) for Cx43 knockdown; another non-targeting siRNA sequence was purchased as control. The sequences used are listed in Table 3.6. For the dye transfer experiment, FAM-labeled sequences were used. The labels were at the 5' end of the forward strands.

Table 3.6 siRNA sequences for connexin 43 down-regulation

siRNA name	**target gene**	**Cx protein**	**forward strand (5'-3')**	**reverse strand (5'-3')**
siCx43	*GJA1*	Cx43	CUGAUGACCUGGAGAUCUA(dTdT)	UAGAUCUCCAGGUCAUCAG(dTdT)
siScram	Nil	Nil	CCUACGCCACCAAUUUCGU(dTdT)	ACGAAAUUGGUGGCGUAGG(dTdT)

25 pmol siRNA was mixed with 3 µl HiPerfect transfection reagent (Qiagen, Hamburg, Germany) in 100 µl DMEM and the mixture was allowed to settle at room temperature for 20 min to allow the formation of the transfection complex in the medium. The 100 µl transfection medium was added slowly to the cells in the culture plate with gentle swirling to ensure uniform distribution. In each well,

50 nM was used as the final concentration of the siRNA. The cells were incubated in a humidified 5% CO_2 incubator at 37°C for 24 hours before performing other experiments.

3.2.6.2 Western blot

The procedures used for Western blot in this section was similar to those described in Section 3.2.4. The siRNA-treated cells were washed twice with PBS before extraction. 50 µl RIPA-cOmplete buffer was added and carefully mixed in each well of a 4-well plate sample. The lysate from the wells was pooled together in a 1.5 ml microcentrifugation tube for 1-hour sonication. This was followed by one hour of on-ice incubation before 4°C centrifugation at 13,200 rpm for 20 min. The supernatant was collected and the protein concentration measured.

3.2.6.3 Lucifer yellow dye transfer

3.2.6.3.1 Solutions and pharmacological agents

Unless stated otherwise, all the chemicals used were purchased from Sigma-Aldrich (St. Louis, MO, USA). The dye transfer bathing solution was made of (in mM) 113.0 NaCl, 4.56 KCl, 21.0 $NaHCO_3$, 0.6 $MgSO_4$, 7.5 D-Glucose, 1.0 L-Glutathione reduced, 1.0 Na_2HPO_4, 10.0 HEPES and 1.4 $CaCl_2$. Its pH and osmolality were adjusted to 7.4 with NaOH and 300 mOsm/kg with D-mannitol, respectively. The pipette solution was made of (in mM) 25 NaCl, 110 L-aspartic acid, 120 N-Methyl-D-glucamine (NMDG), 0.38 $CaCl_2$, 12 4-(2-hydroxyethyl)-1-

piperazineethanesulfonic acid (HEPES) and 1 mg/ml Lucifer yellow CH, lithium salt (Invitrogen, Camarillo, CA, USA).

3.2.6.3.2 Setup

The micropipette was made of a 1.65/1.1 OD/ID (mm) glass capillary (World Precision Instruments, Sarasota, FL, USA) using a Flaming/Brown micropipette puller Model P-97 (Sutter Instrument, San Raphael, CA, USA). Its tip was finely polished using a microforge (Model MF-830; Narishige, Tokyo, Japan). Micropipettes with resistance ranging from 6 to 11 MΩ were used for the experiments. The micropipette was fixed onto the pipette holder connected with an Ag/AgCl electrode. Piezoelectric micromanipulators (Models PCS-6000; EXFO Burleigh, Victor, NY, USA) were used to control the movement of the micropipettes.

The bottom of the bath imaging chamber (Model RC-15, Warner Instruments, Hamden, CT, USA) was sealed using a greased cover glass (Dow Corning Corporation, Midland, MI, USA). This chamber was perfused with the dye transfer bathing solution (with/without drug) at a rate of 1 ml/min with the aid of a peristaltic pump (Model 505S, Watson-Marlow, Wilmington, MA, USA). The temperatures of the chamber and the bathing solution were maintained at 22°C throughout the experiment with a single channel heater controller (Model TC-324B, Warner Instruments, Hamden, CT, USA). The bridge well was filled with 3 M KCl solution and was connected to the bath imaging chamber via a salt bridge (3% agarose in 3 M KCl). The bath imaging chamber was placed over an inverted microscope system Model Eclipse Ti-S (Nikon, Otawara, Tochigi, Japan) equipped with a

digital camera (SPOT idea CMOS 5.0MP; Diagnostic Instruments Inc, Sterling Heights, MI, USA) and an excitation filter (465 – 495 nm).

The whole-cell voltage and current were measured with a patch clamp amplifier (Axopatch 200B, Molecular Devices, Union City, CA). The analogue signal was converted to digital signal by a digitizer (Digidata 1440A, Molecular Devices, Union City, CA).

3.2.6.3.3 Cell couplets preparation for dye transfer

The siRNA-treated cells were washed twice with PBS and transferred onto a Poly-L-lysine-coated cover glass and replenished with fresh culture medium. They were kept at 37°C in a 5% CO_2 incubator before commencing the assay. The cover glass with the cells was transferred to the bath imaging chamber containing bathing solution.

3.2.6.3.4 Patching and dye transfer

Isolated PE-NPE cell couplets with distinct cell borders were chosen for the experiment. Also, only FAM-labeled couplets were chosen for the siRNA dye transfer experiment to ensure the tested ones were transfected with siRNA. The micropipette tip was slowly directed to the PE cell surface and gentle suction was then applied to form a gigaseal between the micropipette tip and the PE cell. After forming the gigaseal, more suction was applied to rupture the cell membrane to enable the diffusion of Lucifer yellow (LY) dye from the micropipette to the PE (donor) cell, and subsequently to the NPE (recipient) cell. The images were

captured every 30 sec for 30 min starting immediately after the membrane rupture.

3.2.6.3.5 Data analysis

The fluorescent intensity was then obtained using software Image-J (National Institutes of Health, Bethesda, MD, USA). We define F ratio as

$$\text{F ratio} = \frac{\text{fluorescence intensity in NPE}}{\text{fluorescence intensity in PE}}$$

The higher the F ratio, the higher the dye transfer rate from PE to NPE cells. The F ratios at 10 min after membrane rupture were chosen for comparison.

3.2.7 Statistical analysis

All data shown are presented as mean ± SEM. One-way ANOVA was used to analyze the qPCR and dye transfer experimental data and t-test for the other experiments comparing means between two groups. A *p*-value < 0.05 was considered to be statistically significant. The notations of *p*-values in the statistical analysis are shown below:

Symbol	***p*-value**
ns	> 0.05
*	< 0.05
**	< 0.01
***	< 0.001

3.3 Results

3.3.1 The expression of connexin isoforms in porcine ciliary body epithelium

RT-PCR was adopted to screen for the different connexin isoforms in freshly-harvested porcine CBE. Every pair of primers was used on at least three occasions to ensure repeatability. For most of the experiments, at least two independent pairs of primers without overlapping sequences were used, except those that had been reported for the screening of corresponding connexin isoforms successfully in pig (Carter et al., 1996).

Representative pictures of gels for each pair of primers are shown in Fig. 3.2. The code shown at the top of each picture indicates the connexin primer being used. *GAPDH* served as a control. The number at the bottom of each lane indicates the expected band size of the PCR product, if any. No PCR products were detected in NTCs, assuring no DNA contamination in the samples.

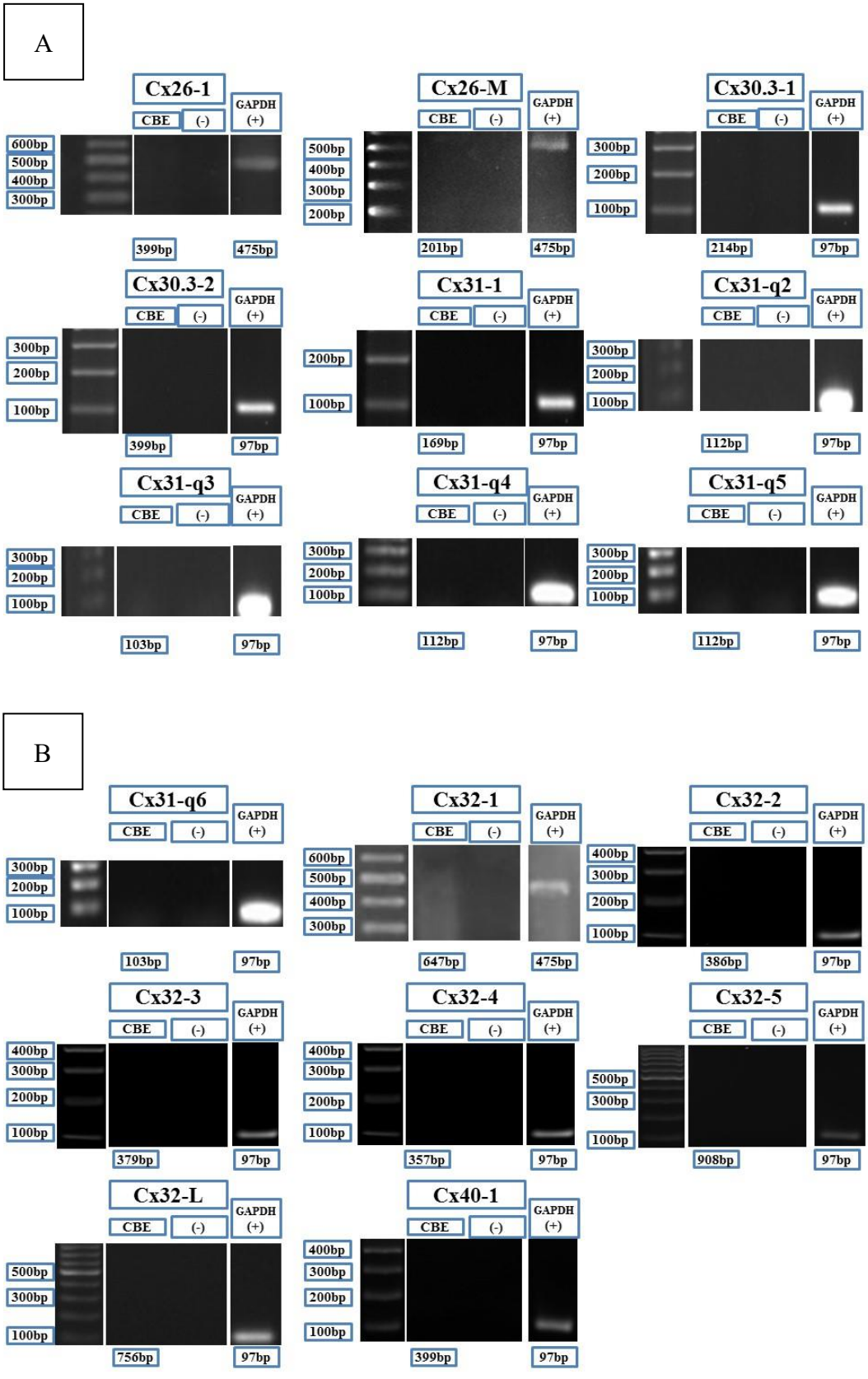
A
Cx26-1
CBE
(-)
GAPDH (+)
600bp
500bp
400bp
300bp
399bp
475bp
Cx26-M
500bp
400bp
300bp
200bp
201bp
475bp
Cx30.3-1
300bp
200bp
100bp
214bp
97bp
Cx30.3-2
399bp
97bp
Cx31-1
200bp
100bp
169bp
97bp
Cx31-q2
112bp
97bp
Cx31-q3
103bp
97bp
Cx31-q4
112bp
97bp
Cx31-q5
112bp
97bp
B
Cx31-q6
103bp
97bp
Cx32-1
647bp
475bp
Cx32-2
386bp
97bp
Cx32-3
379bp
97bp
Cx32-4
357bp
97bp
Cx32-5
500bp
300bp
100bp
908bp
97bp
Cx32-L
756bp
97bp
Cx40-1
399bp
97bp

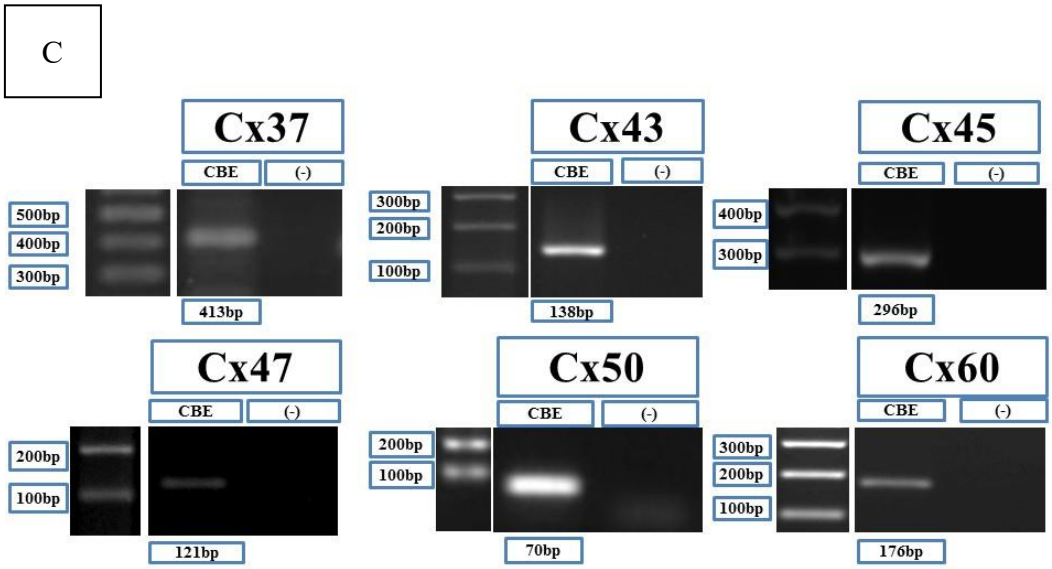

Fig. 3.2 Expression of connexin isoforms in porcine CBE detected by RT-PCR. (A-B) The absence of Cx26, Cx30.3, Cx32 and Cx40 mRNA expression in porcine ciliary body epithelium. (C) The presence of Cx37, Cx43, Cx45, Cx47, Cx50 and Cx60 mRNA expression in porcine ciliary body epithelium. The code (e.g. Cx26-1) shown at the top of each picture indicates the pair of connexin primer being used (For Fig. C, the names of the connexins are used instead of the codes). Symbol "CBE" in the 1st lane indicates the sample being investigated; the symbol (-) in the 2nd lane indicates the no template negative control (NTC); GAPDH (+) in the last lane serves as a control using GAPDH primers. The expected band size of each PCR product is shown at the bottom of the "CBE" lane. At least 3 biological repeats were performed for each pair of primers.

Despite various pairs of primers used, Cx26, Cx30.3, Cx32 and Cx40 were not identified in fresh porcine ciliary body epithelium (Fig. 3.2 A and B). On the other hand, the presence of Cx37, Cx43, Cx45, Cx47, Cx50 and Cx60 were shown (Fig. 3.2C). All the band sizes shown in the samples agreed with the expected band sizes, suggesting that the primers are specific for the genes of interest. The differences in the intensities in Fig. 3.2C do not fully reflect the relative quantity of the connexins, because different exposure time and imaging machines were adopted.

After screening by RT-PCR, the protein expression of those identified connexin isoforms (i.e. Cx37, Cx43, Cx45, Cx47, Cx50 and Cx60) was determined by WB (Fig. 3.3). Our results demonstrated that Cx43, Cx45, Cx47, Cx50 and Cx60 were expressed in native porcine CBE. The band sizes corresponded to those shown in the positive control. Interestingly, Cx37 was identified at mRNA level by RT-PCR, but not detected at protein level by WB.

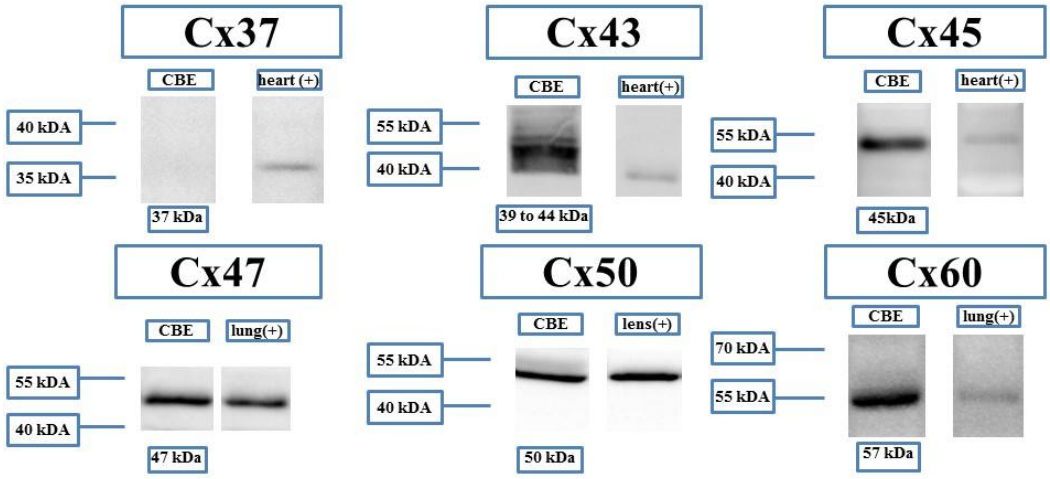

Fig. 3.3 Expression of connexin isoforms in porcine CBE detected by Western blot (WB). Cx43, Cx45, Cx47, Cx50, Cx60 were identified. Cx37 was not detected. The symbol "CBE" represents the lane loaded with ciliary body epithelium sample. The next lane shows the positive control with the label indicating the tissue being used. The expected band size is showed at the bottom of each CBE lane. At least 3 biological repeats were performed for each connexin.

3.3.2 Relative expression and distribution of connexin isoforms

Quantitative RT-PCR (qPCR) was used to investigate the relative expression of the connexin isoforms. The results are shown in Fig. 3.4. In freshly harvested porcine

CBE, the gene expression of Cx43 was found over 200-fold higher than all the other connexin isoforms observed (N = 6, $p < 0.001$, one-way ANOVA). The second most expressed connexin isoform was Cx45, but its expression level was only 0.4% of Cx43's. The expression levels of other connexins were < 0.2% of that of Cx43.

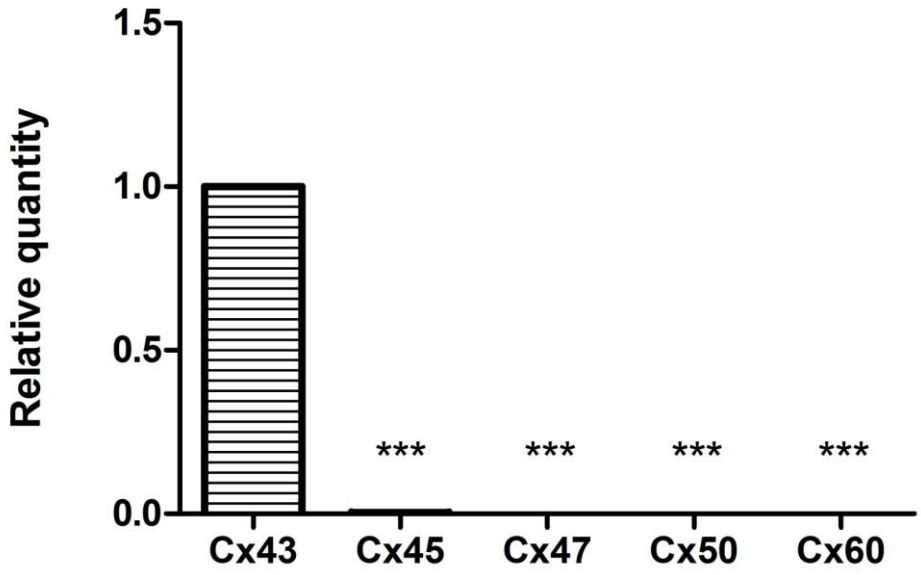

Fig. 3.4 Relative quantity of connexins in fresh porcine CBE by qPCR. The expression of Cx43 was found over 200-fold more than all other connexins. (N = 6, ***: $p < 0.001$, one-way ANOVA, compared to Cx43).

As Cx43 was found to be the most abundant connexin in porcine CBE, its cellular expression in the tissue was studied by immunohistological analysis. As shown in Fig. 3.5A, B and C, Cx43 was primarily localized at the apical surface linking PE and NPE cells. In addition, some Cx43 was detected near the basolateral membrane of PE cells. As shown in Fig. 3.6, primary antibody was omitted from the incubation process in negative controls, which showed no fluorescent stains. Our results

supported the notion that Cx43 is the major connexin present in porcine CBE and it may be responsible for the ion and fluid movement between PE and NPE cell layers.

3.3.3 Effect of connexin 43 knockdown on dye transfer

Based on the results of gene and protein expression, we questioned whether Cx43 was important in transferring fluid from PE to NPE in the process of AHF across porcine CE. To test this hypothesis, we used small interfering RNA (siRNA) to knock down the expression of the connexin and determine whether it affected the fluid movement across isolated porcine PE-NPE cell couplets using Lucifer yellow (LY) dye transfer technique.

After 24 hour-transfection with 50 nM siRNA against Cx43 or scrambled siRNA, the relative mRNA expression of connexin in porcine CE cells was determined by qPCR using SYBR technology. As shown in Fig. 3.7, the relative mRNA expression of Cx43 in porcine CE cells were decreased by 59 ± 3% with Cx43-siRNA treatment compared to the cells treated with scrambled siRNA (N = 4, $p < 0.001$, Student's t-test). Similarly, we found by WB that the relative Cx43 protein expression in porcine CE was reduced by 71 ± 13% in the Cx43-siRNA treatment group compared to the scrambled siRNA control group (N = 3, $p < 0.01$, Student's t-test). The results are summarized in Fig. 3.8.

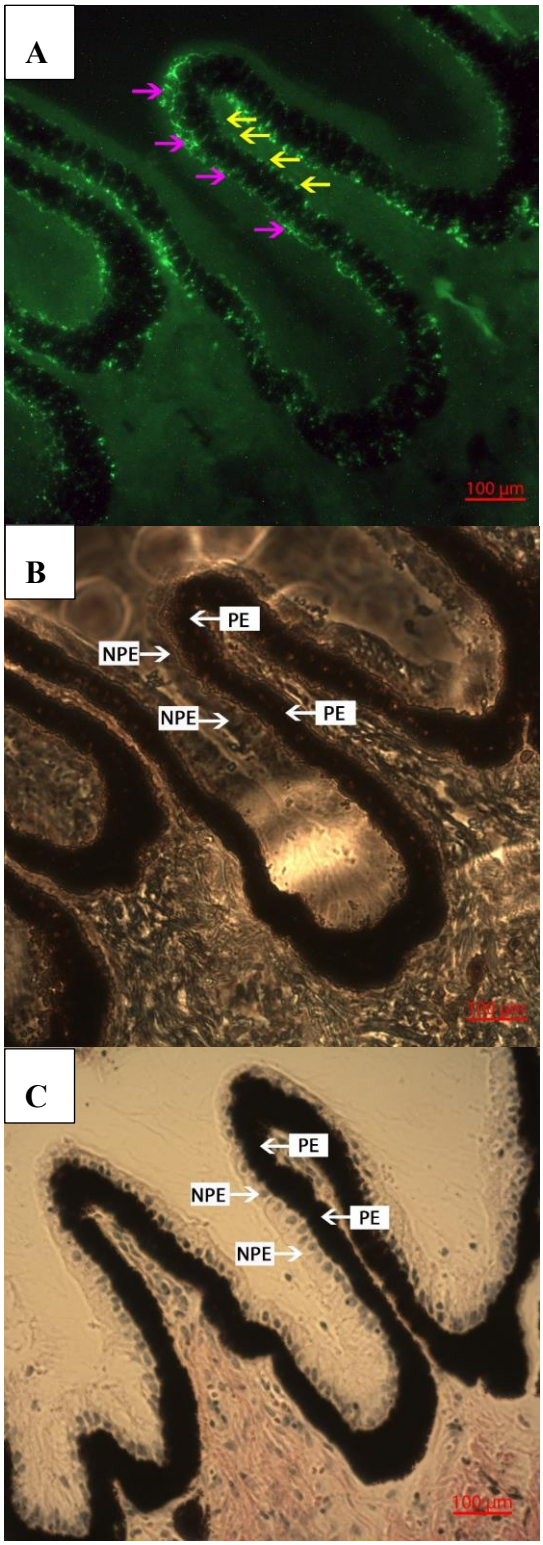

Fig. 3.5 Immunolocalization of Cx43 in porcine CBE. (A) Cx43 was detected at the apical area connecting PE and NPE layers (pink arrows) and at the basolateral side of the PE layers (yellow arrows). (B) The same area of the tissue under bright field. (C) Adjacent part of the same tissue treated with hematoxylin and eosin stain. PE cells and NPE cells are indicated by white arrows.

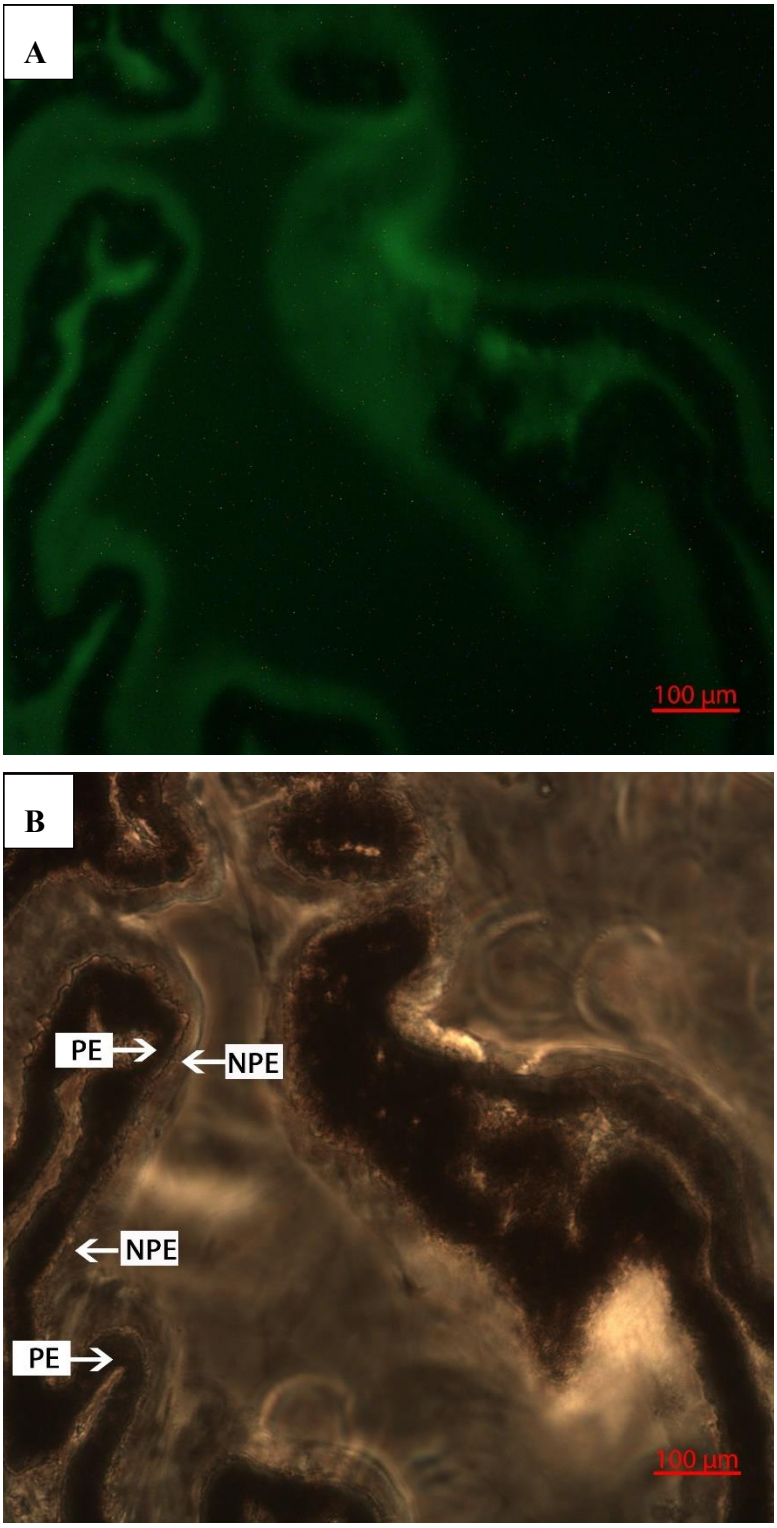

Fig. 3.6 (A) Negative control of immunolocalization of Cx43 in porcine CBE. (B) The same area of the tissue under bright field. PE cells and NPE cells are indicated by white arrows.

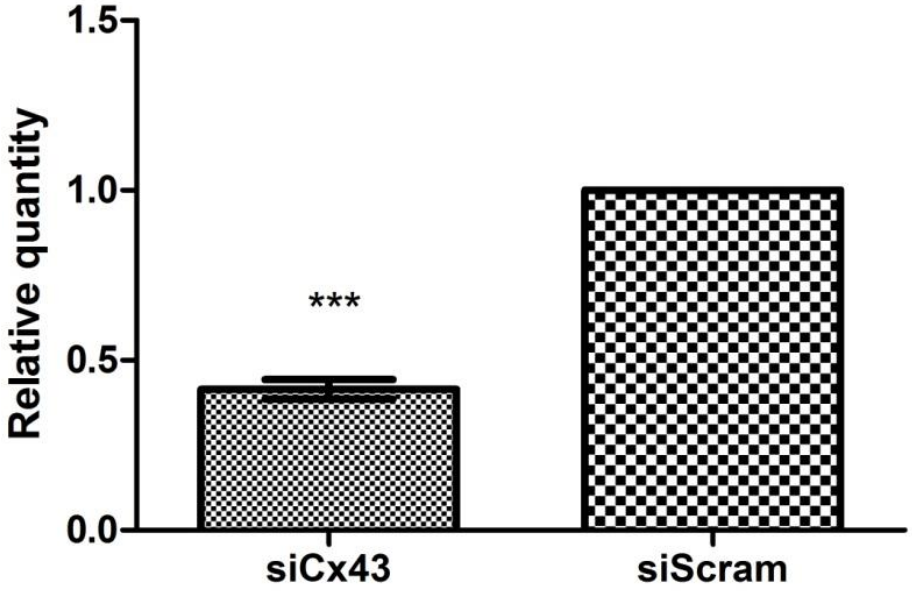

Fig. 3.7 Relative quantity of Cx43 mRNA expression in porcine CE after siRNA treatment by qPCR. After 24-hour transfection, the mRNA expression of Cx43 was reduced by 59 ± 3% (N = 4, ***: $p < 0.001$, Student's t-test). siCx43: porcine CE treated with siRNA against Cx43; siScram: porcine CE with scrambled siRNA treatment.

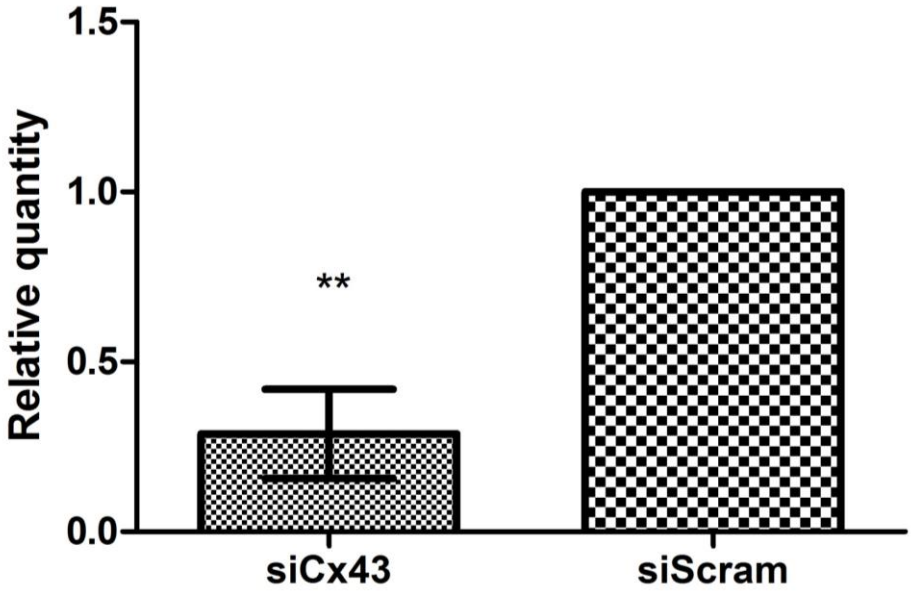

Fig. 3.8 Relative quantity of Cx43 protein expression in porcine CE after siRNA treatment by Western blot (WB). After 24-hour transfection, the protein expression of Cx43 was reduced by 71 ± 13% (N = 3, **: $p < 0.01$, Student's t-test). siCx43: porcine CE treated with siRNA against Cx43; siScram: porcine CE with scrambled siRNA treatment.

For dye transfer experiments, the changes of fluorescence levels in typical isolated porcine PE-NPE cell couplets under control and siRNA-treated conditions are illustrated in Fig. 3.9 and Fig. 3.10, respectively. Fig. 3.11 summarizes the changes in ratios of relative fluorescence intensities of NPE-to-PE (F ratios) under various conditions. For normal PE-NPE cell couplets (norm, N = 10), there was a continuous LY dye diffusion from PE cell to NPE cell, as reflected by the progressive increase in F ratio. An equilibrium reached 10 min after breaking in the plasma membrane. At 10 min, the F ratio was 1.70 ± 0.17. After that, the F ratio remained relatively stable until the end of the experiment. Based on this result, 10 min was chosen as the time point for the F ratio comparison under various conditions.

For couplets treated with non-selective gap junction inhibitor heptanol (3.5 mM, N = 5), the F ratio decreased with time, reaching a steady value by 10 min (Fig. 3.11). At 10 min, the F ratio was found to be 0.16 ± 0.04 and remained low afterwards. Compared with the normal couplets, heptanol inhibited the F ratio by 90% ($p < 0.01$, Kruskal-Wallis test).

For couplets treated with scrambled siRNA (siScram, N = 7), the change in F ratio was similar to that of normal couplets, as demonstrated in Fig. 3.11. The F ratio was observed to be 1.79 ± 0.32 at 10 min. No statistically significant difference in F ratios was observed between control and siScram-treated groups at all time points ($p > 0.05$, Kruskal-Wallis test). This indicated that the scrambled siRNA did not affect the gap junction permeability of the cell couplets.

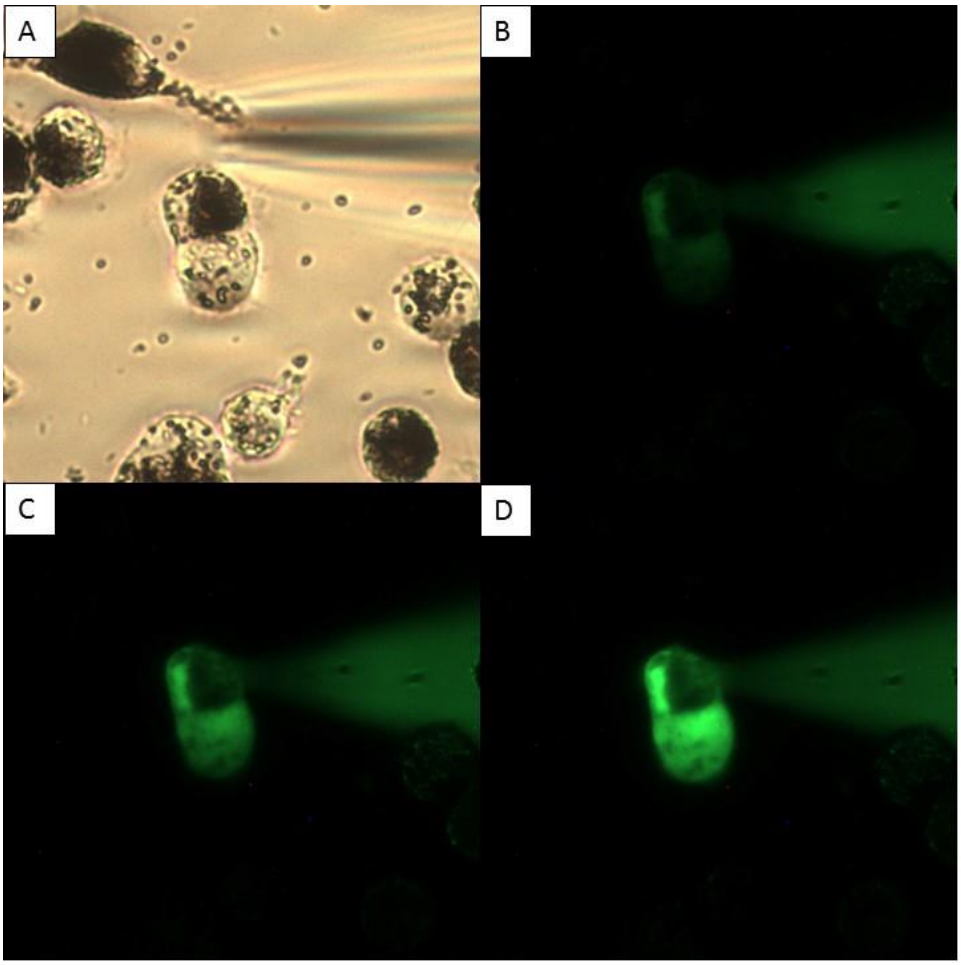

Fig. 3.9 A typical dye transfer experiment showing the changes of fluorescence level in isolated porcine PE-NPE cell couplet under control condition. (A) bright field image before forming the gigaseal; (B) 2 min; (C) 5 min; and (D) 10 min after membrane rupture.

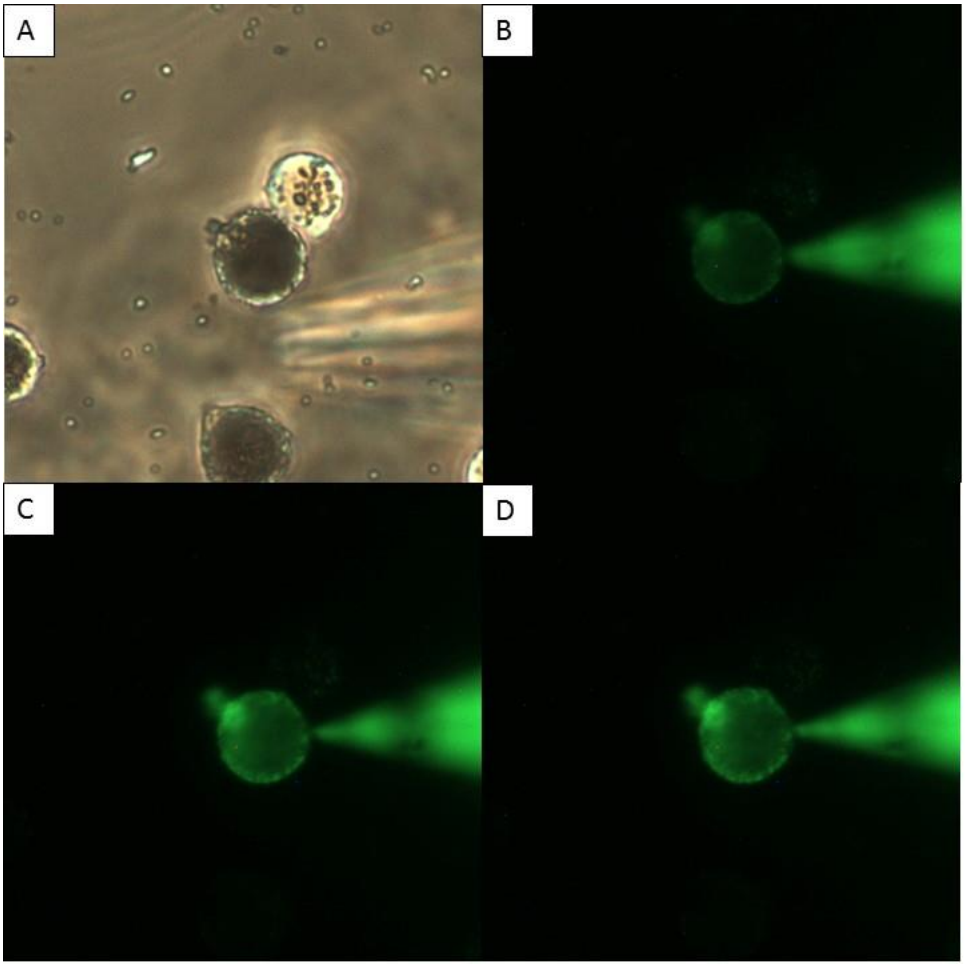

Fig. 3.10 A typical dye transfer experiment showing the changes of fluorescence level in isolated porcine PE-NPE cell couplet with siRNA targeted against Cx43. (A) bright field image before forming the gigaseal; (B) 2 min; (C) 5 min; and (D) 10 min after membrane rupture.

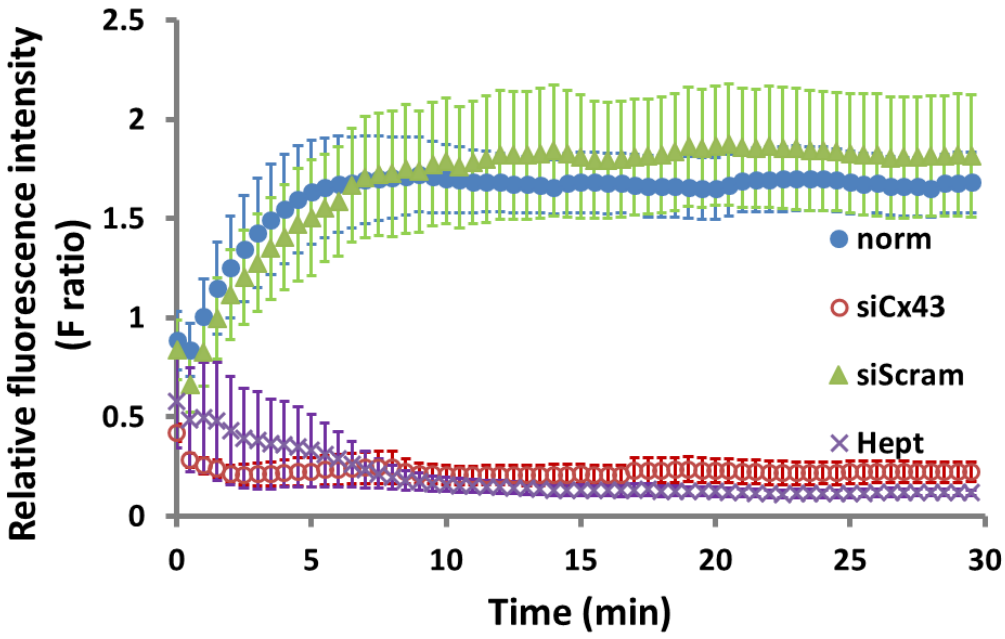

Fig. 3.11 Relative fluorescence intensity (F ratio) over time under various conditions in Lucifer yellow dye transfer experiment. norm: normal isolated porcine PE-NPE cell couplets (N = 10); siCx43: couplets treated with siRNA against Cx43 (N = 8); siScram: couplets treated with scrambled siRNA (N = 7); Hept: couplets treated with 3.5 mM heptanol (N = 5).

For the cell couplets transfected with siRNA against Cx43 (siCx43, N = 8), the F ratio decreased rapidly in the first 2 min and became stable in 5 min (Fig. 3.11). At 10 min, the F ratio was 0.21 ± 0.05. As shown in Fig. 3.12, the F ratios at selected time points among siScram-treated, siCx43-treated and heptanol groups were compared. Significant differences in F ratios were found between siCx43 and siScram groups since 3 min after membrane rupture ($p < 0.05$, Kruskal-Wallis test). At 10 min, there was an 88% reduction in F ratio for couplets treated with siCx43 as compared to siScram ($p < 0.001$, Kruskal-Wallis test). No significant difference of F ratios was observed between the heptanol and siCx43 groups throughout the

experimental period ($p > 0.05$, Kruskal-Wallis test) (Fig. 3.11 and Fig. 3.12). Our results indicated that the inhibitory effect of Cx43 blockage on dye transfer rate was similar to that of non-selective gap junction blocker heptanol.

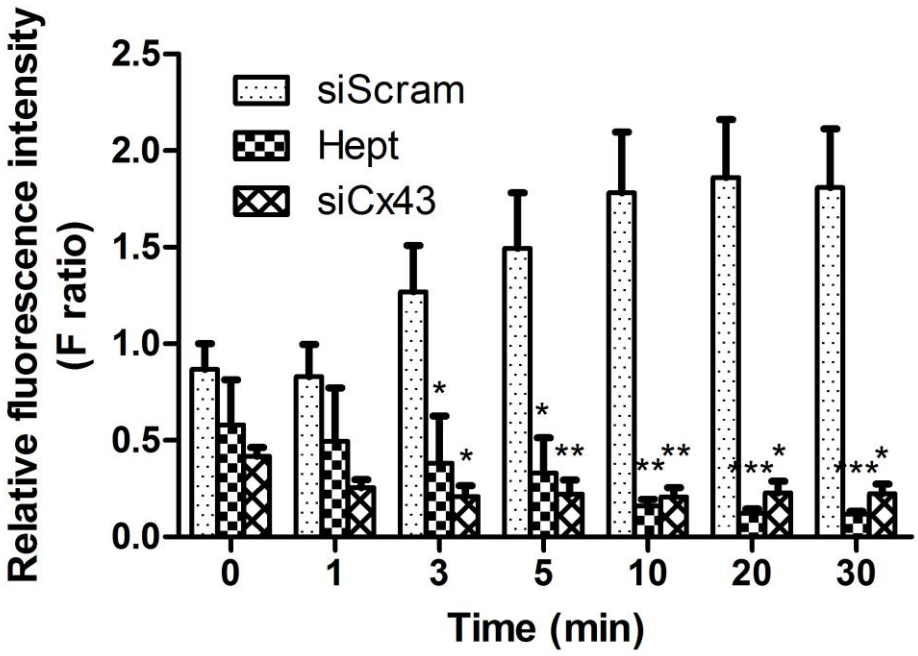

Fig. 3.12 Relative fluorescence intensity (F ratio) at selected time points under various conditions in Lucifer yellow dye transfer experiment (*: $p < 0.05$, **: $p < 0.01$, ***: $p < 0.001$, Kruskal-Wallis test, compared to the siScram control group). siCx43: couplets treated with siRNA against Cx43 (N = 8); siScram: couplets treated with scrambled siRNA (N = 7); Hept: couplets treated with 3.5 mM heptanol, a non-selective gap junction blocker (N = 5).

3.4 Discussion

In this study, we have characterized the gap junctions in porcine CBE. Our results showed that Cx43 was the most abundant connexin present in porcine CBE. It was primarily located on the apical surface linking between PE and NPE cells. Knockdown of Cx43 with siRNA caused a significant inhibition of gene and protein expression, resulting in a 90% reduction of dye diffusion from PE to NPE cells. Our findings support the notion that Cx43 provides a major route for fluid movement across porcine PE-NPE cell couplets.

3.4.1 Species variation in aqueous humor secretion

Species variation in the mechanisms of AHF has been reported previously (Do and Civan, 2009). For example, in rabbits and guinea pigs, it was reported that the HCO_3^- concentration in the aqueous humor is significantly higher than in blood plasma, while the Cl^- concentration in the aqueous humor was lower than in blood plasma (Kinsey and Reddy, 1964; Duke-Elder, 1968; Gerometta et al., 2005). The reverse is true in humans. Besides, both HCO_3^- and Cl^- secretion were shown to be important for driving AHF in rabbits (Wolosin et al., 1993; Crook et al., 2000; Candia et al., 2005; Gerometta et al., 2005); but no net HCO_3^- flux was detected in bovine CEs (To et al., 2001). On the other hand, Cl^- transport plays an important role in mediating AHF in many animal species including cat (Holland and Gipson, 1970), ox (Do and To, 2000) and pig (Kong et al., 2006). These results indicate that the transport mechanisms and regulation of AHF may vary among species. It has been suggested that the porcine eye may be a good animal model to mimic human ocular conditions because: 1) human eyes are not easily assessable due to ethical

issues and their practical value for transplantation; 2) fresh porcine eyes are readily available in the slaughter house without compromising lives for experiment; 3) the physical dimensions and anatomical properties of porcine eyeball are similar to those of humans (Beauchemin, 1974; Simoens et al., 1992); 4) the electrolyte composition of the aqueous humor in pig is similar to that in humans (Civan, 2008); 5) the characteristics of aqueous humor dynamics in pig are similar to those in human (Shahidullah et al., 2005); and 6) the biocompatibility of pig to human eye has been demonstrated in a recent artificial corneal graft study (Yoshida et al., 2014). Our recent findings of cAMP- and forskolin-induced Isc stimulation in porcine CE (Cheng et al., 2016) were also in good agreement with the results obtained in human ciliary process (Wu et al., 2013), suggesting that pig is a good animal model for AHF study.

3.4.2 Significance of characterization of gap junctions in ciliary epithelium

As discussed in Section 3.1.3, the modulation of gap junction permeability in CE may play an important role in regulating AHF and IOP. At present, there are no clinically-available anti-glaucoma drugs that lower IOP by uncoupling the intercellular gap junctions in CE. If a drug that targets the specific composition of connexin in CE is developed, it can be used as an ocular hypotensive agent or combined with other existing anti-glaucoma agents to improve the efficacy of IOP-lowering effect.

Heptanol was previously shown to inhibit the transepithelial electrical parameters and fluid transfer in bovine and porcine eyes (Do and To, 2000; Kong et al., 2006;

Law et al., 2009). Since it is a non-selective gap junction blocker, it may potentially affect other gap junctions present in the neighboring tissues. For example, Cx46 is found to be present in the crystalline lens. Disruption of Cx46 may cause Ca^{2+} imbalance in lens fiber, leading to cataract formation (Shakespeare et al., 2009). In order to preserve the normal physiology of the eye, it is preferable to develop agents that target the specific gap junction isoforms in the CE.

3.4.3 Species variation in composition of connexins in ciliary epithelium

In previous studies, various connexin isoforms have been identified in the CE of different species (Coca-Prados et al., 1992; Wolosin et al., 1997b; Coffey et al., 2002; Calera et al., 2006; Calera et al., 2009; Wang et al., 2010). The relative contribution of these connexins in regulating AHF remains unclear. Since pig is considered a good animal model for mimicking human conditions, its gap junction profiling in CE and the gap junctions' functional significance in mediating fluid movement were investigated.

We have demonstrated the presence of Cx43, Cx45, Cx47, Cx50 and Cx60 in porcine CBE. Cx43 was found to be the most abundant connexin expressed. It was localized primarily at the apical borders connecting between PE and NPE layers. Our result was consistent with a recent study conducted by Shahidullah and Delamere (2014) in which both Cx43 and Cx50 were detected in the porcine CE by immunohistochemical staining. They detected Cx43 at the border between PE and NPE cells, as well as on the basolateral membrane of PE cells; while Cx50 located on the basolateral surface of NPE cells. In addition, the connexin hemichannels

were present on the basolateral membranes of porcine CE as extracellular dye was shown to be taken up by the CE and detected in the NPE layer (Shahidullah and Delamere, 2014). In addition to pig, Cx50 was also expressed in the basolateral membrane of rabbit NPE cells (Wolosin et al., 1997b). Other connexins, such as Cx26, Cx31 and Cx40 that have been reported in rat (Wolosin et al., 1997b; Coffey et al., 2002) and bovine CE (Coca-Prados et al., 1992), but not observed in porcine CE, suggesting the possibility of species variation in the transport machinery. In the present study, we have also studied the relative abundance of various connexins by qPCR and found that the expression of Cx43 was over 200-fold higher than the other connexins observed in CBE.

It is worth noting that although Cx37 was detected at the mRNA level, its protein expression was not observed in our study. This discrepancy could be the result from the post-translational modification in which Cx37 was modified after translation. Another possibility was that the amount of Cx37 protein was not sufficient for detection by WB. Nevertheless, our results were similar to a recent study where Cx37 was also not identified in porcine CE (Shahidullah and Delamere, 2014).

3.4.4 Gap junction permeability

Our findings showed that Cx43 was the most abundant connexin isoform expressed in porcine CBE. Since it was primarily located on the apical surface between PE and NPE cells, it might provide an important route of solute transfer between the two layers. Therefore, we have evaluated its functional significance in mediating fluid movement across porcine PE-NPE cell couplets.

As shown in Fig. 3.7 and Fig. 3.8, the mRNA and protein expression of Cx43 in porcine CE cells was reduced by 60% and 70%, respectively, after a 24-hour transfection with siRNA against Cx43. The dye transfer, as reflected by the relative fluorescence intensity (F ratio), was inhibited by 90% at 10 min compared to siScram control. The reduction level was similar to the porcine CE cells treated with heptanol. It suggests that the contribution of connexins in fluid transfer across CE is mainly from the Cx43 isoform. Our results were in agreement with a previous study where the dye transfer was reduced by 60% in bovine CE cell couplets (Wang et al., 2010). The higher F ratio in the steady state detected in porcine compared to the bovine CE cell couplets may be due to the difference in pigmentation among different species, thereby, influencing the fluorescence levels in PE cells and, thus, F ratio. Our findings also revealed that the inhibition of dye transfer exerted by siRNA against Cx43 was similar to that of heptanol treatment, strongly suggesting that Cx43 may potentially constitute the major conduit for ion and solute exchanges between PE and NPE cells.

Since Lucifer yellow dye transfer is an *in vitro* experiment using isolated PE-NPE cell couplets, our results may not completely reflect the function of the CE *in vivo.* For example, in live animals, the Cx43-knockdown may be compensated by the formation of heterotypic gap junction channels with other connexin isoforms (Brink et al., 2000). Also, the contribution of other connexins in mediating fluid flow was not investigated in the current study. Further studies, especially *in vivo* animal study, are required to further the understanding of gap junction in aqueous humor formation.

3.4.5 Connexin 43 as a target for novel anti-glaucoma drugs

Our results were consistent with previous studies showing that gap junctions linking between PE and NPE cells are important in regulating AHF (Kong et al., 2006; Law et al., 2009). Knockdown of Cx43 significantly inhibited the fluid flow by 90%, indicating its potential role in driving the aqueous humor inflow and IOP (Calera et al., 2009). None of the existing anti-glaucoma agents targets Cx43, providing a possibility of developing a new pharmacologic agent for glaucoma therapy. As Cx43 is also expressed in other ocular tissues, such as cornea (Zhai et al., 2014) and crystalline lens (Shakespeare et al., 2009), it is important to determine if down-regulation of Cx43 would affect the normal physiology of the eye. It has been demonstrated that antisense oligodeoxynucleotides against Cx43 (Cx43-AsODN) could be used to assist corneal epithelium healing for patients with severe corneal injury (Ormonde et al., 2012). In parallel with this finding, down-regulation of Cx43 was shown to aid corneal wound healing instead of disrupting the integrity of the cornea (Elbadawy et al., 2016). In an *in vivo* study, no complications on cornea, ocular and surrounding tissues were reported upon instillation of anti-peptide against Cx43 in diabetic rats (Moore et al., 2014). In the crystalline lens, Cx43 knockout mice has not resulted in the development of cataract (DeRosa et al., 2009). Together, these studies suggested that down-regulation of Cx43 might not disrupt the normal physiology of the ocular tissues around the ciliary body. It supported Cx43 as the potential target for anti-glaucoma agents. However, further studies are required to determine the precise effect of down-regulating Cx43 on ocular tissues.

In the retina, it has been demonstrated that gap junctions are involved in spreading the apoptotic signals in retinal ganglion cells and Muller cells (Akopian et al., 2014).

The use of a non-selective gap junction blocker, meclofenamic acid, reduced the ganglion cell loss by 70% (Akopian et al., 2014). The identification of Cx43 in retina (Kerr et al., 2010) and the down-regulation of Cx43 reducing neuronal cell death (Cronin et al., 2008) suggested the potential role of down-regulation of Cx43 in retinal ganglion cell protection (Kerr et al., 2010; Prasanna et al., 2011). In addition, free, uncoupled hemichannels formed by connexins can release extracellular signals affecting the neighboring cells (Chen et al., 2015a). For example, Cx43 hemichannels have been shown to transport inflammatory signals in the retinal cells (Danesh-Meyer et al., 2008). This study showed that cell death and optic nerve edema was significantly reduced by the down-regulatory expression of Cx43 with Cx43-AsODN in the ischemic reperfusion glaucoma model (Danesh-Meyer et al., 2008). Systemic or intravitreal injection of Cx43 mimetic peptide was also found to be effective in protecting retinal ganglion cells from ischemic reperfusion by blocking Cx43 hemichannels (Danesh-Meyer et al., 2012; Chen et al., 2015b). These findings supported the hypothesis of using connexin, especially Cx43, as a potential target for the treatment of glaucoma.

CHAPTER 4 Effects of temperature alternation and melatonin on aqueous humor secretion

4.1 Introduction

As described in Section 2.1.2, aqueous humor formation (AHF) follows a circadian rhythm. Numerous researches have, therefore, aimed to explore its regulatory mechanism(s) (Brubaker, 1998). It has been shown that hormones such as epinephrine, corticosteroids and melatonin are potential regulators for the AHF circadian rhythm. Epinephrine displays a diurnal rhythm in its blood plasma concentration (Linsell et al., 1985) and it is also present in the aqueous humor (Cooper et al., 1984; Autzen et al., 1985). Nevertheless, the circadian rhythm of AHF was reported to be sustained even without epinephrine production or sympathetic innervation (Larson and Brubaker, 1988; Maus et al., 1994). The aforementioned evidence suggested that epinephrine might not be the only regulator in maintaining the circadian rhythm of AHF. Since secreted melatonin also displays a circadian rhythm (Claustrat, 2014) and it has been demonstrated to reduce IOP in humans (Samples et al., 1988), melatonin was chosen to be investigated in this study.

4.1.1 Melatonin as a potential candidate for regulating aqueous humor inflow

Melatonin is an indole-derived compound naturally synthesized in the human body (Alarma-Estrany and Pintor, 2007). It is mainly secreted by the pineal gland of the brain (Ekmekcioglu and Thalhammer, 2014). Melatonin can also be secreted by ocular structures such as the retina and the ciliary body (Wiechmann and Summers,

2008), although its contribution to total plasma melatonin levels is subtle (Claustrat, 2014).

Two melatonin membrane receptors, MT_1 and MT_2 and a putative membrane receptor MT_3 (MT_3 receptor) have been identified (Claustrat, 2014). MT_1 and MT_2 receptors are G protein-coupled, while the MT_3 receptor has been suggested to be a cytosolic enzyme quinone reductase 2 (QR2) and not a membrane receptor by other scholars (von Gall et al., 2002). Since melatonin receptors are widely distributed in the body, melatonin can synchronize the various physiological functions such as maintenance of tissue metabolism, immune response, core body temperature, blood pressure, hormonal homeostasis, and other circadian rhythms in the body (Claustrat, 2014; Ekmekcioglu and Thalhammer, 2014).

4.1.1.1 Melatonin and the circadian rhythm

Melatonin and its receptors are suggested to be responsible for circadian rhythm. Its secretion oscillates in a circadian rhythm which provides the basis as rhythmic time cue (Claustrat, 2014). Its property of rhythmic synthesis is guarded by a rate limiting enzyme, aralkylamine N-acetyltransferase (AA-NAT) (Wiechmann and Summers, 2008) and maintained by external time cues—light and darkness (Orr et al., 1976; Cohen, 1982; Fukuhara et al., 2004; Wiechmann and Summers, 2008). Several studies have shown that melatonin intake or activation of melatonin receptors can alter the phase of circadian rhythms, such as the sleep-wake cycle (Ekmekcioglu and Thalhammer, 2014). Timed administration of melatonin can be adopted to adjust the phase of the sleep-wake cycle (Arendt et al., 1997). Melatonin intake has also been found to entrain the sleep-wake cycle for the blind, who lacks

light cues in order to synchronize their sleep rhythm with the surrounding environment (Sack et al., 2000). Clinically, a melatonin analogue ramelteon has been used as a treatment for insomnia (Spadoni et al., 2011). When melatonin receptors MT_1 and MT_2 are disrupted, the circadian rhythm of insulin secretion becomes inhibited (Muhlbauer et al., 2009). It provides further support for the significance of melatonin and its receptors in maintaining circadian rhythms and a normal lifestyle (Challet, 2015).

It has been demonstrated that melatonin is produced at a rate of 10 to 80 μg/night in the human body (Geoffriau et al., 1999). The concentration of melatonin in blood plasma during the daytime has also been found to be significantly lower than at night (Viggiano et al., 1994; Lundmark et al., 2007), contributing to a diurnal variation in plasma concentrations (Chiquet et al., 2006).

The melatonin level in the aqueous humor has been shown to display a similar diurnal change as in blood plasma (Lundmark et al., 2007). Melatonin levels were found increased by 2-3 fold at night in rabbits (Liu and Dacus, 1991) and humans (Chiquet et al., 2006; Aydin and Sahin, 2016). This diurnal rhythm evident in melatonin provides a good foundation for studying its effects on AHF and IOP.

4.1.1.2 Expression of MT receptors in the ciliary body

Melatonin receptors have been identified in the ciliary body of various species (Alarma-Estrany and Pintor, 2007). Changes in the melatonin levels have been thought to affect the physiological regulation of aqueous humor dynamics. In ciliary body, the MT_1 receptor has been found in rabbits while MT_2 receptors have been

reported in rabbits and humans (Osborne and Chidlow, 1994; Roberts et al., 2000). The MT_3 receptor has also been demonstrated in Xenopus laevis (Wiechmann and Wirsig-Wiechmann, 2001). The presence of MT receptors in the ciliary body suggests that it may play a role in regulating AHF.

4.1.1.3 Effect of melatonin and its analogues on aqueous humor formation and intraocular pressure

The effects of melatonin on IOP have been extensively studied previously. Topical instillation of melatonin or its analogue has been shown to lower IOP in many different species including rabbit (Pintor et al., 2001; Pintor et al., 2003), mouse (Martinez-Aguila et al., 2016) and monkey (Serle et al., 2004). In particular, studies on human subjects regarding the oral intake of melatonin or its analogues have shown a noted IOP reduction (Samples et al., 1988; Ismail and Mowafi, 2009; Pescosolido et al., 2015). Nevertheless, some other studies have not demonstrated the IOP-lowering effect of melatonin in cats (Rohde et al., 1985) and rabbits (Kiuchi et al., 1993).

In addition, there is no consensus on the signaling pathway for melatonin to achieve IOP reduction. It has been suggested that both MT_1 and MT_2 receptors are responsible for the reduction in a knockout mice study (Alcantara-Contreras et al., 2011). However, some other studies have demonstrated that selective MT_2 antagonists inhibited the IOP-lowering effects of melatonin and its analogues, suggesting MT_2 receptors responsible for IOP regulation (Martinez-Aguila et al., 2013; Martinez-Aguila et al., 2016). In contrast, MT_3 receptors have been advocated to be involved in melatonin-induced IOP reduction (Pintor et al., 2001;

Serle et al., 2004). This controversy hinders us from understanding the precise functional roles of MT_1, MT_2 and MT_3 in regulating AHF and the potential significance of various melatonin receptors has yet to be evaluated.

4.1.2 Temperature cue for regulating aqueous humor inflow

As described Section 2.1.2, the rate of AHF in humans displays a 50% reduction at night (Brubaker, 1998). This magnitude of reduction has not yet been achieved by any clinical anti-glaucoma agents (Bartlett and Jaanus, 2008). Similar to aqueous humor drainage, the small diurnal temperature fluctuation in the eye may partially contribute to the observed changes in AHF rate.

Temperature effects on AHF rate has previously been studied. It has been found that lowering temperature would lower the rate (Becker, 1961), and similarly, *vice versa* (Krupin et al., 1977). However, the temperatures in these studies were outside normal physiological range. Moreover, the ocular temperature is expected to increase at night due to eyelid closure, which will synchronize the body temperature to that of the eye; yet a reduction in AHF rate has been observed in a human study (Brubaker, 1998). Therefore, it is worthwhile to conduct further experiments, using small temperature change within the physiological range, to explain these seemingly contradictory findings. The expression of gap junction protein e.g. Cx43 was found to be affected by temperature in both *in vitro* (Zhang et al., 2012) and *in vivo* (Saitongdee et al., 2000) studies. Since Cx43 was shown to be important for regulating AHF as discussed in CHAPTER 3, the effect of temperature alternation on gap junction permeability was studied.

4.1.3 Aims of the study

Since the secretion of aqueous humor follows a circadian rhythm, temperature variation and melatonin may play a role to the observed reduction in AHF at night (Buhr et al., 2010; Claustrat, 2014). In this present study, we aimed to study the effects of small temperature change (by 4°C) and melatonin on AHF in porcine eyes. For temperature alternation experiments, transepithelial electrical parameters, which are indicators of AHF, were monitored. Western blot (WB) analysis was used to examine the changes of Cx43 protein expression upon temperature changes. In addition, the effect of temperature on gap junction permeability across isolated PE-NPE cell couplets was also evaluated. As for melatonin, its effects on transepithelial electrical parameters and gap junction permeability were determined. The roles of various melatonin receptor antagonists on transepithelial transport were also studied.

4.2 Materials and methods

4.2.1 Transepithelial electrical measurements with the Ussing-Zerahn-type chamber

4.2.1.1 Experimental setup

A modified Ussing-Zerahn-type chamber (Ussing chamber) was used to monitor the transepithelial electrical parameters including potential difference (PD), short-circuit current (Isc) and transmural resistance (Rt). The Ussing chamber was custom-made, illustrated in Fig. 4.1. Two tissue-mounting blocks (A) and (B) were made of Perspex and were in conjugate pairs (Fig. 4.2). At the center of each block, there was an oval-shaped aperture with an exposed area of 0.10 cm^2. The aperture was surrounded by a rubber O-ring lubricated with silicone grease (Dow Corning, Corporation, Midland, MI, USA) to prevent water leakage and to minimize the tissue damage throughout the experiment. The fixation pins around the aperture were used to keep the tissue preparation in place.

The Perspex tissue-bathing chambers were assembled on the tissue-mounting blocks and mounted on the chamber-mounting rack shown in Fig. 4.1. The whole chamber was then connected to a borosilicate glass re-circulating bath. 95% O_2 and 5% CO_2 was supplied to the chamber through the gas inlets on both sides of the chamber. The temperature of the bathing solution was controlled by a water bath system (PolyScience, Niles, IL, USA). In temperature alternation experiments, the temperature was changed from 22°C to 26°C, and *vice versa*. For other experiments, the temperature was maintained at room temperature, i.e. 22°C.

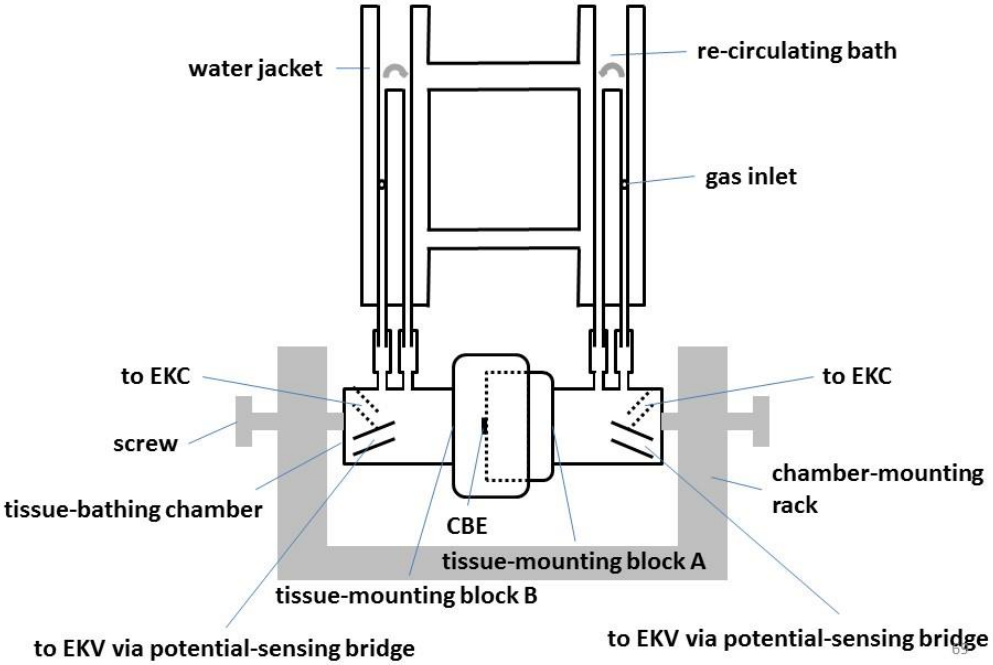

Fig. 4.1 Schematic diagram of the Ussing-Zerahn-type chamber (Ussing chamber). EKC: current-clamp electrode; EKV: voltage-clamp electrode; CBE: ciliary body epithelium preparation.

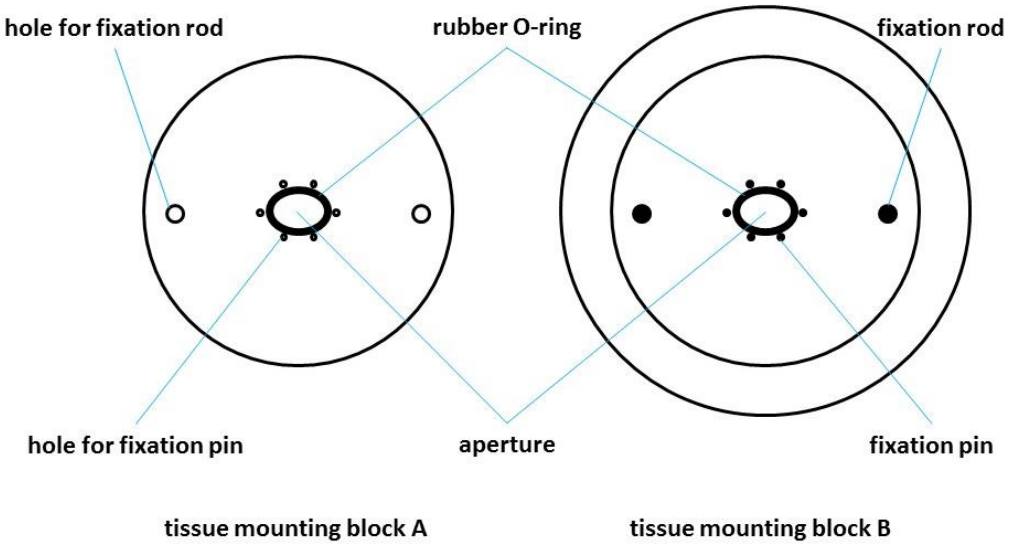

Fig. 4.2 Schematic diagram of tissue mounting-blocks.

For electrical measurements, each pair of tissue-bathing chambers were connected to a pair of voltage-clamp electrodes (EKV, World Precision Instruments, Sarasota, USA) via a potential-sensing bridge (Do and To, 2000; Cheng et al., 2016) and a pair of current-clamp electrodes (EKC). The electrodes were made of Ag/AgCl and connected to a dual voltage current clamp unit DVC-1000 (World Precision Instruments, Sarasota, FL, USA). EKVs were used to measure the potential difference (PD) across the CBE preparation while EKCs were used to apply a known current through the preparation for the measurement of transmural resistance (Rt). The potential-sensing bridge (H-bridge, Fig. 4.3A) was made of polyvinyl chloride (PVC) tubes and stopcocks that helped to neutralize the electrical drift throughout the experiment. As shown in Fig. 4.3, the PD across the preparation was measured when the horizontal bridge was closed (position P1). When the stopcocks were switched to position P2, the electrical measurements stopped and the electrical drift, if any, could be corrected. The data acquisition was achieved with a PowerLab 8/30 PL3508 and software Chart™ 5 (ADInstruments, Sydney, Australia).

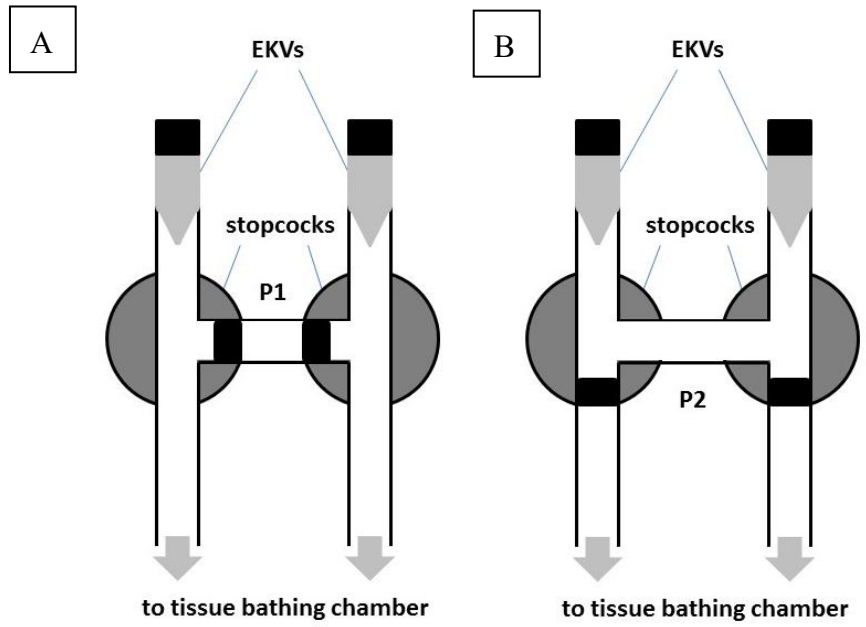

Fig. 4.3 Schematic diagram of potential-sensing bridge (H-bridge) (A) in position P1 and (B) in position P2. EKV: voltage-clamp electrode.

4.2.1.2 Preparation of porcine ciliary body epithelium

The extra-ocular muscle and fatty tissues were carefully removed from a fresh porcine eye. An incision was made at the limbus to the equator of the eye. Another incision was made perpendicular to the first cut. Afterwards, the cornea was removed before separating the sclera from the iris base and the choroid. Then, a sector of the CBE was excised. The vitreous attached to the CBE preparation was carefully trimmed and minimized. The preparation was then bathed in HEPES-buffered Ringer's solution before mounting on the Ussing chamber.

4.2.1.3 Tissue mounting and transepithelial electrical measurements

A thin layer of silicone grease (Dow Corning Corporation, Midland, MI, USA) was applied to the surfaces of tissue-mounting blocks and O-rings to avoid water leakage. The CBE preparation was properly positioned so that only the pars plicata region was exposed to the bathing solution. The tissue-mounting blocks and tissue-bathing chambers were assembled and mounted onto the chamber mounting rack. The assembled chambers were then connected to the re-circulating bath.

The chambers were filled with the HEPES-buffered Ringer's solution with the electrodes in position, as shown in Fig. 4.1. A total of 15 ml Ringer's solution was filled in each side of the chamber. The Ringer's solution was then bubbled continuously with 95% O_2 and 5% CO_2; and the temperature of the solution was kept at either 22°C or 26°C depending on the experimental conditions.

The potential difference (PD) across the CBE preparation was continuously monitored during the experiment. The transmural resistance (Rt) was measured by applying an external current (I) of 5 μA across the tissue preparation. Depending on the change in potential difference ΔPD, the transmural resistance (Rt) was calculated by the following equation:

$$\mathrm{Rt} = \frac{\Delta \mathrm{PD}}{\mathrm{I}}$$

Afterwards, the short-circuit current (Isc) was determined using the following formula:

$$\mathrm{Isc} = \frac{\mathrm{PD}}{\mathrm{Rt}}$$

4.2.1.4 Solutions and pharmacological agents

Unless stated otherwise, all the chemicals used were purchased from Sigma-Aldrich (St. Louis, MO, USA). The HEPES-buffered Ringer's solution was used as the Ussing chamber bathing solution and composed of (in mM) 113.0 NaCl, 4.56 KCl, 21.0 $NaHCO_3$, 0.6 $MgSO_4$, 7.5 D-Glucose, 1.0 L-Glutathione reduced, 1.0 Na_2HPO_4, 10.0 HEPES and 1.4 $CaCl_2$. The pH and osmolality of the solution were adjusted to 7.4 with NaOH and 300 mOsm/kg with D-mannitol, respectively.

The drugs used in this study were: heptanol, niflumic acid (NFA), melatonin, luzindole, prazosin (Santa Cruz Biotechnology, Dallas, TX, USA). All the drugs except heptanol were dissolved in the vehicle dimethyl sulfoxide (DMSO) prior to addition to the Ussing chamber bathing solution. The final DMSO concentration was less than 0.1% in the bathing solution.

4.2.2 Western blot

The detailed procedures in obtaining isolated CE cells were previously described (Section 3.2.4). The freshly isolated CE cells were incubated at 37°C inside a 5% CO_2 humidified incubator for 24 hours. Then, the culture medium was replenished with DMEM with 1% PS 10% FBS supplements after washing twice with PBS. The incubation temperature was then changed to 33°C or maintained at 37°C for 12 hours, depending on the experimental conditions. Afterwards, 12 hour-33°C cell incubation temperature was either maintained at 33°C (C33, constant 33°C) or increased to 37°C (E37, ending 37°C) for 30 min. For the other patch of cells with 12-hour 37°C incubation, the temperature was maintained at 37°C (C37, constant

37°C) or reduced to 33°C (E33, ending 33°C) for 30 min. The cells from 4 treatment conditions were then washed with PBS of corresponding temperatures before protein extraction using RIPA-cOmplete lysis buffer. The quantity of Cx43 in the samples were analyzed with Western blot technique described in Section 3.2.4.

4.2.3 Lucifer yellow dye transfer

The dye transfer experiment was described in details in Section 3.2.6.3. The measurements of LY dye transfer across freshly isolated porcine PE-NPE cell couplets were conducted at either 22°C or 26°C throughout the experiment. For temperature alternation experiments, the incubation temperature was increased from 22°C to 26°C at 2.5 min after the start of the experiment. For melatonin experiments, melatonin was added to the bathing solution either 45 min before (i.e. melatonin pretreatment) or at the time of membrane rupture.

4.2.4 Statistical analysis

All data shown are presented as mean ± SEM. One-way repeated measures ANOVA was used to analyze the Ussing chamber experiments with sequential addition of drugs. Student's t-test was used to analyze the changes of Cx43 protein expression upon temperature alterations. One-way ANOVA was used to analyze the F-ratio at any given time point in LY dye transfer experiment and the effect of melatonin receptor antagonists on Isc. A p-value < 0.05 was considered to be statistically significant. The notations of p-values used in the statistical analysis are shown below:

Symbol	*p*-value
ns	> 0.05
*	< 0.05
**	< 0.01
***	< 0.001

4.3 Results

4.3.1 Baseline electrical parameters in Ussing chamber experiments

The baseline transepithelial electrical parameters of porcine CBE in Ussing chamber experiments at room temperature of 22°C are summarized in Table 4.1. A negative PD of -0.68 mV (the aqueous side being more negative compared to the stromal side) was found and its value was consistent with our previous studies (Kong et al., 2006; Cheng et al., 2016). Only preparations with stable electrical parameters were used.

Table 4.1 Baseline electrical parameters of porcine CBE in Ussing chamber experiments at 22°C. N = number of experiments; PD = potential difference; Isc = short-circuit current; and Rt = transmural resistance.

N	PD (mV)	Isc ($\mu A \cdot cm^{-2}$)	Rt ($\Omega \cdot cm^2$)
68	-0.68 ± 0.08	11.31 ± 0.88	63.6 ± 3.6

4.3.2 Effect of temperature alternation on transepithelial electrical measurements

Table 4.2 illustrates the effects of changing bathing solution temperature on transepithelial electrical parameters. Our results showed that the baseline PD and

Isc were significantly higher in preparations conducted at an initial temperature of 22°C compared with 26°C. The PD and Isc of the 22°C group were 81% and 69% higher than that of the 26°C group, respectively ($p < 0.001$ for both PD and Isc, Student's t-test). However, Rt had no statistically significant difference between the two groups ($p > 0.05$, Student's t-test).

Table 4.2 Measurements of transepithelial electrical parameters at different temperatures.

(A) Electrical parameters with an initial temperature of 22°C				
Temp	**N**	**PD (mV)**	**Isc (μA·cm^{-2})**	**Rt (Ω·cm^2)**
Initial 22°C	21	-0.85 ± 0.06	13.85 ± 1.06	64.0 ± 3.7
Final 26°C		-0.44 ± 0.04	7.50 ± 0.89	63.2 ± 3.3
(B) Electrical parameters with an initial temperature of 26°C				
Temp	**N**	**PD (mV)**	**Isc (μA·cm^{-2})**	**Rt (Ω·cm^2)**
Initial 26°C	23	-0.47 ± 0.05	6.86 ± 0.67	69.1 ± 2.3
Final 22°C		-0.86 ± 0.08	12.34 ± 1.09	70.6 ± 2.5

To determine whether temperature alternation had any effect on PD and Isc, the incubation temperature was increased from 22°C by 4°C, or decreased from 26°C by 4°C. When the bathing solution temperature increased, the Isc was reduced by 50% from 13.85 to 7.50 μA·cm^{-2}, as shown in Table 4.2. Similarly, lowering the

bathing solution temperature had the opposite effects; the Isc was increased by 80% from 6.86 to 12.34 $\mu A \cdot cm^{-2}$. There was no statistically significant difference in any electrical parameters measured at the same incubation temperature between the two groups (p >0.05 for all of the electrical parameters, Student's t-test).

Fig. 4.4 and Fig. 4.5 illustrate the sequential effects of temperature alternation on Isc with different initial temperatures. For preparations with lower initial incubation temperature, the normalized Isc was significantly reduced when the bathing temperature was increased by 4°C (Fig. 4.4, N = 7, $p < 0.001$, one-way repeated measures ANOVA). The changes of Isc were reversible and repeatable ($p > 0.05$). For preparations with higher initial incubation temperature, the percentage increase of Isc when the temperature reduced by 4°C was 80-90% (Fig. 4.5, N = 7, $p < 0.001$, one-way repeated measures ANOVA). Similarly, the changes noted were reversible ($p > 0.05$). On average, 20-30 min was required to achieve a stable Isc subsequent to either increasing or decreasing the bathing temperature.

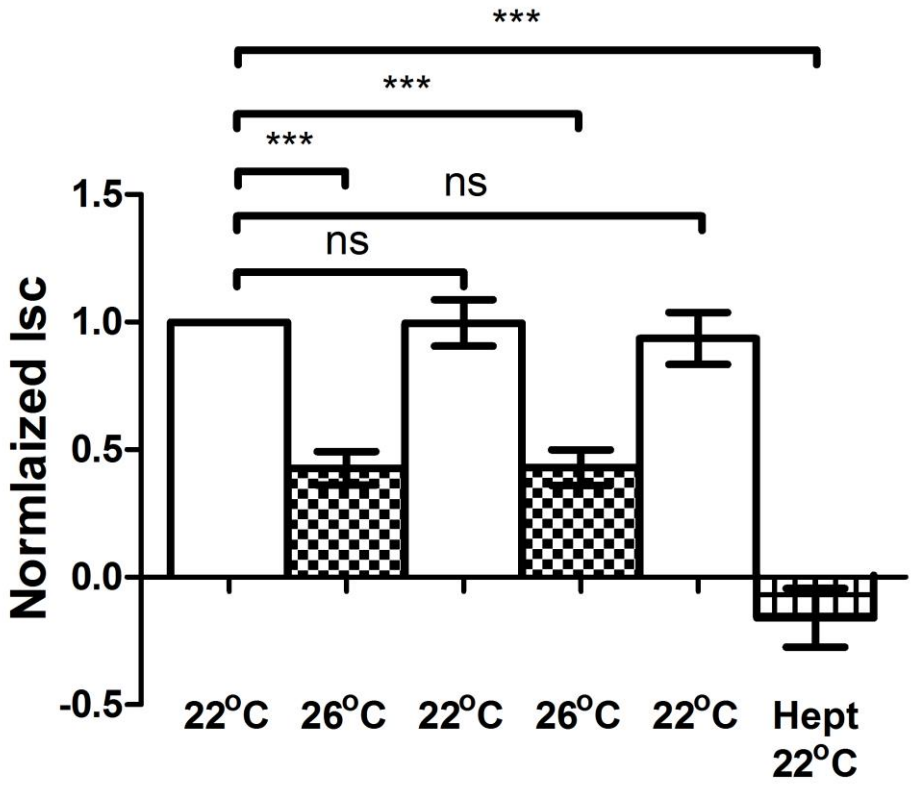

Isc ($\mu A/cm^2$)	13.1 ±1.9	5.4 ±0.9	13.4 ±2.4	5.7 ±1.1	12.9 ±2.8

Fig. 4.4 Effects of temperature alternation on short-circuit current (Isc) (initial temperature set at 22°C) (N = 7, ns: not statistically significant; ***: $p < 0.001$, one-way repeated measures ANOVA). Hept: 3.5 mM heptanol added on both sides.

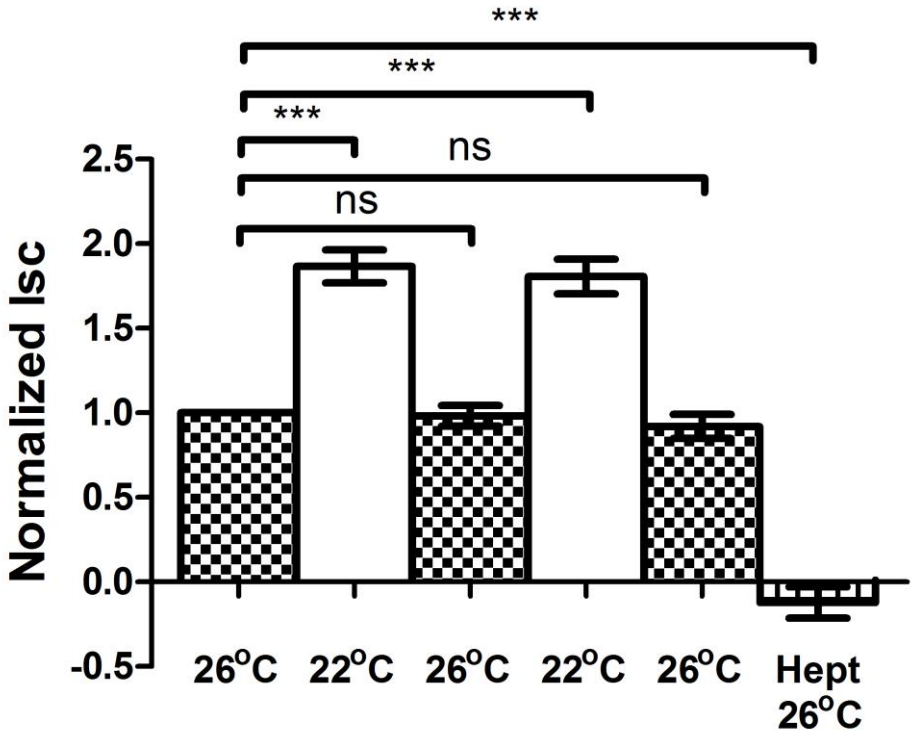

Isc ($\mu A/cm^2$)	7.4 ±1.2	13.4 ±1.8	7.2 ±1.2	13.1 ±1.9	6.9 ±1.3

Fig. 4.5 Effects of temperature alternation on short-circuit current (Isc) (initial temperature set at 26°C) (N = 7, ns: not statistically significant; ***: $p < 0.001$, one-way repeated measures ANOVA). Hept: 3.5 mM heptanol added on both sides.

4.3.3 Effect of heptanol on temperature-induced short-circuit current changes

To investigate whether gap junctions were involved in temperature-induced Isc changes, 3.5 mM heptanol was added to the bathing solution after two cycles of temperature alternation (Fig. 4.4 and Fig. 4.5). When the drug was added to both the stromal and aqueous sides, it abolished the Isc irrespective of the initial and

final incubation temperatures ($p < 0.001$, one-way repeated measure ANOVA). As shown in Fig. 4.6 and Fig. 4.7, increasing or decreasing the bathing temperature produced similar changes in Isc, as described in Fig. 4.4 and Fig. 4.5. The addition of heptanol to both sides totally inhibited the Isc and abolished the subsequent Isc changes induced by temperature alternation in both directions. These findings indicate the potential involvement of gap junctions in mediating temperature-induced Isc responses.

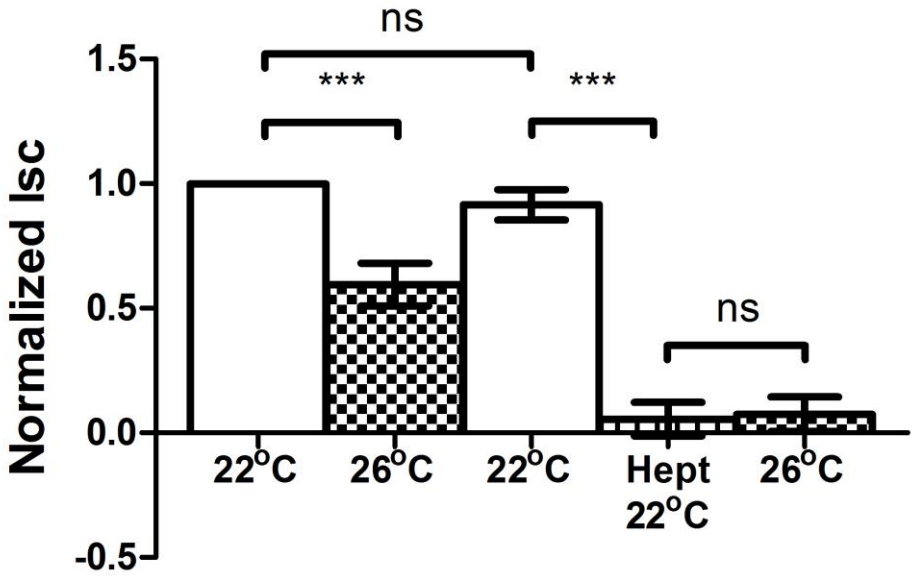

Isc ($\mu A/cm^2$)	7.4 ±1.2	13.4 ±1.8	7.2 ±1.2	13.1 ±1.9	6.9 ±1.3

Fig. 4.6 Effect of heptanol on temperature-induced short-circuit current (Isc) inhibition triggered by increasing temperature (N = 7, ns: not statistically significant; ***: $p < 0.001$, one-way repeated measures ANOVA). Hept: 3.5 mM heptanol added on both sides.

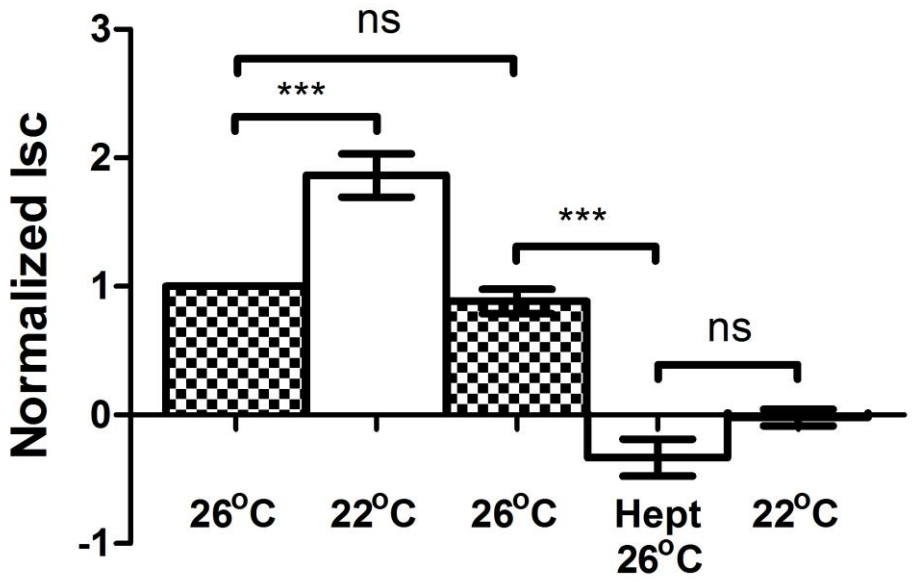

Isc ($\mu A/cm^2$)	5.2 ±0.7	10.0 ±1.9	4.9 ±1.0	-1.5 ±0.6	-0.2 ±0.4

Fig. 4.7 Effect of heptanol on temperature-induced short-circuit current (Isc) stimulation triggered by decreasing temperature (N = 8, ns: not statistically significant, ***: $p < 0.001$, one-way repeated measures ANOVA). Hept: 3.5 mM heptanol added on both sides.

4.3.4 Effect of temperature on connexin 43 expression

To examine whether the temperature-induced Isc responses were associated with changes in Cx43 protein expression, Western blot (WB) was adopted. In Fig. 4.8, the isolated CE cells were incubated at a physiologically relevant temperature of 33°C for 12 hours and the incubation temperature was maintained at 33°C (C33) or raised by 4°C to 37°C (E37) for 30 min before sample collection. Similarly, as shown in Fig. 4.9, the cells were incubated at 37°C for 12 hours and the incubation

temperature was either maintained at 37°C (C37) or reduced by 4°C to 33°C (E33) for 30 min. We found that the expression Cx43 was reduced by 13 ± 5 % with a short-time rise in incubation temperature (Fig. 4.8 , N = 8, $p < 0.05$, Student's t-test). On the other hand, reducing the incubation temperature increased Cx43 expression by 16 ± 3 % (Fig. 4.9, N = 7, $p < 0.001$, Student's t-test).

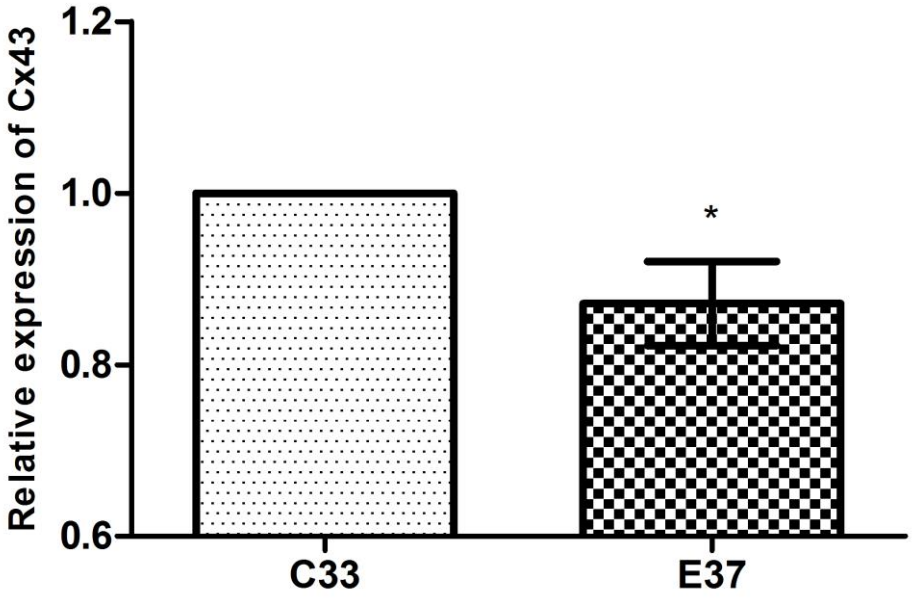

Fig. 4.8 Relative Cx43 protein expression after temperature increase from 33°C to 37°C for 30 min (N = 8; *: $p < 0.05$, Student's t-test).

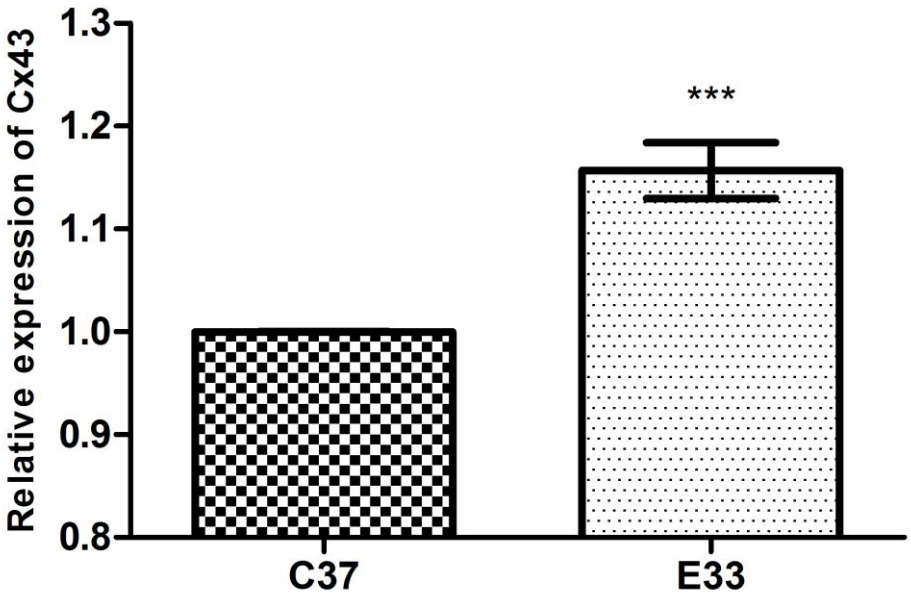

Fig. 4.9 Relative Cx43 protein expression after temperature decrease from 37°C to 33°C for 30 min (N = 7; ***: $p < 0.001$, Student's t-test).

4.3.5 Effect of temperature alternation on gap junction permeability

As for the expression level of the most expressed gap junction protein, Cx43 altered upon temperature change, we wondered whether the gap junction permeability was changed, leading to Isc responses. Therefore, the rate of dye diffusion from PE to NPE cell couplets was determined at lower and higher temperatures of 22°C and 26°C, respectively.

Our results indicated that there were no significant differences in F ratios at any time point between the 22°C and 26°C groups throughout the experiment (Fig. 4.10, $p > 0.05$, one way ANOVA). In order to determine whether the individual cell

difference might mask the temperature effect, we conducted another experiment with a lower initial incubation temperature for 2.5 min and the temperature was increased by 4°C afterwards (Fig. 4.10; labelled with 22°C to 26°C). No significant changes in F ratios were detected among all three groups at any time point ($p > 0.05$, one-way ANOVA).

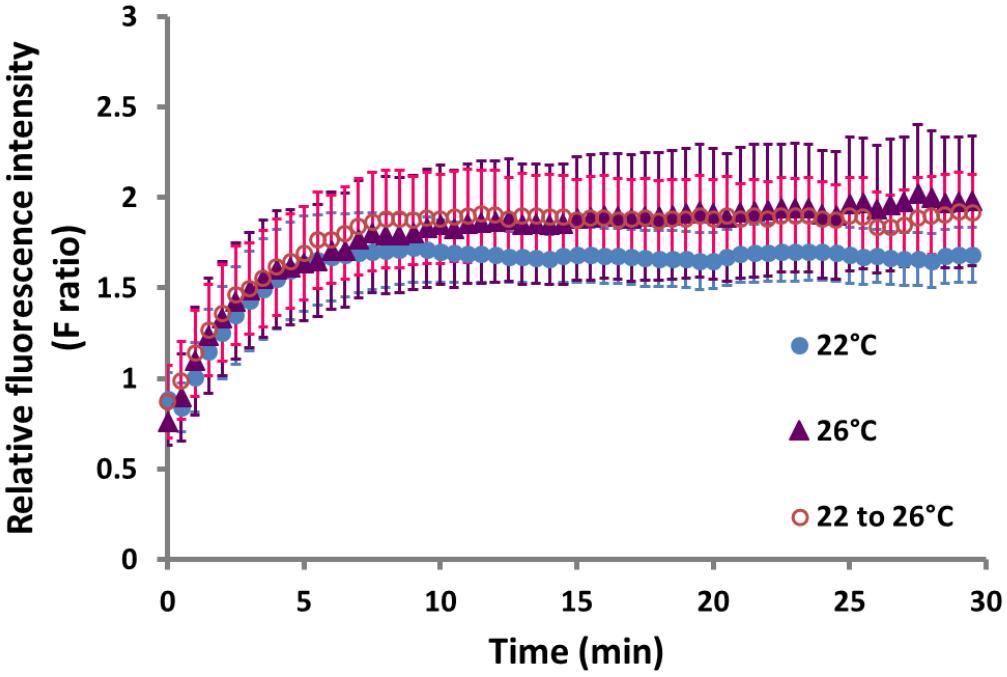

Fig. 4.10 Relative fluorescence intensity (F ratio) over time under different temperature conditions in Lucifer yellow dye transfer experiment. 22 to 26°C: temperature change from 22°C to 26°C at 2.5 min.

4.3.6 Effect of melatonin on short-circuit current

The effects of melatonin on Isc across porcine CBE was studied. Three concentrations (1, 10 and 100 μM) and two administration sites (aqueous side or

both stromal and aqueous sides) were adopted. A dose-dependent response of bilateral melatonin on Isc was illustrated in Fig. 4.11. At 1 and 10 μM, melatonin had no effect on Isc. At 100 μM, it significantly stimulated the Isc by 38 ± 6% (N = 6, $p < 0.001$, one-way repeated measures ANOVA). The melatonin-induced Isc stimulation was inhibited by 1 mM NFA, a non-selective Cl^- channel blocker. Likewise, an addition of melatonin to the aqueous side caused a similar dose-dependent Isc response. A melatonin-induced Isc stimulation was only observed at 100 μM (40 ± 9%), but not at 1 and 10 μM (Fig. 4.12, N = 11, $p < 0.001$, one-way repeated measures ANOVA). Subsequent addition of 1 mM NFA triggered a significant inhibition of normalized Isc: to 0.11 ± 0.08 (N = 5, $p < 0.001$, one-way repeated measures ANOVA) for preparations with prior bilateral administration of melatonin and to -0.06 ± 0.06 (N = 6, $p < 0.001$, one-way repeated measures ANOVA) for preparations with prior melatonin administration on the aqueous side. These results suggested that melatonin likely acted on the Cl^- secretion across porcine CBE. Therefore, for subsequent experiments, melatonin and its receptor antagonists were only administrated to the aqueous side. Additionally, the latency period after the administration of melatonin between the bilateral (41.9 ± 7.7 min) and aqueous (52.4 ± 9.3 min) applications were similar ($p > 0.05$, Student's t-test).

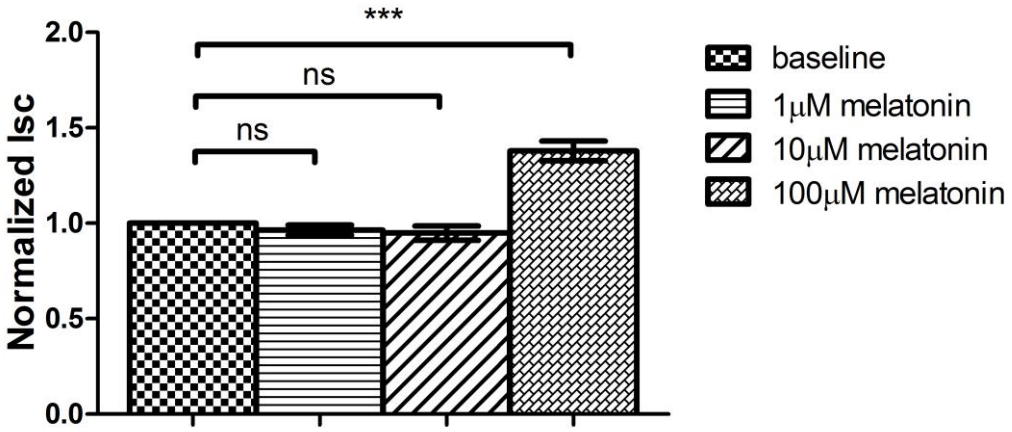

Fig. 4.11 Effects of melatonin, when added to stromal and aqueous sides simultaneously, on short-circuit current (Isc) (N = 6, ns: not statistically significant, ***: $p < 0.001$, one-way repeated measures ANOVA).

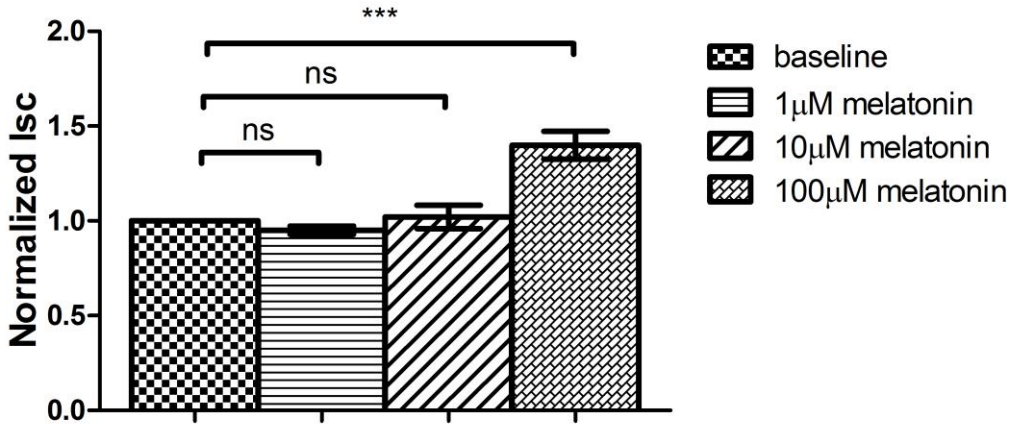

Fig. 4.12 Effects of melatonin, when added to aqueous side only, on short-circuit current (Isc) (N = 11, ns: not statistically significant, ***: $p < 0.001$, one-way repeated measures ANOVA).

4.3.7 Effect of melatonin on gap junction

As melatonin has been reported to modulate gap junction communication (Cos and Fernandez, 2000; Blackman et al., 2001), the effect of melatonin on gap junction was studied using Ussing chamber (Fig. 4.13). Heptanol has been added on both stromal and aqueous sides prior to melatonin administration. It was found that heptanol abolished Isc across the CBE preparation (N = 8, $p < 0.001$, one-way repeated measures ANOVA) and subsequent melatonin-induced Isc (N = 8, $p > 0.05$, one-way repeated measures ANOVA). The results indicated that melatonin might probably act on gap junctions to enhance the Isc.

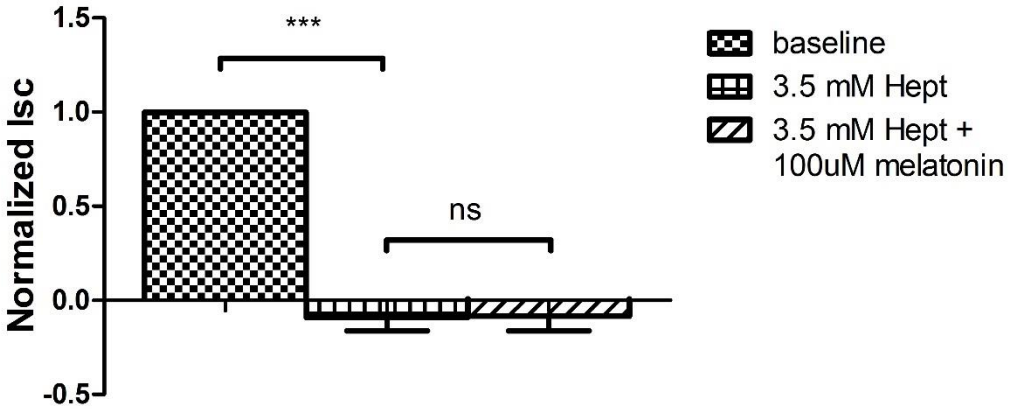

Fig. 4.13 Effect of heptanol pretreatment on melatonin-induced short-circuit current (Isc) response (N = 8, ns: not statistically significant, ***: $p < 0.001$, one-way repeated measures ANOVA). Hept: heptanol, added on both stromal and aqueous sides; melatonin: added on aqueous side.

To investigate whether melatonin-induced Isc stimulation was elicited by modulating of gap junction permeability, LY dye transfer technique was employed. Fig. 4.14 shows the relative fluorescence intensities (F ratios) of the two melatonin-treated groups (i.e. melatonin and melatonin pretreatment) and the control group throughout the 30-min recording period. Comparisons of the F ratios at selected time points were also summarized in Fig. 4.15. Our results showed that 100 μM melatonin significantly increased the gap junction permeability in porcine PE-NPE cells. As illustrated in Fig. 4.14, there were significant differences in F ratios between the melatonin and control groups after 15 min of dye transfer measurement. At 15 min, for example, the F ratios of the melatonin and the control groups were 2.64 ± 0.38 and 1.68 ± 0.15, respectively. This finding indicated that melatonin caused a 60% increase in F ratio compared with the control (Fig. 4.15, $p < 0.05$, one-way AONVA). In addition, pretreatment of 100 μM melatonin for 45 min also triggered a sustained increase in gap junction permeability. At 15 min, the F ratios of the melatonin-pretreated and the control groups were 3.06 ± 0.44 and 1.68 ± 0.15 respectively, suggesting an 80% increase in F ratio in the melatonin-pretreated group as compared with the control (Fig. 4.15, $p < 0.05$, one-way ANOVA). Although the F ratios of melatonin-pretreated group appeared higher than that of melatonin group at all time points, the differences between them were not statistically significant throughout the 30-min experimental period (Fig. 4.14 and Fig. 4.15, $p > 0.05$, one-way ANOVA).

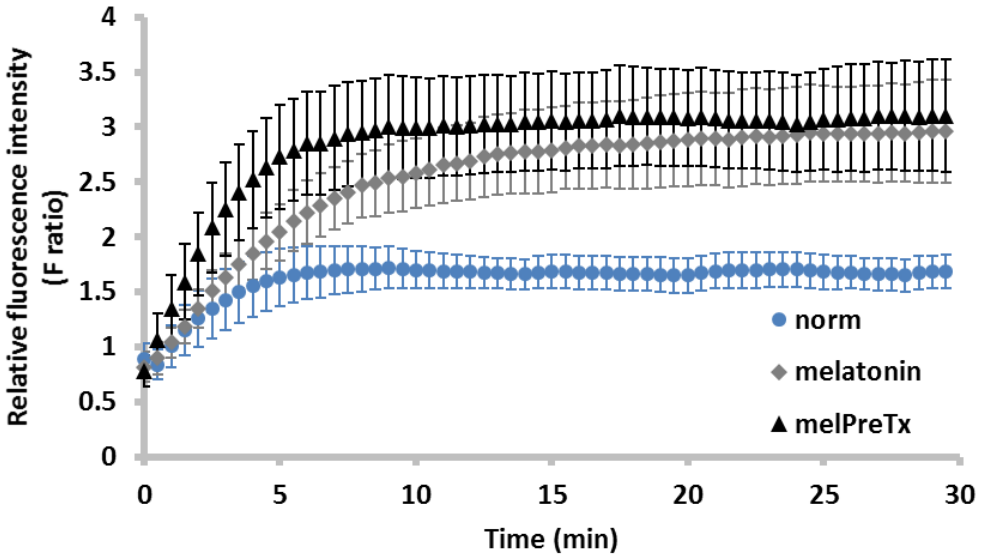

Fig. 4.14 Relative fluorescence intensity (F ratio) over time with melatonin treatment. norm: normal (N = 10); melatonin: 100 μM melatonin (N = 9); melPreTx: 100 μM melatonin pretreatment for 45 min (N = 7).

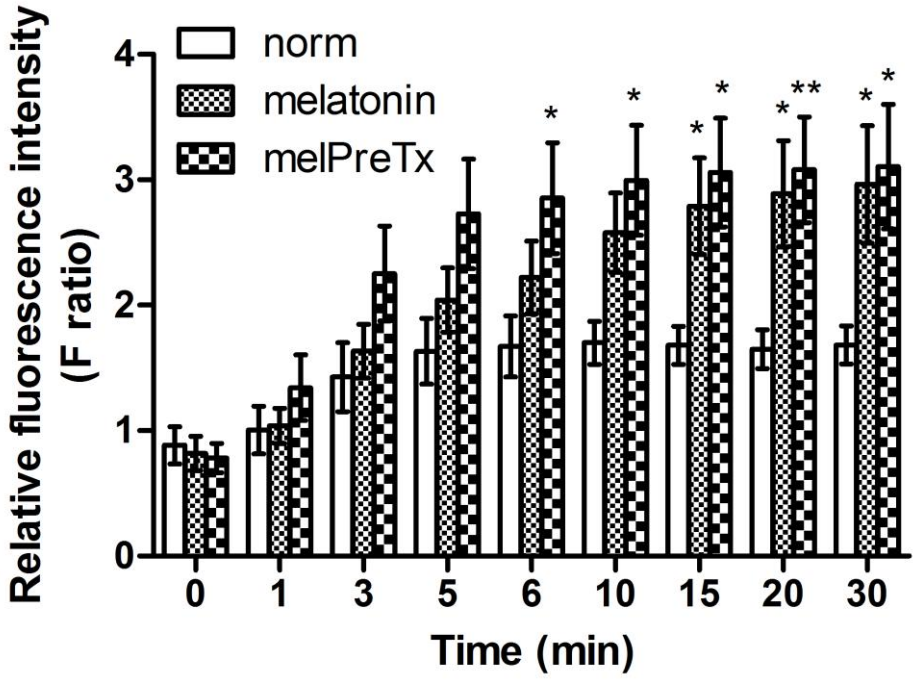

Fig. 4.15 Relative fluorescence intensity (F ratio) at selected time points with melatonin treatment (*: $p < 0.05$, **: $p < 0.01$, one-way ANOVA, compared to the norm at the same time point). norm: normal; melatonin (N = 10): 100 μM melatonin (N = 9); melPreTx:

100 μM melatonin pretreatment for 45 min (N = 7).

4.3.8 Effects of melatonin receptor antagonists on short-circuit current

Two melatonin receptors antagonists were used in this study: luzindole (10 μM), an MT_1/MT_2 receptor antagonist and prazosin (1.5 μM and 10 μM), a putative MT_3 receptor antagonist. Both antagonists were added to the aqueous side of the CBE preparation prior to 100 μM melatonin treatment (aqueous side).

Luzindole did not affect the baseline Isc, as shown in Fig. 4.16. The pretreatment of luzindole increased the melatonin-induced Isc stimulation paradoxically. The percentage increase of the normalized Isc with 10 μM luzindole pretreatment was 92 ± 19% compared to the baseline (N = 9, $p < 0.001$, one-way repeated measures ANOVA). This stimulatory effect on Isc was significantly larger than with melatonin alone (Fig. 4.17, $p < 0.05$, Student's t-test). In both cases, an addition of 1 mM NFA significantly inhibited the melatonin-induced Isc stimulation either in the presence (N = 5, $p < 0.001$, one-way repeated measures ANOVA) or absence of luzindole (N = 6, $p < 0.001$, one-way repeated measures ANOVA). The latency period for melatonin to take effect was not significantly different with or without luzindole pretreatment ($p > 0.44$, Student's t-test).

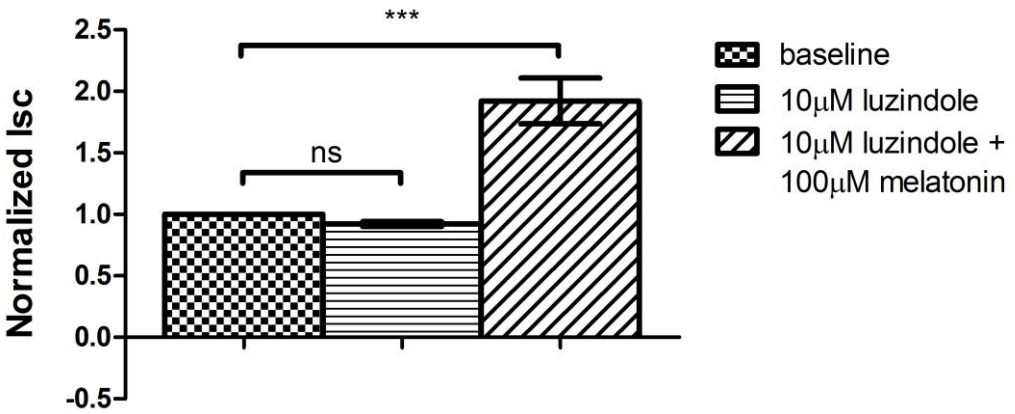

Fig. 4.16 Effect of luzindole pretreatment on melatonin-induced short-circuit current (Isc) response (N = 10, ns: not statistically significant, ***: $p < 0.001$, one-way repeated measures ANOVA). All drugs were added on the aqueous side.

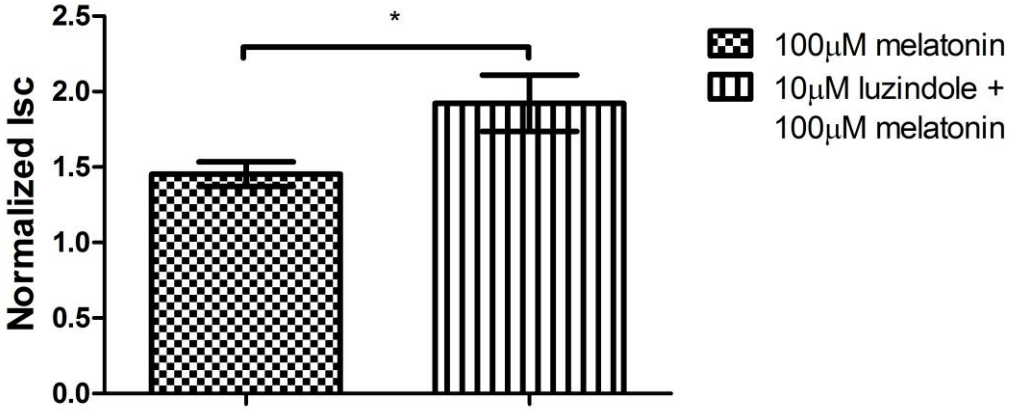

Fig. 4.17 Effects of melatonin on short-circuit current (Isc) with / without luzindole pretreatment (*: $p < 0.05$, Student's t-test). All drugs were added on the aqueous side.

In this study, two concentrations of prazosin (1.5 μM and 10 μM) were used. As illustrated in Fig. 4.18, at 1.5 μM, prazosin had no significant effects on both baseline Isc and the melatonin-induced Isc stimulation. At 10 μM, a pretreatment

of prazosin did not affect the baseline Isc but significantly inhibited the subsequent melatonin-induced Isc stimulation (Fig. 4.19, N = 10, $p > 0.05$, one-way repeated measures ANOVA). The effect of prazosin pretreatment on melatonin-induce Isc is summarized and compared with the preparations with no prazosin pretreatment in Fig. 4.20. For both conditions, the addition of 1 mM NFA abolished the Isc (N = 4 for 1.5 μM prazosin, N = 5 for 10 μM prazosin, $p < 0.001$, Student's t-test in both conditions), indicating the potential involvement of Cl^- secretion in melatonin-mediated response. Similar to luzindole, the latency periods of melatonin-triggered Isc response were similar between melatonin alone group and 1.5 μM prazosin-pretreated group ($p > 0.05$, Student's t-test).

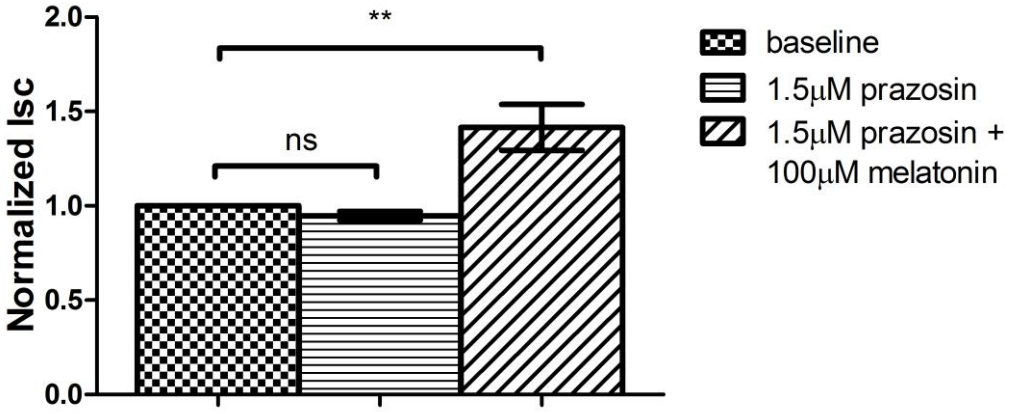

Fig. 4.18 Effect of 1.5 μM prazosin pretreatment on melatonin-induced short-circuit current (Isc) response (N = 10, ns: not statistically significant, **: $p < 0.01$, one-way repeated measures ANOVA). All drugs were added on the aqueous side.

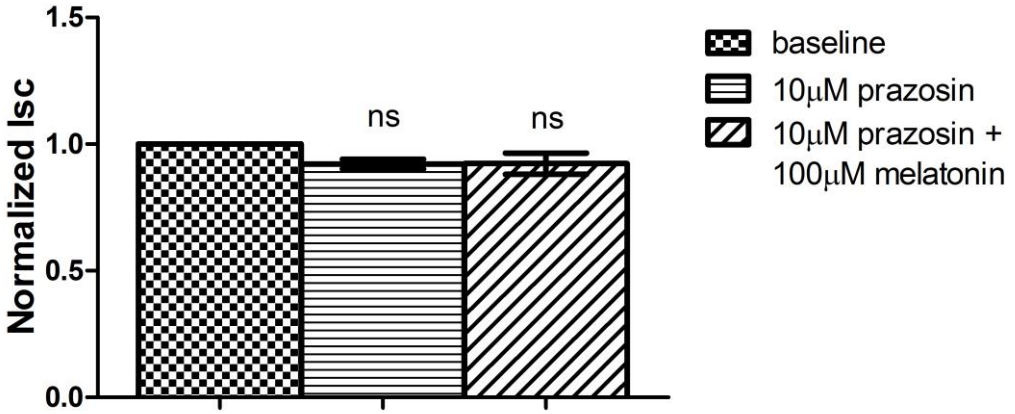

Fig. 4.19 Effect of 10 μM prazosin pretreatment on melatonin-induced short-circuit current (Isc) response (N = 10, ns: not statistically significant, one-way repeated measures ANOVA). All drugs were added on the aqueous side.

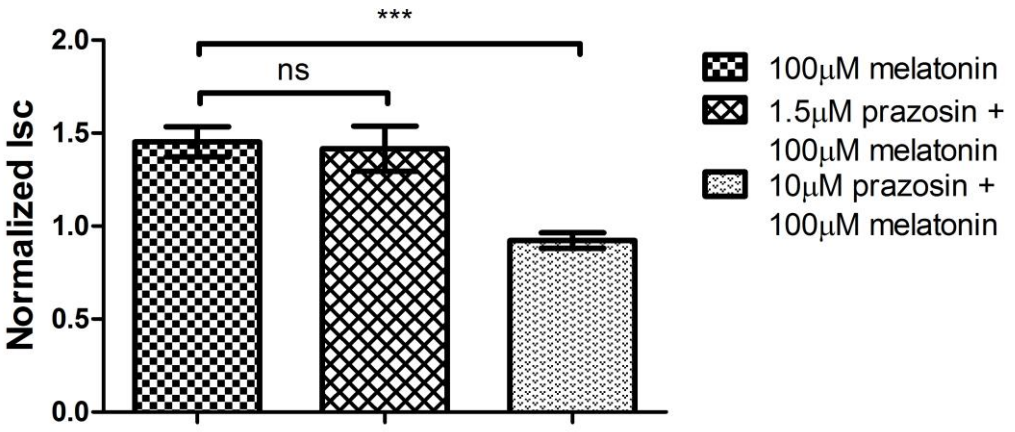

Fig. 4.20 Effects of melatonin on short-circuit current (Isc) with / without prazosin pretreatment (ns: not statistically significant, ***: $p < 0.001$, one-way ANOVA). All drugs were added on the aqueous side.

4.4 Discussion

4.4.1 Effect of temperature alternation on aqueous humor secretion

In this study, we have demonstrated that the Isc across porcine CBE was reversibly reduced by a half with a physiological temperature rise of 4°C. Heptanol abolished the temperature-induced Isc response, suggesting the potential involvement of the gap junctions in temperature-induced Isc alternation. Increasing the temperature by 4°C for 30 min significantly decreased the expression of Cx43 by approximately 15%, but did not alter the gap junction permeability across isolated PE-NPE cell couplets. Our findings suggest that gap junctions may not be a direct target responsible for the changes in AHF mediated by physiological temperature alternation.

4.4.1.1 Baseline transepithelial electrical parameters

Consistent with our previous studies (Kong et al., 2006; Cheng et al., 2016), a negative PD (i.e. aqueous side being more negative than stromal side) was observed across porcine CBE. The magnitudes of baseline PD and Isc were found to be -0.68 ± 0.08 mV and 11.31 ± 0.88 $\mu A \cdot cm^{-2}$, respectively. Similar results were also reported in other species such as dog (Iizuka et al., 1984), rabbit (Burstein et al., 1984; Krupin et al., 1984), ox (To et al., 1998b; Do and To, 2000) and human (Wu et al., 2013). The negative PD suggests that there is a net anion transport, possibly Cl^- or HCO_3^-, from ciliary stroma to the posterior chamber of the eye, as reflected by a higher concentration of Cl^- or HCO_3^- in the aqueous humor (Gerometta et al.,

2005; Civan, 2008).

4.4.1.2 Effect of temperature on short-circuit current

As shown in Table 4.2, increasing the temperature by 4°C inhibited the Isc by 46% (A) while reducing the temperature by 4°C increased the Isc by 80% (B). The temperature-mediated Isc responses were reversible when the temperature was returned to its initial level (Fig. 4.4 and Fig. 4.5). Our results showed that the group with an initial temperature of 22°C had a higher baseline PD and Isc compared to the group with an initial temperature of 26°C. This discrepancy was possibly attributed to the differences in initial temperatures. When the temperature was changed from either 22°C to 26°C or 26°C to 22°C, no statistically significant difference in PD and Isc was found between the two groups at the same temperatures. Moreover, the Rt from the two groups was similar, suggesting that the integrity of the tissues was comparable between groups.

At the beginning, we had attempted to use a higher bathing temperature to mimic the physiological temperatures. However, it was found that the PD across CBE tissue was reduced dramatically when the bathing temperature was increased to > 30°C, rendering it difficult to detect the Isc responses. Similar findings had also been reported previously in porcine CBE (Kong et al., 2006). Therefore, room temperatures, 22°C and 26°C were chosen as the studied temperatures and a fluctuation of 4°C likely reflected the diurnal temperature variation in the anterior eye.

Our results showed that the temperature-induced Isc responses were reversible in both directions (i.e. from 22°C to 26°C and from 26°C to 22°C). In addition, no significant changes of Rt were observed during temperature alternation, indicating that the Isc response did not result from tissue deterioration. Our findings were in agreement with the clinical observation that an increased ocular temperature at night due to eyelid closure might lead to an inhibition of AHF (Brubaker, 1998).

Although the Isc measured by Ussing chamber was considered as a good indicator of aqueous humor formation rate in porcine ciliary body epithelium (Kong et al., 2006; Candia et al., 2007; Cheng et al., 2016), other factors, such as electroneutral transporter Na^+-K^+-$2Cl^-$ co-transporter, may affect the fluid flow without altered Isc. Further experiments using fluid flow chamber can help confirm the change in fluid formation rate suggested by the change of Isc in our results (Candia et al., 2007). Also, in living organism, the intraocular pressure may affect aqueous inflow. Such a phenomenon was not reflected in our *in vitro* experiment. Thus, further animal study is needed to confirm our findings.

4.4.1.3 Effect of temperature on gap junction

As mentioned in CHAPTER 3, gap junctions play an important role in regulating solute and fluid movement across CE. We speculated that the changes in Isc might be mediated by the regulation of gap junction permeability. To address this hypothesis, we tested the effect of heptanol on temperature-induced Isc responses. As shown in Fig. 4.6 and Fig. 4.7, an addition of 3.5 mM heptanol abolished the subsequent Isc changes triggered by temperature alternation in both directions. These results suggested that gap junctions might contribute to the observed diurnal

changes in AHF.

Given the important role of Cx43 in mediating fluid flow from PE to NPE cells, we investigated the expression of Cx43 upon temperature alternation. To maintain the health of the CE cells, they were incubated in physiologically related temperatures and 4°C gap was adopted to mimic the diurnal physiological temperature variation in anterior eye. We demonstrated that there was a 13% decrease of Cx43 protein expression with 4°C temperature rise (Fig. 4.8) and a 16% increase in its expression with a temperature drop (Fig. 4.9). It has been shown that the degradation rate of Cx43 protein was very rapid with the half-life of 1 to 2 hours (Musil et al., 1990; Laird et al., 1991; Darrow et al., 1995), allowing faster detection of expression level changes within a short period. In our study, a short-term 30 min incubation period was chosen based upon the results obtained from the transepithelial measurements.

Our results were consistent with the previous studies in which the expression level of Cx43 could be influenced by the ambient temperature. It has been reported that Cx43 expression in heart ventricles increases significantly during hibernation (Saitongdee et al., 2000; Fedorov et al., 2005). Laing et al. (1998) also found that increasing the ambient temperature to 43.5°C for 30 min caused a drastic reduction in Cx43 expression in rat cardiac myocytes. However, a recent study conducted in golden hamster neural tube revealed that hyperthermia increased the expression of Cx43 (Zhang et al., 2012). This difference may be attributed, at least in part, to the species variation, heating conditions as well as methodology adopted.

Based on these findings, it is suspected that a decrease in Cx43 expression triggered by temperature rise may influence the fluid movement across the PE-NPE cell couplets. To test this hypothesis, we investigated the change in LY dye transfer rate

with temperature changes. In this study, freshly harvested porcine PE-NPE cell couplets were incubated at either 22°C or 26°C. The reason for choosing room temperatures instead of physiologically related temperatures was to maintain the same experimental condition as the other physiological experiment—Ussing chamber—adopted, for direct comparisons among these physiological experiments. The relative fluorescence ratio of NPE-to-PE (F ratio) was monitored over a period of 30 min. Our results showed no significant difference in F ratios at all time points between the 22°C and 26°C groups (Fig. 4.10), suggesting that the gap junction permeability was not altered at different temperatures. We wondered whether raising the temperature by 4°C in the same cell couplet affected the gap junction permeability. Measurement of dye transfer was conducted at 22°C for the initial 2.5 min and the temperature was changed to 26°C thereafter. As shown in Fig. 4.10, no significant changes in dye transfer rate were detected. Our results suggested that the change in gap junction permeability, if any, was not sufficient to be detected by LY dye transfer technique. It also implied that the temperature-induced Isc response may be mediated by a regulation of epithelial ion transport independent of gap junctions linked between PE and NPE cells.

The thermoTRP channels are one of the potential candidates that may be associated with temperature-induced Isc response. TRPV1 and TRPV4 channels have been identified in CE cells (Shahidullah et al., 2012; Martinez-Garcia et al., 2013; Alkozi and Pintor, 2015; Delamere et al., 2016). TRPV1 and TRPV4 are heat-sensitive channels that allow cation inflow, such as Ca^{2+} to trigger temperature sensation and response (Nilius and Flockerzi, 2014). Recently, TRPV4 has also been shown to involve in the swelling-activated Ca^{2+} influx in NPE cells (Jo et al., 2016), suggesting its functional significance in regulating AHF. Altogether, our results

showed that a small temperature variation of 4°C could lead to a significant change in Isc; thereby, potentially affecting the AHF rate. This finding was in line with the clinical observation that the reduction of AHF at night is possibly associated with an increase in anterior ocular temperature due to eyelid closure.

4.4.2 Effect of melatonin on aqueous humor secretion

It has been found that AHF rate is reduced at night, when the melatonin concentrations in the blood plasma and aqueous humor are elevated (Brubaker, 1998). This led our interest to explore whether there was a causative relationship between melatonin elevation and AHF reduction. Several studies have shown that topical administration of melatonin or its analogues could reduce IOP in rabbits and monkeys (Pintor et al., 2001; Serle et al., 2004; Martinez-Aguila et al., 2013). Human studies have also shown that an oral intake of melatonin or its analogues reduced IOP (Samples et al., 1988; Conway et al., 2000; Ismail and Mowafi, 2009; Pescosolido et al., 2015), even though AHF had not been found to be affected with melatonin intake (Viggiano et al., 1994).

4.4.2.1 Effect of melatonin on short-circuit current and gap junction permeability

Our results showed that an addition of 1 or 10 μM melatonin to both stromal and aqueous sides had no effect on Isc. At 100 μM, melatonin triggered an increase in Isc by 40%, which could subsequently be blocked by 1 mM NFA. An addition of melatonin to the aqueous side produced similar responses to that of melatonin administrated to both sides. This finding indicated that the effect of melatonin might

be primarily mediated in NPE cells. This was in agreement with a recent study that melatonin exerted its effect primarily on rabbit NPE cells (Huete-Toral et al., 2015). However, in that study, melatonin and its analogue 5-MCA-NAT were found to inhibit Cl^- efflux from NPE cells (Huete-Toral et al., 2015). This discrepancy could partly be explained by species differences. It has been suggested that species variation existed in the mechanism of ion transport across CE among different animals (Do and Civan, 2009). In rabbits, AHF is primarily driven by HCO_3^- secretion, and to a lesser extent by Cl^- transport (Gerometta et al., 2005). The inhibition of Cl^- efflux in NPE cells may not necessarily reflect a reduction in AHF (Crook et al., 2000). In contrast, AHF is primarily driven by Cl^- secretion in some other species such as ox, pig and human (Candia et al., 2005; Gerometta et al., 2005). It has been demonstrated that Isc was a good indicator to reflect the spontaneous fluid flow across CE in porcine eye (Candia et al., 2007). Our results also agreed with a previous study that melatonin stimulated Isc and Cl^- release in a human colonic cell line (Chan et al., 1998).

It has been demonstrated that melatonin plays an important role in regulating gap junction communication and permeability in many cell types (Ubeda et al., 1995; Kojima et al., 1997; Martinez and Saez, 2000; Blackman et al., 2001). We investigated whether the increase in Isc was mediated by a modulation of gap junction permeability in porcine PE-NPE cell couplets. In agreement with transepithelial measurements, our results showed that melatonin significantly increased the dye transfer across isolated cell couplets. The reported physiological concentration of melatonin in aqueous humor varied from pg/ml (Liu and Dacus, 1991; Chiquet et al., 2006) to ng/ml (Martin et al., 1992; Alkozi et al., 2016) in different studies, which might be due to different methods of measurement adopted.

Nevertheless, the concentration of melatonin we used fell within the working range adopted in the literatures (Kojima et al., 1997; Chan et al., 1998; Dortch-Carnes and Tosini, 2013; Huete-Toral et al., 2015; Martinez-Aguila et al., 2016). Our results suggest that melatonin increases gap junction permeability between PE and NPE cells, potentially facilitating the Cl^- secretion across porcine CE.

4.4.2.2 Effects of melatonin receptor antagonists on short-circuit current

Our results demonstrated that a pretreatment of 10 μM non-selective MT_1/MT_2 receptor antagonist luzindole did not block, but enhanced the melatonin-induced Isc stimulation. A pretreatment of 1.5 μM prazosin, an MT_3 receptor antagonist, had no effect on melatonin-induced Isc response; while at 10 μM, it abolished the Isc stimulation by melatonin. The absence of inhibitory effect exerted by luzindole suggested that melatonin did not act through MT_1/MT_2 receptors. Our findings were in good agreement with a recent study where the melatonin-induced Cl^- efflux by NPE cells was enhanced by MT_1/MT_2 receptor antagonists (Huete-Toral et al., 2015). In addition, when prazosin was added to the aqueous side at 1.5 μM, it failed to block melatonin-induced Isc stimulation. The inhibitory effect was only observed at a higher concentration of 10 μM. This finding was different from the study conducted by Huete-Toral et al., in which 1.5 μM prazosin was sufficient to inhibit the melatonin-mediated response. This difference can be explained by: 1) species difference in affinity to prazosin at the binding sites to trigger the response (Jerez et al., 2010; Angus and Wright, 2016; Peitzman et al., 2016); 2) difference in sample preparations as cultured NPE cells were used by Huete-Toral et al., whereas, CBE tissues were used in the present study. The intact CBE may have vitreous attached

to NPE cells, potentially acting as a barrier hindering the access of drug to the target site(s) (Cheng et al., 2016); and 3) diurnal variations in the expression level of melatonin receptors, as reported in other ocular tissues (Rada and Wiechmann, 2006). This may affect the amount of melatonin receptors available for antagonist interaction.

4.4.2.3 Potential mechanisms of melatonin-induced effect on aqueous humor secretion

Our *in vitro* findings suggest that melatonin may potentially increase Cl^- secretion and AHF rate, possibly through MT_3, not MT_1/MT_2 receptors. Melatonin-induced Isc stimulation may partly be mediated by an increase in gap junction permeability between PE and NPE cells (Cos and Fernandez, 2000; Blackman et al., 2001). Our findings were different from the clinical observation that melatonin lowers IOP in both experimental animals and humans (Samples et al., 1988; Pintor et al., 2001; Martinez-Aguila et al., 2016). In our study, isolated porcine CBE preparations were used. Therefore, possible influences from extraneous factors such as hydrostatic pressure, vascular and hormonal factors were eliminated. However, in living animals, the administration of melatonin and its analogues may not solely affect the ciliary epithelium, but also other ocular tissues around it. For example, melatonin was found to stimulate voltage dependent Na^+ current in cultured human TM cells (Rich et al., 1999), potentially influencing the outflow facility and IOP. In addition, oxidative stress has been shown to increase the aqueous humor outflow resistance by affecting the integrity of TM cells (Kahn et al., 1983; Zhou et al., 1999). The administration of melatonin as an antioxidant may help relieve oxidative stress (Hardeland, 2014), thus, it may help reduce the outflow resistance and ocular

hypertension (Zhou et al., 1999; Izzotti et al., 2003).

Furthermore, melatonin has been proposed to trigger physiological effects via various signaling pathways such as cAMP, phospholipase C, cGMP, Akt, and calmodulin (Godson and Reppert, 1997; Karlsson et al., 2000; Fukunaga et al., 2002; Choi et al., 2008; Hernandez-Pacheco et al., 2008; Luchetti et al., 2010). It is likely that melatonin may affect ion transporters or channels in addition to gap junctions, leading to an alteration of AHF rate. For example, Cl^- release from NPE cells is an important step for AHF (Do and Civan, 2004), although the identities of Cl^- channels have not been fully understood. In our study, the melatonin-induced Isc stimulation was completely blocked by NFA, suggesting that Cl^- channel might be a potential target for the regulation. Further studies are required to determine the mechanistic effects of melatonin and its antagonists on Cl^- channel activity in NPE cells.

In summary, melatonin was found to increase the gap junction permeability between PE and NPE cells. This may facilitate Cl^- secretion across porcine CBE. The stimulatory effect of melatonin on AHF was possibly mediated by MT_3 and not MT_1 and MT_2 receptors. Finally, temperature alternation and melatonin may potentially influence aqueous humor flow, but their associations with the observed diurnal changes in the aqueous humor flow and IOP await further investigation.

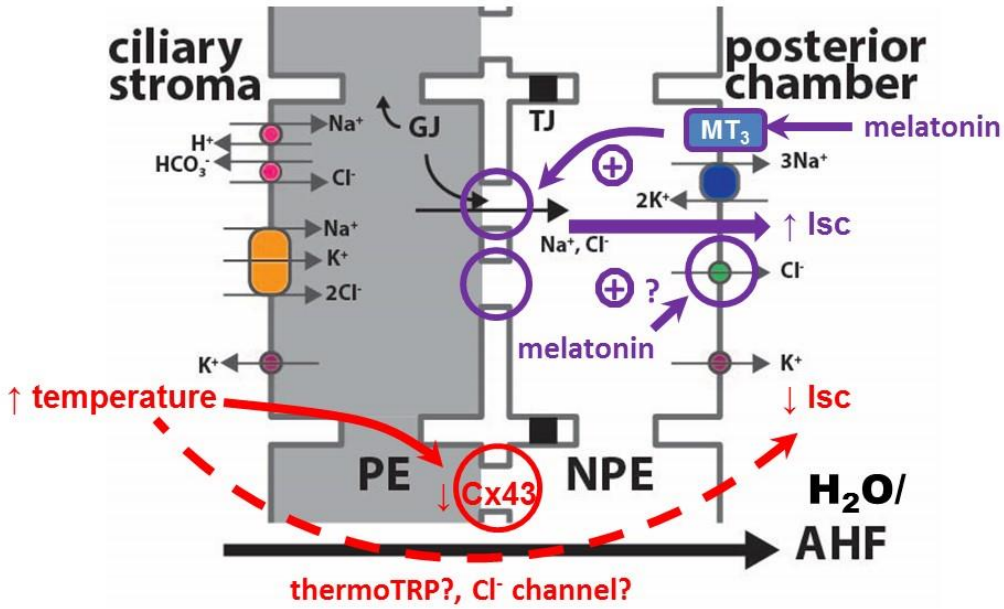

Fig. 4.21 Proposed pathways of the effects of temperature and melatonin on short-circuit current. PE: pigmented ciliary epithelium; NPE: non-pigmented epithelium. GJ: gap junction; TJ: tight junction; Isc: short-circuit current; MT_3: putative MT_3 receptor.

CHAPTER 5 Conclusion

In this study, we have investigated the effects of physiological temperature oscillation on the activity of matrix metalloproteinase-9 and -2 (MMP-9 and MMP-2) secreted from the human trabecular meshwork (hTM5) cells. In addition, the gap junction connexins in porcine ciliary epithelium were characterized and the effects of simulated physiological temperature alternation and melatonin on the aqueous humor inflow in porcine eyes studied.

We adopted that a temperature change of 4°C which mimicked the physiological temperature oscillation caused by eyelid closure during sleep and investigated its effects on the activity of secreted MMP-9 and MMP-2 from a transformed TM cell line (hTM5). Zymography results showed that raising the temperature by 4°C increased the activity of MMP-9 and MMP-2 and that the effects were reversible. Temperature cycling did not entrain the oscillations of the enzyme activity nor the oscillations of the expression of the clock genes *Cry2* and *Per2* in hTM5 cells. Our results suggested that the oscillations of the MMP activity did not display as a circadian rhythm with the peripheral clock located in the hTM5 cells. Heat shock transcription factor 1 (HSF1) inhibitor KNK437 reduced the MMP-9, but not the MMP-2 temperature cycling-driven oscillations. However, inhibition of TRPV1 or TRPM8 did not affect the oscillations of the MMP activity driven by temperature cycling. The alternation of MMP-9 and -2 activity in TM cells may potentially result in extracellular matrix (ECM) remodeling and thus influence the conventional outflow facility.

In addition to aqueous humor drainage, we have characterized the expression of gap junction connexins (Cxs) in porcine ciliary epithelium (CE) by RT-PCR and

Western blot (WB). Our results have demonstrated the presence of Cx43, Cx45, Cx47, Cx50 and Cx60 mRNAs and proteins in porcine CE. Cx43 was found to be the most abundantly expressed connexin in CE with over 200-fold greater presence than the other connexins. The connection of Cx43 to the PE and NPE layers was also shown structurally by immunohistochemistry. siRNA-mediated gene silencing of Cx43 significantly down-regulated the expression of Cx43 mRNA and protein in porcine CE cells. The knockdown of Cx43 also resulted in a significant reduction of the rate of fluid diffusion across the isolated PE-NPE cell couplets at a level comparable to a non-selective gap junction blocker heptanol treatment. The results support the important role of Cx43 in providing the major conduit for fluid transfer from PE to NPE cells in ciliary epithelium.

Furthermore, we have studied the temperature alternation and melatonin on the regulation of aqueous humor inflow. It was found that the short-circuit current (Isc) across porcine CE was significantly reduced by almost half when the temperature of the bathing solution was increased by 4°C. The inhibitory effect on Isc was fully reversible when the temperature was returned to its baseline value. Increasing the incubation temperature for 30 min reduced the protein expression of Cx43 in the ciliary epithelium, while decreasing the temperature showed the opposite effect. However, dye transfer experiment did not detect any changes in gap junction permeability by temperature alternation, suggesting that temperature might not target the gap junction.

As for inflow regulation by melatonin, we have found that melatonin stimulated the transepithelial measurements and promoted the fluid transfer across PE-NPE cell couplets. A pretreatment of the MT_1/MT_2 antagonist luzindole did not block, but further stimulated the melatonin-induced Isc. However, the pretreatment of putative

MT_3 receptor antagonist prazosin completely blocked the melatonin-induced Isc. Our findings indicate that melatonin facilitates the solute and fluid flow from PE to NPE cells, potentially through the putative MT_3 receptor.

Overall, our findings suggest that Cx43 provides the major route for fluid transfer from porcine PE to NPE cells. Temperature change and melatonin potentially influence the aqueous humor flow, but their associations with the observed diurnal changes in aqueous humor flow and IOP await further investigation.

References:

Abrams, C.K., Rash, J.E., 2009. Connexins in the Nervous System, in: Harris, A., Locke, D. (Eds.), Connexins: a Guide. Springer, New York, NY.

Acott, T.S., Kelley, M.J., 2008. Extracellular matrix in the trabecular meshwork. Exp Eye Res. 86, 543-561.

Akopian, A., Atlasz, T., Pan, F., Wong, S., Zhang, Y., Volgyi, B., Paul, D.L., Bloomfield, S.A., 2014. Gap junction-mediated death of retinal neurons is connexin and insult specific: a potential target for neuroprotection. J Neurosci. 34, 10582-10591.

Alarma-Estrany, P., Pintor, J., 2007. Melatonin receptors in the eye: location, second messengers and role in ocular physiology. Pharmacol Ther. 113, 507-522.

Alcantara-Contreras, S., Baba, K., Tosini, G., 2011. Removal of melatonin receptor type 1 increases intraocular pressure and retinal ganglion cells death in the mouse. Neurosci Lett. 494, 61-64.

Alkozi, H., Sanchez-Naves, J., de Lara, M.J., Carracedo, G., Fonseca, B., Martinez-Aguila, A., Pintor, J., 2016. Elevated intraocular pressure increases melatonin levels in the aqueous humour. Acta Ophthalmol. 95, e185-e189.

Alkozi, H.A., Pintor, J., 2015. TRPV4 activation triggers the release of melatonin from human non-pigmented ciliary epithelial cells. Exp Eye Res. 136, 34-37.

Angus, J.A., Wright, C.E., 2016. Novel α_1-adrenoceptor antagonism by the fluroquinolone antibiotic trovafloxacin. Eur J Pharmacol. 791, 179-184.

Arendt, J., Skene, D.J., Middleton, B., Lockley, S.W., Deacon, S., 1997. Efficacy of melatonin treatment in jet lag, shift work, and blindness. J Biol Rhythms. 12, 604-617.

Asejczyk-Widlicka, M., Pierscionek, B.K., 2007. Fluctuations in intraocular pressure and the potential effect on aberrations of the eye. Br J Ophthalmol. 91, 1054-1058.

Autzen, T., Larsen, F.E., Christensen, N.J., 1985. Human aqueous humor catecholamines. Curr Eye Res. 4, 1269-1271.

Aydin, E., Sahin, S., 2016. Increased melatonin levels in aqueous humor of patients with proliferative retinopathy in type 2 diabetes mellitus. Int J Ophthalmol. 9, 721-724.

Babizhayev, M.A., Brodskaya, M.W., 1989. Fibronectin detection in drainage outflow system of human eyes in ageing and progression of open-angle glaucoma. Mech Ageing Dev. 47, 145-157.

Balsalobre, A., Damiola, F., Schibler, U., 1998. A serum shock induces circadian gene expression in mammalian tissue culture cells. Cell. 93, 929-937.

Bartlett, J.D., Jaanus, S.D., 2008. Clinical Ocular Pharmacology, 5th ed. Butterworth-Heinemann/Elsevier, St. Louis, MO.

Beauchemin, M.L., 1974. The fine structure of the pig's retina. Albrecht Von Graefes Arch Klin Exp Ophthalmol. 190, 27-45.

Becker, B., 1961. The effect of hypothermia on aqueous humor dynamics. III. Turnover of ascorbate and sodium. Am J Ophthalmol. 51, 1032-1039.

Becker, B., 1963. Ouabain and Aqueous Humor Dynamics in the Rabbit Eye. Invest Ophthalmol. 2, 325-331.

Behar-Cohen, F.F., Goureau, O., D'Hermies, F., Courtois, Y., 1996. Decreased intraocular pressure induced by nitric oxide donors is correlated to nitrite production in the rabbit eye. Invest Ophthalmol Vis Sci. 37, 1711-1715.

Behrendt, H.J., Germann, T., Gillen, C., Hatt, H., Jostock, R., 2004. Characterization of the mouse cold-menthol receptor TRPM8 and vanilloid receptor type-1 VR1 using a fluorometric imaging plate reader (FLIPR) assay. Br J Pharmacol. 141, 737-745.

Beyer, E., Berthoud, V.M., 2009. The Family of Connexin Genes, in: Harris, A., Locke, D. (Eds.), Connexins: a Guide. New York, NY, New York, NY.

Bill, A., 1966. Conventional and uveo-scleral drainage of aqueous humour in the cynomolgus monkey (Macaca irus) at normal and high intraocular pressures. Exp Eye Res. 5, 45-54.

Bill, A., 1975. Blood circulation and fluid dynamics in the eye. Physiol Rev. 55, 383-417.

Bill, A., Phillips, C.I., 1971. Uveoscleral drainage of aqueous humour in human eyes. Exp Eye Res. 12, 275-281.

Blackman, C.F., Andrews, P.W., Ubeda, A., Wang, X., House, D.E., Trillo, M.A., Pimentel, M.E., 2001. Physiological levels of melatonin enhance gap junction communication in primary cultures of mouse hepatocytes. Cell Biol Toxicol. 17, 1-9.

Boussommier-Calleja, A., 2013. Mouse models of intraocular pressure, with applications to glaucoma, Department of Bioengineering. Imperial College London, London.

Boussommier-Calleja, A., Li, G., Wilson, A., Ziskind, T., Scinteie, O.E., Ashpole, N.E., Sherwood, J.M., Farsiu, S., Challa, P., Gonzalez, P., Downs, J.C., Ethier, C.R., Stamer, W.D., Overby, D.R., 2015. Physical Factors Affecting Outflow Facility Measurements in Mice. Invest Ophthalmol Vis Sci. 56, 8331-8339.

Bowler, J.M., Peart, D., Purves, R.D., Carre, D.A., Macknight, A.D., Civan, M.M., 1996. Electron probe X-ray microanalysis of rabbit ciliary epithelium. Exp Eye Res. 62, 131-139.

Bradley, J.M., Anderssohn, A.M., Colvis, C.M., Parshley, D.E., Zhu, X.H., Ruddat, M.S., Samples, J.R., Acott, T.S., 2000. Mediation of laser trabeculoplasty-induced matrix metalloproteinase expression by IL-1β and TNFα. Invest Ophthalmol Vis Sci. 41, 422-430.

Bradley, J.M., Kelley, M.J., Zhu, X., Anderssohn, A.M., Alexander, J.P., Acott, T.S., 2001. Effects of mechanical stretching on trabecular matrix metalloproteinases. Invest Ophthalmol Vis Sci. 42, 1505-1513.

Bradley, J.M., Vranka, J., Colvis, C.M., Conger, D.M., Alexander, J.P., Fisk, A.S.,

Samples, J.R., Acott, T.S., 1998. Effect of matrix metalloproteinases activity on outflow in perfused human organ culture. Invest Ophthalmol Vis Sci. 39, 2649-2658.

Brink, P.R., Valiunas, V., Christ, G.J., 2000. Homotypic, Heterotypic, and Heteromeric Gap Junction Channels, in: Peracchia, C. (Ed.), Gap Junctions : Molecular Basis of Cell Communication in Health and Disease. Academic Press, San Diego, pp. 43-60.

Brubaker, R.F., 1991. Flow of aqueous humor in humans [The Friedenwald Lecture]. Invest Ophthalmol Vis Sci. 32, 3145-3166.

Brubaker, R.F., 1998. Clinical measurement of aqueous dynamics: implications for addressing glaucoma, in: Civan, M.M. (Ed.), The eye's aqueous humor : from secretion to glaucoma. Academic Press,, San Diego.

Buhr, E.D., Takahashi, J.S., 2013. Molecular Components of the Mammalian Circadian Clock, in: Kramer, A., Merrow, M. (Eds.), Circadian Clocks. Springer, Heidelberg, pp. 3-27.

Buhr, E.D., Yoo, S.H., Takahashi, J.S., 2010. Temperature as a universal resetting cue for mammalian circadian oscillators. Science. 330, 379-385.

Burstein, N.L., Fischbarg, J., Liebovitch, L., Cole, D.F., 1984. Electrical potential, resistance, and fluid secretion across isolated ciliary body. Exp Eye Res. 39, 771-779.

Calera, M.R., Topley, H.L., Liao, Y., Duling, B.R., Paul, D.L., Goodenough, D.A., 2006. Connexin43 is required for production of the aqueous humor in the murine eye. J Cell Sci. 119, 4510-4519.

Calera, M.R., Wang, Z., Sanchez-Olea, R., Paul, D.L., Civan, M.M., Goodenough, D.A., 2009. Depression of intraocular pressure following inactivation of connexin43 in the nonpigmented epithelium of the ciliary body. Invest Ophthalmol Vis Sci. 50, 2185-2193.

Candia, O.A., To, C.H., Gerometta, R.M., Zamudio, A.C., 2005. Spontaneous fluid transport across isolated rabbit and bovine ciliary body preparations. Invest

Ophthalmol Vis Sci. 46, 939-947.

Candia, O.A., To, C.H., Law, C.S., 2007. Fluid transport across the isolated porcine ciliary epithelium. Invest Ophthalmol Vis Sci. 48, 321-327.

Carter, T.D., Chen, X.Y., Carlile, G., Kalapothakis, E., Ogden, D., Evans, W.H., 1996. Porcine aortic endothelial gap junctions: identification and permeation by caged InsP3. J Cell Sci. 109, 1765-1773.

Caterina, M.J., Leffler, A., Malmberg, A.B., Martin, W.J., Trafton, J., Petersen-Zeitz, K.R., Koltzenburg, M., Basbaum, A.I., Julius, D., 2000. Impaired nociception and pain sensation in mice lacking the capsaicin receptor. Science. 288, 306-313.

Challet, E., 2015. Keeping circadian time with hormones. Diabetes Obes Metab. 17 Suppl 1, 76-83.

Chan, H.C., Lui, K.M., Wong, W.S., Poon, A.M., 1998. Effect of melatonin on chloride secretion by human colonic T84 cells. Life Sci. 62, 2151-2158.

Chen, Y.S., Green, C.R., Danesh-Meyer, H.V., Rupenthal, I.D., 2015a. Neuroprotection in the treatment of glaucoma-A focus on connexin43 gap junction channel blockers. Eur J Pharm Biopharm. 95, 182-193.

Chen, Y.S., Green, C.R., Wang, K., Danesh-Meyer, H.V., Rupenthal, I.D., 2015b. Sustained intravitreal delivery of connexin43 mimetic peptide by poly(D,L-lactide-co-glycolide) acid micro- and nanoparticles - Closing the gap in retinal ischaemia. Eur J Pharm Biopharm. 95, 378-386.

Cheng, A.K., Civan, M.M., To, C.H., Do, C.W., 2016. cAMP Stimulates Transepithelial Short-Circuit Current and Fluid Transport Across Porcine Ciliary Epithelium. Invest Ophthalmol Vis Sci. 57, 6784-6794.

Chiquet, C., Claustrat, B., Thuret, G., Brun, J., Cooper, H.M., Denis, P., 2006. Melatonin concentrations in aqueous humor of glaucoma patients. Am J Ophthalmol. 142, 325-327.

Choi, S.I., Joo, S.S., Yoo, Y.M., 2008. Melatonin prevents nitric oxide-induced apoptosis by increasing the interaction between 14-3-3β and p-Bad in SK-N-MC

cells. J Pineal Res. 44, 95-100.

Chowdhury, S., Jarecki, B.W., Chanda, B., 2014. A molecular framework for temperature-dependent gating of ion channels. Cell. 158, 1148-1158.

Chu, T.C., Candia, O.A., 1987. Electrically silent Na^+ and Cl^- fluxes across the rabbit ciliary epithelium. Invest Ophthalmol Vis Sci. 28, 445-450.

Civan, M.M., 1998. The eye's aqueous humor : from secretion to glaucoma. Academic Press, San Diego.

Civan, M.M., 2003. The fall and rise of active chloride transport: implications for regulation of intraocular pressure. J Exp Zool A Comp Exp Biol. 300, 5-13.

Civan, M.M., 2008. Formation of the Aqueous Humor: Transport Components and Their Integration, in: Civan, M.M. (Ed.), The eye's aqueous humor. Academic Press, San Diego.

Civitelli, R., Donahue, H.J., 2009. Connexins in the Nervous System, in: Harris, A., Locke, D. (Eds.), Connexins: a Guide. Humana Press, New York.

Clapham, D.E., 2003. TRP channels as cellular sensors. Nature. 426, 517-524.

Clark, A.F., Brotchie, D., Read, A.T., Hellberg, P., English-Wright, S., Pang, I.H., Ethier, C.R., Grierson, I., 2005. Dexamethasone alters F-actin architecture and promotes cross-linked actin network formation in human trabecular meshwork tissue. Cell Motil Cytoskeleton. 60, 83-95.

Clark, A.F., Miggans, S.T., Wilson, K., Browder, S., McCartney, M.D., 1995. Cytoskeletal changes in cultured human glaucoma trabecular meshwork cells. J Glaucoma. 4, 183-188.

Claustrat, B., 2014. Melatonin: An introduction to Its Physiological and Pharmacological Effects in Humans, in: Srinivasan, V., Brzezinski, A., Oter, S., Shillcutt, S. (Eds.), Melatonin and Melatonergic Drugs in Clinical Practice. Springer, New Delhi.

Coca-Prados, M., Ghosh, S., 2008. Functional Modulators Linking Inflow with

Outflow of Aqueous Humor, in: Civan, M.M. (Ed.), The eye's aqueous humor. Academic Press, San Diego.

Coca-Prados, M., Ghosh, S., Gilula, N.B., Kumar, N.M., 1992. Expression and cellular distribution of the α1 gap junction gene product in the ocular pigmented ciliary epithelium. Curr Eye Res. 11, 113-122.

Coffey, K.L., Krushinsky, A., Green, C.R., Donaldson, P.J., 2002. Molecular profiling and cellular localization of connexin isoforms in the rat ciliary epithelium. Exp Eye Res. 75, 9-21.

Cohen, A.I., 1982. Increased levels of 3',5'-cyclic adenosine monophosphate induced by cobaltous ion or 3-isobutylmethylxanthine in the incubated mouse retina: evidence concerning location and response to ions and light. J Neurochem. 38, 781-796.

Cole, D.F., 1962. Transport across the Isolated Ciliary Body of Ox and Rabbit. Br J Ophthalmol. 46, 577-591.

Cole, D.F., 1977. Secretion of the aqueous humour. Exp Eye Res. 25 Suppl, 161-176.

Collaborative Normal-Tension Glaucoma Study Group, 1998a. Comparison of glaucomatous progression between untreated patients with normal-tension glaucoma and patients with therapeutically reduced intraocular pressures. Collaborative Normal-Tension Glaucoma Study Group. Am J Ophthalmol. 126, 487-497.

Collaborative Normal-Tension Glaucoma Study Group, 1998b. The effectiveness of intraocular pressure reduction in the treatment of normal-tension glaucoma. Collaborative Normal-Tension Glaucoma Study Group. Am J Ophthalmol. 126, 498-505.

Conway, S., Canning, S.J., Howell, H.E., Mowat, E.S., Barrett, P., Drew, J.E., Delagrange, P., Lesieur, D., Morgan, P.J., 2000. Characterisation of human melatonin mt_1 and MT_2 receptors by CRE-luciferase reporter assay. Eur J Pharmacol. 390, 15-24.

Cooper, R.L., Constable, I.J., Davidson, L., 1984. Aqueous humor catecholamines. Curr Eye Res. 3, 809-813.

Cordeiro, S., Seyler, S., Stindl, J., Milenkovic, V.M., Strauss, O., 2010. Heat-sensitive TRPV channels in retinal pigment epithelial cells: regulation of VEGF-A secretion. Invest Ophthalmol Vis Sci. 51, 6001-6008.

Cos, S., Fernandez, R., 2000. Melatonin effects on intercellular junctional communication in MCF-7 human breast cancer cells. J Pineal Res. 29, 166-171.

Counillon, L., Touret, N., Bidet, M., Peterson-Yantorno, K., Coca-Prados, M., Stuart-Tilley, A., Wilhelm, S., Alper, S.L., Civan, M.M., 2000. Na^+/H^+ and CI^-/HCO_3^- antiporters of bovine pigmented ciliary epithelial cells. Pflugers Arch. 440, 667-678.

Crambert, G., Hasler, U., Beggah, A.T., Yu, C., Modyanov, N.N., Horisberger, J.D., Lelievre, L., Geering, K., 2000. Transport and pharmacological properties of nine different human Na, K-ATPase isozymes. J Biol Chem. 275, 1976-1986.

Crawford, H.C., Stack, M.S., 2015. Matrix Metalloproteinase Modification of Extracellular Matrix-Mediated Signaling, in: Sagi, I., Gaffney, J.P. (Eds.), Matrix Metalloproteinase Biology. Wiley-Blackwell, Hoboken, pp. 103-113.

Cronin, M., Anderson, P.N., Cook, J.E., Green, C.R., Becker, D.L., 2008. Blocking connexin43 expression reduces inflammation and improves functional recovery after spinal cord injury. Mol Cell Neurosci. 39, 152-160.

Crook, R.B., Takahashi, K., Mead, A., Dunn, J.J., Sears, M.L., 2000. The role of NaKCl cotransport in blood-to-aqueous chloride fluxes across rabbit ciliary epithelium. Invest Ophthalmol Vis Sci. 41, 2574-2583.

Dailey, R.A., Brubaker, R.F., Bourne, W.M., 1982. The effects of timolol maleate and acetazolamide on the rate of aqueous formation in normal human subjects. Am J Ophthalmol. 93, 232-237.

Dan, J., Belyea, D., Gertner, G., Leshem, I., Lusky, M., Miskin, R., 2005. Plasminogen activator inhibitor-1 in the aqueous humor of patients with and without glaucoma. Arch Ophthalmol. 123, 220-224.

Danesh-Meyer, H.V., Huang, R., Nicholson, L.F., Green, C.R., 2008. Connexin43 antisense oligodeoxynucleotide treatment down-regulates the inflammatory response in an in vitro interphase organotypic culture model of optic nerve ischaemia. J Clin Neurosci. 15, 1253-1263.

Danesh-Meyer, H.V., Kerr, N.M., Zhang, J., Eady, E.K., O'Carroll, S.J., Nicholson, L.F., Johnson, C.S., Green, C.R., 2012. Connexin43 mimetic peptide reduces vascular leak and retinal ganglion cell death following retinal ischaemia. Brain. 135, 506-520.

Darrow, B.J., Laing, J.G., Lampe, P.D., Saffitz, J.E., Beyer, E.C., 1995. Expression of multiple connexins in cultured neonatal rat ventricular myocytes. Circ Res. 76, 381-387.

De Groef, L., Van Hove, I., Dekeyster, E., Stalmans, I., Moons, L., 2013. MMPs in the trabecular meshwork: promising targets for future glaucoma therapies? Invest Ophthalmol Vis Sci. 54, 7756-7763.

De Groef, L., Van Hove, I., Dekeyster, E., Stalmans, I., Moons, L., 2014. MMPs in the neuroretina and optic nerve: modulators of glaucoma pathogenesis and repair? Invest Ophthalmol Vis Sci. 55, 1953-1964.

De Wit, C., Wolfle, S.E., 2009. Connexins in the Vasculature, in: Harris, A., Locke, D. (Eds.), Connexins: a Guide. Springer, New York.

Delamere, N.A., Mandal, A., Shahidullah, M., 2016. The Significance of TRPV4 Channels and Hemichannels in the Lens and Ciliary Epithelium. J Ocul Pharmacol Ther. 32, 504-508.

DeRosa, A.M., Mese, G., Li, L., Sellitto, C., Brink, P.R., Gong, X., White, T.W., 2009. The cataract causing Cx50-S50P mutant inhibits Cx43 and intercellular communication in the lens epithelium. Exp Cell Res. 315, 1063-1075.

Dhaka, A., Murray, A.N., Mathur, J., Earley, T.J., Petrus, M.J., Patapoutian, A., 2007. TRPM8 is required for cold sensation in mice. Neuron. 54, 371-378.

Diamond, J.M., Bossert, W.H., 1967. Standing-gradient osmotic flow. A mechanism for coupling of water and solute transport in epithelia. J Gen Physiol. 50, 2061-

2083.

Do, C.W., Civan, M.M., 2004. Basis of chloride transport in ciliary epithelium. J Membr Biol. 200, 1-13.

Do, C.W., Civan, M.M., 2009. Species variation in biology and physiology of the ciliary epithelium: similarities and differences. Exp Eye Res. 88, 631-640.

Do, C.W., To, C.H., 2000. Chloride secretion by bovine ciliary epithelium: a model of aqueous humor formation. Invest Ophthalmol Vis Sci. 41, 1853-1860.

Dortch-Carnes, J., Tosini, G., 2013. Melatonin receptor agonist-induced reduction of SNP-released nitric oxide and cGMP production in isolated human non-pigmented ciliary epithelial cells. Exp Eye Res. 107, 1-10.

Duke-Elder, S., 1968. The physiology of eye and vision, in: Duke-Elder, S. (Ed.), System of Ophthalmology, vol 4, pp. 164–168.

Dunlap, J.C., 2004. Molecular Biology of Circadian Pacemaker Systems, in: Dunlap, J.C., Loros, J.J., DeCoursey, P.J. (Eds.), Chronobiology: Biological Timekeeper. Sinauer Associates, Inc, Sunderland, Massachusetts.

Dunn, J.J., Lytle, C., Crook, R.B., 2001. Immunolocalization of the Na-K-Cl cotransporter in bovine ciliary epithelium. Invest Ophthalmol Vis Sci. 42, 343-353.

Edery, I., 2010. Circadian rhythms. Temperatures to communicate by. Science. 330, 329-330.

Ekmekcioglu, C., Thalhammer, T., 2014. Melatonin Receptors and Their Role in Human Diseaes, in: Srinivasan, V., Brzezinski, A., Oter, S., Shillcutt, S. (Eds.), Melatonin and Melatonergic Drugs in Clinical Practice. Springer, New Delhi.

Elbadawy, H.M., Mirabelli, P., Xeroudaki, M., Parekh, M., Bertolin, M., Breda, C., Cagini, C., Ponzin, D., Lagali, N., Ferrari, S., 2016. Effect of Connexin 43 inhibition by the mimetic peptide Gap27 on corneal wound healing, inflammation and neovascularization. Br J Pharmacol. 173, 2880-2893.

Everaerts, W., Zhen, X., Ghosh, D., Vriens, J., Gevaert, T., Gilbert, J.P., Hayward,

N.J., McNamara, C.R., Xue, F., Moran, M.M., Strassmaier, T., Uykal, E., Owsianik, G., Vennekens, R., De Ridder, D., Nilius, B., Fanger, C.M., Voets, T., 2010. Inhibition of the cation channel TRPV4 improves bladder function in mice and rats with cyclophosphamide-induced cystitis. Proc Natl Acad Sci U S A. 107, 19084-19089.

Fedorov, V.V., Li, L., Glukhov, A., Shishkina, I., Aliev, R.R., Mikheeva, T., Nikolski, V.P., Rosenshtraukh, L.V., Efimov, I.R., 2005. Hibernator Citellus undulatus maintains safe cardiac conduction and is protected against tachyarrhythmias during extreme hypothermia: possible role of Cx43 and Cx45 up-regulation. Heart Rhythm. 2, 966-975.

Filla, M.S., Schwinn, M.K., Sheibani, N., Kaufman, P.L., Peters, D.M., 2009. Regulation of cross-linked actin network (CLAN) formation in human trabecular meshwork (HTM) cells by convergence of distinct β1 and β3 integrin pathways. Invest Ophthalmol Vis Sci. 50, 5723-5731.

Firouzi, M., Ramanna, H., Kok, B., Jongsma, H.J., Koeleman, B.P., Doevendans, P.A., Groenewegen, W.A., Hauer, R.N., 2004. Association of human connexin40 gene polymorphisms with atrial vulnerability as a risk factor for idiopathic atrial fibrillation. Circ Res. 95, e29-33.

Fleenor, D.L., Pang, I.H., Clark, A.F., 2003. Involvement of AP-1 in interleukin-1alpha-stimulated MMP-3 expression in human trabecular meshwork cells. Invest Ophthalmol Vis Sci. 44, 3494-3501.

Friedenwald, J.S., 1949. The formation of the intraocular fluid. Am J Ophthalmol. 32 Pt. 2, 9-27.

Fujimoto, T., Inoue, T., Inoue-Mochita, M., Tanihara, H., 2016. Live cell imaging of actin dynamics in dexamethasone-treated porcine trabecular meshwork cells. Exp Eye Res. 145, 393-400.

Fukuhara, C., Liu, C., Ivanova, T.N., Chan, G.C., Storm, D.R., Iuvone, P.M., Tosini, G., 2004. Gating of the cAMP signaling cascade and melatonin synthesis by the circadian clock in mammalian retina. J Neurosci. 24, 1803-1811.

Fukunaga, K., Horikawa, K., Shibata, S., Takeuchi, Y., Miyamoto, E., 2002.

Ca^{2+}/calmodulin-dependent protein kinase II-dependent long-term potentiation in the rat suprachiasmatic nucleus and its inhibition by melatonin. J Neurosci Res. 70, 799-807.

Garnock-Jones, K.P., 2014. Ripasudil: first global approval. Drugs. 74, 2211-2215.

Gehr, B.T., Weiss, C., Porzsolt, F., 2006. The fading of reported effectiveness. A meta-analysis of randomised controlled trials. BMC Med Res Methodol. 6, 25.

Geiser, M.H., Bonvin, M., Quibel, O., 2004. Corneal and retinal temperatures under various ambient conditions: a model and experimental approach. Klin Monbl Augenheilkd. 221, 311-314.

Geoffriau, M., Claustrat, B., Veldhuis, J., 1999. Estimation of frequently sampled nocturnal melatonin production in humans by deconvolution analysis: evidence for episodic or ultradian secretion. J Pineal Res. 27, 139-144.

Gerometta, R., Spiga, M.G., Borras, T., Candia, O.A., 2010. Treatment of sheep steroid-induced ocular hypertension with a glucocorticoid-inducible MMP1 gene therapy virus. Invest Ophthalmol Vis Sci. 51, 3042-3048.

Gerometta, R.M., Malgor, L.A., Vilalta, E., Leiva, J., Candia, O.A., 2005. Cl- concentrations of bovine, porcine and ovine aqueous humor are higher than in plasma. Exp Eye Res. 80, 307-312.

Ghosh, S., Hernando, N., Martin-Alonso, J.M., Martin-Vasallo, P., Coca-Prados, M., 1991. Expression of multiple Na^+,K^+-ATPase genes reveals a gradient of isoforms along the nonpigmented ciliary epithelium: functional implications in aqueous humor secretion. J Cell Physiol. 149, 184-194.

Glynn, I.M., 2002. A hundred years of sodium pumping. Annu Rev Physiol. 64, 1-18.

Godson, C., Reppert, S.M., 1997. The Mel_{1a} melatonin receptor is coupled to parallel signal transduction pathways. Endocrinology. 138, 397-404.

Gollob, M.H., Jones, D.L., Krahn, A.D., Danis, L., Gong, X.Q., Shao, Q., Liu, X., Veinot, J.P., Tang, A.S., Stewart, A.F., Tesson, F., Klein, G.J., Yee, R., Skanes, A.C.,

Guiraudon, G.M., Ebihara, L., Bai, D., 2006. Somatic mutations in the connexin 40 gene (GJA5) in atrial fibrillation. N Engl J Med. 354, 2677-2688.

Gong, H., Tripathi, R.C., Tripathi, B.J., 1996. Morphology of the aqueous outflow pathway. Microsc Res Tech. 33, 336-367.

Grieshaber, M.C., Pienaar, A., Olivier, J., Stegmann, R., 2010. Clinical evaluation of the aqueous outflow system in primary open-angle glaucoma for canaloplasty. Invest Ophthalmol Vis Sci. 51, 1498-1504.

Guo, M.S., Wu, Y.Y., Liang, Z.B., 2012. Hyaluronic acid increases MMP-2 and MMP-9 expressions in cultured trabecular meshwork cells from patients with primary open-angle glaucoma. Mol Vis. 18, 1175-1181.

Guo, Y., Ma, J., Wu, L., Wang, Q., Li, X., Li, X., Zhang, Y., Zhang, J., Yao, L., Zhang, J., Liu, W., 2013. Hyperthermia-induced NDRG2 upregulation inhibits the invasion of human hepatocellular carcinoma via suppressing ERK1/2 signaling pathway. PLoS One. 8, e61079.

Hamelin, P., 1987. Lorry driver's time habits in work and their involvement in traffic accidents. Ergonomics. 30, 1323-1333.

Hardeland, R., 2014. Melatonin's Antioxidant Properties: Molecular Mechanisms, in: Srinivasan, V., Brzezinski, A., Oter, S., Shillcutt, S. (Eds.), Melatonin and Melatonergic Drugs in Clinical Practice. Springer, New Delhi.

Harris, A., Locke, D., 2009. Permeability of Connexin Channels, in: Harris, A., Locke, D. (Eds.), Connexins: a Guide. Springer, New York.

Hawkes, S.P., Li, H., Taniguchi, G.T., 2010. Zymography and reverse zymography for detecting MMPs and TIMPs. Methods Mol Biol. 622, 257-269.

Helbig, H., Korbmacher, C., Erb, C., Nawrath, M., Knuuttila, K.G., Wistrand, P., Wiederholt, M., 1989. Coupling of ^{22}Na and ^{36}Cl uptake in cultured pigmented ciliary epithelial cells: a proposed role for the isoenzymes of carbonic anhydrase. Curr Eye Res. 8, 1111-1119.

Hernandez-Pacheco, A., Araiza-Saldana, C.I., Granados-Soto, V., Mixcoatl-Zecuatl,

T., 2008. Possible participation of the nitric oxide-cyclic GMP-protein kinase G-K^+ channels pathway in the peripheral antinociception of melatonin. Eur J Pharmacol. 596, 70-76.

Hoare, M.J., Grierson, I., Brotchie, D., Pollock, N., Cracknell, K., Clark, A.F., 2009. Cross-linked actin networks (CLANs) in the trabecular meshwork of the normal and glaucomatous human eye in situ. Invest Ophthalmol Vis Sci. 50, 1255-1263.

Holland, M.G., Gipson, C.C., 1970. Chloride ion transport in the isolated ciliary body. Invest Ophthalmol. 9, 20-29.

Hosseini, M., Rose, A.Y., Song, K., Bohan, C., Alexander, J.P., Kelley, M.J., Acott, T.S., 2006. IL-1 and TNF induction of matrix metalloproteinase-3 by c-Jun N-terminal kinase in trabecular meshwork. Invest Ophthalmol Vis Sci. 47, 1469-1476.

Hu, X., Beeton, C., 2010. Detection of functional matrix metalloproteinases by zymography. J Vis Exp. 45, e2445.

Huete-Toral, F., Crooke, A., Martinez-Aguila, A., Pintor, J., 2015. Melatonin receptors trigger cAMP production and inhibit chloride movements in nonpigmented ciliary epithelial cells. J Pharmacol Exp Ther. 352, 119-128.

Hussain, M.U., 2014. Connexins: The Gap Junction Proteins. Springer, New Delhi.

Iizuka, S., Kishida, K., Tsuboi, S., Emi, K., Manabe, R., 1984. Electrical characteristics of the isolated dog ciliary body. Curr Eye Res. 3, 417-421.

Inatani, M., Tanihara, H., Katsuta, H., Honjo, M., Kido, N., Honda, Y., 2001. Transforming growth factor-β2 levels in aqueous humor of glaucomatous eyes. Graefes Arch Clin Exp Ophthalmol. 239, 109-113.

Inomata, H., Bill, A., 1977. Exit sites of uveoscleral flow of aqueous humor in cynomolgus monkey eyes. Exp Eye Res. 25, 113-118.

Inomata, H., Bill, A., Smelser, G.K., 1972. Unconventional routes of aqueous humor outflow in Cynomolgus monkey (Macaca irus). Am J Ophthalmol. 73, 893-907.

Ismail, S.A., Mowafi, H.A., 2009. Melatonin provides anxiolysis, enhances analgesia, decreases intraocular pressure, and promotes better operating conditions during cataract surgery under topical anesthesia. Anesth Analg. 108, 1146-1151.

Izzotti, A., Sacca, S.C., Cartiglia, C., De Flora, S., 2003. Oxidative deoxyribonucleic acid damage in the eyes of glaucoma patients. Am J Med. 114, 638-646.

Jerez, S., Sierra, L., Scacchi, F., Peral de Bruno, M., 2010. Hypercholesterolemia modifies angiotensin II desensitisation and cross talk between α_1-adrenoceptor and angiotensin AT_1 receptor in rabbit aorta. Eur J Pharmacol. 635, 149-155.

Jo, A.O., Lakk, M., Frye, A.M., Phuong, T.T., Redmon, S.N., Roberts, R., Berkowitz, B.A., Yarishkin, O., Krizaj, D., 2016. Differential volume regulation and calcium signaling in two ciliary body cell types is subserved by TRPV4 channels. Proc Natl Acad Sci U S A. 113, 3885-3890.

Johnson, C.H., Elliott, J., Foster, R., Honma, K.-I., Kronauer, R., 2004. Fundamental Properties of Circadian Rhythms, in: Dunlap, J.C., Loros, J.J., DeCoursey, P.J. (Eds.), Chronobiology : biological timekeeping. Sinauer Associates, Sunderland, pp. 67-105.

Johnson, D.H., 1997. The effect of cytochalasin D on outflow facility and the trabecular meshwork of the human eye in perfusion organ culture. Invest Ophthalmol Vis Sci. 38, 2790-2799.

Johnson, D.H., 2007. Histologic findings after argon laser trabeculoplasty in glaucomatous eyes. Exp Eye Res. 85, 557-562.

Johnson, M., McLaren, J.W., Overby, D.R., 2017. Unconventional aqueous humor outflow: A review. Exp Eye Res. 158, 94-111.

Kahn, M.G., Giblin, F.J., Epstein, D.L., 1983. Glutathione in calf trabecular meshwork and its relation to aqueous humor outflow facility. Invest Ophthalmol Vis Sci. 24, 1283-1287.

Karlsson, A.M., Lerner, M.R., Unett, D., Lundstrom, I., Svensson, S.P., 2000. Melatonin-induced organelle movement in melanophores is coupled to tyrosine

phosphorylation of a high molecular weight protein. Cell Signal. 12, 469-474.

Kelley, M.J., Rose, A.Y., Song, K., Chen, Y., Bradley, J.M., Rookhuizen, D., Acott, T.S., 2007. Synergism of TNF and IL-1 in the induction of matrix metalloproteinase-3 in trabecular meshwork. Invest Ophthalmol Vis Sci. 48, 2634-2643.

Kerr, N.M., Johnson, C.S., de Souza, C.F., Chee, K.S., Good, W.R., Green, C.R., Danesh-Meyer, H.V., 2010. Immunolocalization of gap junction protein connexin43 (GJA1) in the human retina and optic nerve. Invest Ophthalmol Vis Sci. 51, 4028-4034.

Kinsey, V.E., Reddy, V.N., 1964. Chemistry and dynamics of aqueous humor, in: Prince, J.H. (Ed.), The Rabbit in Eye Research, pp. 215–316.

Kishida, K., Sasabe, T., Iizuka, S., Manabe, R., Otori, T., 1982. Sodium and chloride transport across the isolated rabbit ciliary body. Curr Eye Res. 2, 149-152.

Kiuchi, Y., Mockovak, M.E., Gregory, D.S., 1993. Melatonin does not increase IOP significantly in rabbits. Curr Eye Res. 12, 181-190.

Knepper, P.A., Goossens, W., Hvizd, M., Palmberg, P.F., 1996. Glycosaminoglycans of the human trabecular meshwork in primary open-angle glaucoma. Invest Ophthalmol Vis Sci. 37, 1360-1367.

Kodama, T., Reddy, V.N., Macri, F.J., 1985. Pharmacological study on the effects of some ocular hypotensive drugs on aqueous humor formation in the arterially perfused enucleated rabbit eye. Ophthalmic Res. 17, 120-124.

Kojima, T., Mochizuki, C., Mitaka, T., Mochizuki, Y., 1997. Effects of melatonin on proliferation, oxidative stress and Cx32 gap junction protein expression in primary cultures of adult rat hepatocytes. Cell Struct Funct. 22, 347-356.

Kong, C.W., Li, K.K., To, C.H., 2006. Chloride secretion by porcine ciliary epithelium: New insight into species similarities and differences in aqueous humor formation. Invest Ophthalmol Vis Sci. 47, 5428-5436.

Krupin, T., Bass, J., Oestrich, C., Podos, S.M., Becker, B., 1977. The effect of

hyperthermia on aqueous humor dynamics in rabbits. Am J Ophthalmol. 83, 561-564.

Krupin, T., Civan, M.M., 1996. Physiologic basis of aqueous humor formation, in: Ritch, R., Shields, M., Krupin, T. (Eds.), The Glaucomas: Basic Sciences, volume 1. Mosby.

Krupin, T., Reinach, P.S., Candia, O.A., Podos, S.M., 1984. Transepithelial electrical measurements on the isolated rabbit iris-ciliary body. Exp Eye Res. 38, 115-123.

Laing, J.G., Tadros, P.N., Green, K., Saffitz, J.E., Beyer, E.C., 1998. Proteolysis of connexin43-containing gap junctions in normal and heat-stressed cardiac myocytes. Cardiovasc Res. 38, 711-718.

Laird, D.W., Puranam, K.L., Revel, J.P., 1991. Turnover and phosphorylation dynamics of connexin43 gap junction protein in cultured cardiac myocytes. Biochem J. 273, 67-72.

Larson, R.S., Brubaker, R.F., 1988. Isoproterenol stimulates aqueous flow in humans with Horner's syndrome. Invest Ophthalmol Vis Sci. 29, 621-625.

Last, J.A., Pan, T., Ding, Y., Reilly, C.M., Keller, K., Acott, T.S., Fautsch, M.P., Murphy, C.J., Russell, P., 2011. Elastic modulus determination of normal and glaucomatous human trabecular meshwork. Invest Ophthalmol Vis Sci. 52, 2147-2152.

Laux-Fenton, W.T., Donaldson, P.J., Kistler, J., Green, C.R., 2003. Connexin expression patterns in the rat cornea: molecular evidence for communication compartments. Cornea. 22, 457-464.

Law, C.S., Candia, O.A., To, C.H., 2009. Inhibitions of chloride transport and gap junction reduce fluid flow across the whole porcine ciliary epithelium. Invest Ophthalmol Vis Sci. 50, 1299-1306.

Lee, Y.M., Kang, S.M., Chung, J.H., 2012. The role of TRPV1 channel in aged human skin. J Dermatol Sci. 65, 81-85.

Lepple-Wienhues, A., Stahl, F., Wiederholt, M., 1991. Differential smooth muscle-like contractile properties of trabecular meshwork and ciliary muscle. Exp Eye Res. 53, 33-38.

Li, A., Leung, C.T., Peterson-Yantorno, K., Stamer, W.D., Civan, M.M., 2011. Cytoskeletal dependence of adenosine triphosphate release by human trabecular meshwork cells. Invest Ophthalmol Vis Sci. 52, 7996-8005.

Linsell, C.R., Lightman, S.L., Mullen, P.E., Brown, M.J., Causon, R.C., 1985. Circadian rhythms of epinephrine and norepinephrine in man. J Clin Endocrinol Metab. 60, 1210-1215.

Liu, H., Fan, S., Gulati, V., Camras, L.J., Zhan, G., Ghate, D., Camras, C.B., Toris, C.B., 2011. Aqueous humor dynamics during the day and night in healthy mature volunteers. Arch Ophthalmol. 129, 269-275.

Liu, J.H., 1998. Circadian rhythm of intraocular pressure. J Glaucoma. 7, 141-147.

Liu, J.H., Dacus, A.C., 1991. Endogenous hormonal changes and circadian elevation of intraocular pressure. Invest Ophthalmol Vis Sci. 32, 496-500.

Liu, Y., Qin, N., 2011. TRPM8 in health and disease: cold sensing and beyond. Adv Exp Med Biol. 704, 185-208.

Liu, Z., Chu, G., 2013. Chronobiology in mammalian health. Mol Biol Rep. 40, 2491-2501.

Llobet, A., Gasull, X., Gual, A., 2003. Understanding trabecular meshwork physiology: a key to the control of intraocular pressure? News Physiol Sci. 18, 205-209.

Luchetti, F., Canonico, B., Betti, M., Arcangeletti, M., Pilolli, F., Piroddi, M., Canesi, L., Papa, S., Galli, F., 2010. Melatonin signaling and cell protection function. FASEB J. 24, 3603-3624.

Lundmark, P.O., Pandi-Perumal, S.R., Srinivasan, V., Cardinali, D.P., Rosenstein, R.E., 2007. Melatonin in the eye: implications for glaucoma. Exp Eye Res. 84, 1021-1030.

Lutjen-Drecoll, E., Rittig, M., Rauterberg, J., Jander, R., Mollenhauer, J., 1989. Immunomicroscopical study of type VI collagen in the trabecular meshwork of normal and glaucomatous eyes. Exp Eye Res. 48, 139-147.

Maatta, M., Tervahartiala, T., Harju, M., Airaksinen, J., Autio-Harmainen, H., Sorsa, T., 2005. Matrix metalloproteinases and their tissue inhibitors in aqueous humor of patients with primary open-angle glaucoma, exfoliation syndrome, and exfoliation glaucoma. J Glaucoma. 14, 64-69.

Manabe, S., Gu, Z., Lipton, S.A., 2005. Activation of matrix metalloproteinase-9 via neuronal nitric oxide synthase contributes to NMDA-induced retinal ganglion cell death. Invest Ophthalmol Vis Sci. 46, 4747-4753.

Maren, T.H., 1976. The rates of movement of Na^+, Cl^-, and HCO_3^- from plasma to posterior chamber: effect of acetazolamide and relation to the treatment of glaucoma. Invest Ophthalmol. 15, 356-364.

Markoulli, M., Papas, E., Cole, N., Holden, B.A., 2012. The diurnal variation of matrix metalloproteinase-9 and its associated factors in human tears. Invest Ophthalmol Vis Sci. 53, 1479-1484.

Martin, X.D., Malina, H.Z., Brennan, M.C., Hendrickson, P.H., Lichter, P.R., 1992. The ciliary body--the third organ found to synthesize indoleamines in humans. Eur J Ophthalmol. 2, 67-72.

Martinez-Aguila, A., Fonseca, B., Bergua, A., Pintor, J., 2013. Melatonin analogue agomelatine reduces rabbit's intraocular pressure in normotensive and hypertensive conditions. Eur J Pharmacol. 701, 213-217.

Martinez-Aguila, A., Fonseca, B., Perez de Lara, M.J., Pintor, J., 2016. Effect of Melatonin and 5-Methoxycarbonylamino-N-Acetyltryptamine on the Intraocular Pressure of Normal and Glaucomatous Mice. J Pharmacol Exp Ther. 357, 293-299.

Martinez-Garcia, M.C., Martinez, T., Paneda, C., Gallego, P., Jimenez, A.I., Merayo, J., 2013. Differential expression and localization of transient receptor potential vanilloid 1 in rabbit and human eyes. Histol Histopathol. 28, 1507-1516.

Martinez, A.D., Saez, J.C., 2000. Regulation of astrocyte gap junctions by hypoxia-

reoxygenation. Brain Res Brain Res Rev. 32, 250-258.

Massey, S.C., 2009. Connexins in the Mammalian Retina, in: Harris, A., Locke, D. (Eds.), Connexins: a Guide. Springer, New York.

Maus, T.L., Young, W.F., Jr., Brubaker, R.F., 1994. Aqueous flow in humans after adrenalectomy. Invest Ophthalmol Vis Sci. 35, 3325-3331.

McLaughlin, C.W., Peart, D., Purves, R.D., Carre, D.A., Macknight, A.D., Civan, M.M., 1998. Effects of HCO_3^- on cell composition of rabbit ciliary epithelium: a new model for aqueous humor secretion. Invest Ophthalmol Vis Sci. 39, 1631-1641.

McLaughlin, C.W., Zellhuber-McMillan, S., Macknight, A.D., Civan, M.M., 2007. Electron microprobe analysis of rabbit ciliary epithelium indicates enhanced secretion posteriorly and enhanced absorption anteriorly. Am J Physiol Cell Physiol. 293, C1455-1466.

Milks, L.C., Kumar, N.M., Houghten, R., Unwin, N., Gilula, N.B., 1988. Topology of the 32-kd liver gap junction protein determined by site-directed antibody localizations. EMBO J. 7, 2967-2975.

Moore, K., Ghatnekar, G., Gourdie, R.G., Potts, J.D., 2014. Impact of the controlled release of a connexin 43 peptide on corneal wound closure in an STZ model of type I diabetes. PLoS One. 9, e86570.

Mori, N., Yamada, E., Sears, M.L., 1991. Immunocytochemical localization of Na/K-ATPase in the isolated ciliary epithelial bilayer of the rabbit. Arch Histol Cytol. 54, 259-265.

Morimoto, R.I., 1998. Regulation of the heat shock transcriptional response: cross talk between a family of heat shock factors, molecular chaperones, and negative regulators. Genes Dev. 12, 3788-3796.

Muhlbauer, E., Gross, E., Labucay, K., Wolgast, S., Peschke, E., 2009. Loss of melatonin signalling and its impact on circadian rhythms in mouse organs regulating blood glucose. Eur J Pharmacol. 606, 61-71.

Musil, L.S., Cunningham, B.A., Edelman, G.M., Goodenough, D.A., 1990.

Differential phosphorylation of the gap junction protein connexin43 in junctional communication-competent and -deficient cell lines. J Cell Biol. 111, 2077-2088.

Nickel, R., Forge, A., Jagger, D., 2009. Connexins in the Inner Ear, in: Harris, A., Locke, D. (Eds.), Connexins: a Guide. Springer, New York.

Nilius, B., Flockerzi, V., 2014. Mammalian transient receptor potential (TRP) cation channels. Preface. Handb Exp Pharmacol. 223, v - vi.

Ormonde, S., Chou, C.Y., Goold, L., Petsoglou, C., Al-Taie, R., Sherwin, T., McGhee, C.N., Green, C.R., 2012. Regulation of connexin43 gap junction protein triggers vascular recovery and healing in human ocular persistent epithelial defect wounds. J Membr Biol. 245, 381-388.

Orr, H.T., Lowry, O.H., Cohen, A.I., Ferrendelli, J.A., 1976. Distribution of 3':5'-cyclic AMP and 3':5'-cyclic GMP in rabbit retina in vivo: selective effects of dark and light adaptation and ischemia. Proc Natl Acad Sci U S A. 73, 4442-4445.

Osborne, N.N., Chidlow, G., 1994. The presence of functional melatonin receptors in the iris-ciliary processes of the rabbit eye. Exp Eye Res. 59, 3-9.

Pang, I.H., Clark, A.F., 2008. Outflow Signaling Mechanisms and New Therapeutic Strategies for the Control of Intraocular Pressure, in: Civan, M.M. (Ed.), The eye's aqueous humor. Academic Press, San Diego.

Pang, I.H., Fleenor, D.L., Hellberg, P.E., Stropki, K., McCartney, M.D., Clark, A.F., 2003. Aqueous outflow-enhancing effect of tert-butylhydroquinone: involvement of AP-1 activation and MMP-3 expression. Invest Ophthalmol Vis Sci. 44, 3502-3510.

Pang, I.H., Shade, D.L., Clark, A.F., Steely, H.T., DeSantis, L., 1994. Preliminary characterization of a transformed cell strain derived from human trabecular meshwork. Curr Eye Res. 13, 51-63.

Park, C.H., Lee, M.J., Ahn, J., Kim, S., Kim, H.H., Kim, K.H., Eun, H.C., Chung, J.H., 2004. Heat shock-induced matrix metalloproteinase (MMP)-1 and MMP-3 are mediated through ERK and JNK activation and via an autocrine interleukin-6 loop. J Invest Dermatol. 123, 1012-1019.

Park, Y., Ellis, D., Mueller, B., Stankowska, D., Yorio, T., 2016. Principles of Ocular Pharmacology, in: Barrett, J.E. (Ed.), Handbook of Expermental Pharmacology. Springer, pp. 1-28.

Peitzman, E.R., Zaidman, N.A., Maniak, P.J., O'Grady, S.M., 2016. Carvedilol binding to beta2-adrenergic receptors inhibits CFTR-dependent anion secretion in airway epithelial cells. Am J Physiol Lung Cell Mol Physiol. 310, L50-58.

Perkins, G.A., Goodenough, D.A., Sosinsky, G.E., 1998. Formation of the gap junction intercellular channel requires a 30 degree rotation for interdigitating two apposing connexons. J Mol Biol. 277, 171-177.

Pescosolido, N., Gatto, V., Stefanucci, A., Rusciano, D., 2015. Oral treatment with the melatonin agonist agomelatine lowers the intraocular pressure of glaucoma patients. Ophthalmic Physiol Opt. 35, 201-205.

Peterson, J.A., Tian, B., Bershadsky, A.D., Volberg, T., Gangnon, R.E., Spector, I., Geiger, B., Kaufman, P.L., 1999. Latrunculin-A increases outflow facility in the monkey. Invest Ophthalmol Vis Sci. 40, 931-941.

Peterson, J.A., Tian, B., Geiger, B., Kaufman, P.L., 2000. Effect of latrunculin-B on outflow facility in monkeys. Exp Eye Res. 70, 307-313.

Picht, G., Welge-Luessen, U., Grehn, F., Lutjen-Drecoll, E., 2001. Transforming growth factor beta 2 levels in the aqueous humor in different types of glaucoma and the relation to filtering bleb development. Graefes Arch Clin Exp Ophthalmol. 239, 199-207.

Pintor, J., Martin, L., Pelaez, T., Hoyle, C.H., Peral, A., 2001. Involvement of melatonin MT_3 receptors in the regulation of intraocular pressure in rabbits. Eur J Pharmacol. 416, 251-254.

Pintor, J., Pelaez, T., Hoyle, C.H., Peral, A., 2003. Ocular hypotensive effects of melatonin receptor agonists in the rabbit: further evidence for an MT_3 receptor. Br J Pharmacol. 138, 831-836.

Prasanna, G., Krishnamoorthy, R., Yorio, T., 2011. Endothelin, astrocytes and glaucoma. Exp Eye Res. 93, 170-177.

Preitner, N., Damiola, F., Lopez-Molina, L., Zakany, J., Duboule, D., Albrecht, U., Schibler, U., 2002. The orphan nuclear receptor REV-ERBalpha controls circadian transcription within the positive limb of the mammalian circadian oscillator. Cell. 110, 251-260.

Puente, X.S., Sanchez, L.M., Overall, C.M., Lopez-Otin, C., 2003. Human and mouse proteases: a comparative genomic approach. Nat Rev Genet. 4, 544-558.

Qin, F., 2014. Temperature Sensing by Thermal TRP Channels: Thermodynamic Basis and Molecular Insights, in: Islas, L.D., Qin, F. (Eds.), Thermal sensors. Academic Press, Waltham, MA.

Quigley, H.A., 2011. Glaucoma. Lancet. 377, 1367-1377.

Rada, J.A., Wiechmann, A.F., 2006. Melatonin receptors in chick ocular tissues: implications for a role of melatonin in ocular growth regulation. Invest Ophthalmol Vis Sci. 47, 25-33.

Rao, P.V., Deng, P.F., Kumar, J., Epstein, D.L., 2001. Modulation of aqueous humor outflow facility by the Rho kinase-specific inhibitor Y-27632. Invest Ophthalmol Vis Sci. 42, 1029-1037.

Raviola, G., Raviola, E., 1978. Intercellular junctions in the ciliary epithelium. Invest Ophthalmol Vis Sci. 17, 958-981.

Rensing, L., Ruoff, P., 2002. Temperature effect on entrainment, phase shifting, and amplitude of circadian clocks and its molecular bases. Chronobiol Int. 19, 807-864.

Rich, A., Farrugia, G., Rae, J.L., 1999. Effects of melatonin on ionic currents in cultured ocular tissues. Am J Physiol. 276, C923-929.

Roberts, J.E., Wiechmann, A.F., Hu, D.N., 2000. Melatonin receptors in human uveal melanocytes and melanoma cells. J Pineal Res. 28, 165-171.

Robertson, J.V., Siwakoti, A., West-Mays, J.A., 2013. Altered expression of transforming growth factor beta 1 and matrix metalloproteinase-9 results in elevated intraocular pressure in mice. Mol Vis. 19, 684-695.

Rohde, B.H., McLaughlin, M.A., Chiou, L.Y., 1985. Existence and role of endogenous ocular melatonin. J Ocul Pharmacol. 1, 235-243.

Rohen, J.W., 1983. Why is intraocular pressure elevated in chronic simple glaucoma? Anatomical considerations. Ophthalmology. 90, 758-765.

Rohen, J.W., Kaufman, P.L., Eichhorn, M., Goeckner, P.A., Bito, L.Z., 1989. Functional morphology of accommodation in the raccoon. Exp Eye Res. 48, 523-527.

Rowland, J.M., Sawyer, W.K., Tittel, J., Ford, C.J., 1986. Studies on the circadian rhythm of IOP in rabbits: correlation with aqueous inflow and cAMP content. Curr Eye Res. 5, 201-206.

Roy Chowdhury, U., Hann, C.R., Stamer, W.D., Fautsch, M.P., 2015. Aqueous humor outflow: dynamics and disease. Invest Ophthalmol Vis Sci. 56, 2993-3003.

Sack, R.L., Brandes, R.W., Kendall, A.R., Lewy, A.J., 2000. Entrainment of free-running circadian rhythms by melatonin in blind people. N Engl J Med. 343, 1070-1077.

Saitongdee, P., Milner, P., Becker, D.L., Knight, G.E., Burnstock, G., 2000. Increased connexin43 gap junction protein in hamster cardiomyocytes during cold acclimatization and hibernation. Cardiovasc Res. 47, 108-115.

Salameh, A., Dhein, S., 2005. Pharmacology of gap junctions. New pharmacological targets for treatment of arrhythmia, seizure and cancer? Biochim Biophys Acta. 1719, 36-58.

Samples, J.R., Krause, G., Lewy, A.J., 1988. Effect of melatonin on intraocular pressure. Curr Eye Res. 7, 649-653.

Sandstrom, M.E., Madden, L.A., Taylor, L., Siegler, J.C., Lovell, R.J., Midgley, A., McNaughton, L., 2009. Variation in basal heat shock protein 70 is correlated to core temperature in human subjects. Amino Acids. 37, 279-284.

Santos, A.R., Corredor, R.G., Obeso, B.A., Trakhtenberg, E.F., Wang, Y., Ponmattam, J., Dvoriantchikova, G., Ivanov, D., Shestopalov, V.I., Goldberg, J.L.,

Fini, M.E., Bajenaru, M.L., 2012. β1 integrin-focal adhesion kinase (FAK) signaling modulates retinal ganglion cell (RGC) survival. PLoS One. 7, e48332.

Schlotzer-Schrehardt, U., Lommatzsch, J., Kuchle, M., Konstas, A.G., Naumann, G.O., 2003. Matrix metalloproteinases and their inhibitors in aqueous humor of patients with pseudoexfoliation syndrome/glaucoma and primary open-angle glaucoma. Invest Ophthalmol Vis Sci. 44, 1117-1125.

Scott, J.A., 1988. A finite element model of heat transport in the human eye. Phys Med Biol. 33, 227-241.

Serle, J.B., Wang, R.F., Peterson, W.M., Plourde, R., Yerxa, B.R., 2004. Effect of 5-MCA-NAT, a putative melatonin MT_3 receptor agonist, on intraocular pressure in glaucomatous monkey eyes. J Glaucoma. 13, 385-388.

Severs, N.J., 2009. Connexins in the Heart, in: Harris, A., Locke, D. (Eds.), Connexins: a Guide. Springer, New York.

Shahidullah, M., Al-Malki, W.A., Delamere, N.A., 2011. Mechanism of Aqueous Humor Secretion, Its Regulation and Relevance to Glaucoma, in: Rumelt, S. (Ed.), Glaucoma - Basic and Clinical Concepts. InTech, pp. 3-32.

Shahidullah, M., Delamere, N.A., 2014. Connexins form functional hemichannels in porcine ciliary epithelium. Exp Eye Res. 118, 20-29.

Shahidullah, M., Mandal, A., Delamere, N.A., 2012. TRPV4 in porcine lens epithelium regulates hemichannel-mediated ATP release and Na-K-ATPase activity. Am J Physiol Cell Physiol. 302, C1751-1761.

Shahidullah, M., Wei, G., Delamere, N.A., 2013. DIDS inhibits Na-K-ATPase activity in porcine nonpigmented ciliary epithelial cells by a Src family kinase-dependent mechanism. Am J Physiol Cell Physiol. 305, C492-501.

Shahidullah, M., Wilson, W.S., Yap, M., To, C.H., 2003. Effects of ion transport and channel-blocking drugs on aqueous humor formation in isolated bovine eye. Invest Ophthalmol Vis Sci. 44, 1185-1191.

Shahidullah, M., Yap, M., To, C.H., 2005. Cyclic GMP, sodium nitroprusside and

sodium azide reduce aqueous humour formation in the isolated arterially perfused pig eye. Br J Pharmacol. 145, 84-92.

Shakespeare, T.I., Mathias, R.T., White, T.W., 2009. Connexins in Lens Development and Disease, in: Harris, A., Locke, D. (Eds.), Connexins: a Guide. Springer, New York.

Simoens, P., De Schaepdrijver, L., Lauwers, H., 1992. Morphologic and clinical study of the retinal circulation in the miniature pig. A: Morphology of the retinal microvasculature. Exp Eye Res. 54, 965-973.

Sit, A.J., Coloma, F.M., Ethier, C.R., Johnson, M., 1997. Factors affecting the pores of the inner wall endothelium of Schlemm's canal. Invest Ophthalmol Vis Sci. 38, 1517-1525.

Smith, S.D., Gregory, D.S., 1989. A circadian rhythm of aqueous flow underlies the circadian rhythm of IOP in NZW rabbits. Invest Ophthalmol Vis Sci. 30, 775-778.

Sohl, G., Joussen, A., Kociok, N., Willecke, K., 2010. Expression of connexin genes in the human retina. BMC Ophthalmol. 10, 27.

Sosinsky, G., 2000. Gap Junction Structure: New Structures and New Insights, in: Peracchia, C. (Ed.), Gap junctions : molecular basis of cell communication in health and disease. Academic Press, San Diego.

Spadoni, G., Bedini, A., Rivara, S., Mor, M., 2011. Melatonin receptor agonists: new options for insomnia and depression treatment. CNS Neurosci Ther. 17, 733-741.

Spiga, M.G., Borras, T., 2010. Development of a gene therapy virus with a glucocorticoid-inducible MMP1 for the treatment of steroid glaucoma. Invest Ophthalmol Vis Sci. 51, 3029-3041.

Stawikowski, M.J., Fields, G.B., 2015. Matrix Metalloproteinases: From Structure to Function, in: Sagi, I., Gaffney, J.P. (Eds.), Matrix Metalloproteinase Biology. Wiley-Blackwell, Hoboken, New Jersey.

Stumpff, F., Strauss, O., Boxberger, M., Wiederholt, M., 1997. Characterization of

maxi-K-channels in bovine trabecular meshwork and their activation by cyclic guanosine monophosphate. Invest Ophthalmol Vis Sci. 38, 1883-1892.

Tamm, E.R., 2009. The trabecular meshwork outflow pathways: structural and functional aspects. Exp Eye Res. 88, 648-655.

The AGIS Investigators, 2000. The Advanced Glaucoma Intervention Study (AGIS): 7. The relationship between control of intraocular pressure and visual field deterioration.The AGIS Investigators. Am J Ophthalmol. 130, 429-440.

To, C.H., Do, C.W., Zamudio, A.C., Candia, O.A., 2001. Model of ionic transport for bovine ciliary epithelium: effects of acetazolamide and HCO_3^-. Am J Physiol Cell Physiol. 280, C1521-1530.

To, C.H., Mok, K.H., Do, C.W., Lee, K.L., Millodot, M., 1998a. Chloride and sodium transport across bovine ciliary body/epithelium (CBE). Curr Eye Res. 17, 896-902.

To, C.H., Mok, K.H., Tse, S.K., Siu, W.T., Millodot, M., Lee, K.L., Hodson, S., 1998b. In vitro bovine ciliary body/epithelium in a small continuously perfused Ussing type chamber. Cell Struct Funct. 23, 247-254.

Toris, C.B., Camras, C.B., 1998. Aqueous Humor Dyamics II Clinical Studies, in: Civan, M.M. (Ed.), The eye's aqueous humor : from secretion to glaucoma. Academic Press, San Diego.

Toris, C.B., Yablonski, M.E., Wang, Y.L., Camras, C.B., 1999. Aqueous humor dynamics in the aging human eye. Am J Ophthalmol. 127, 407-412.

Tovar-Vidales, T., Roque, R., Clark, A.F., Wordinger, R.J., 2008. Tissue transglutaminase expression and activity in normal and glaucomatous human trabecular meshwork cells and tissues. Invest Ophthalmol Vis Sci. 49, 622-628.

Townsend, D.J., Brubaker, R.F., 1980. Immediate effect of epinephrine on aqueous formation in the normal human eye as measured by fluorophotometry. Invest Ophthalmol Vis Sci. 19, 256-266.

Tripathi, R.C., Li, J., Chan, W.F., Tripathi, B.J., 1994. Aqueous humor in

glaucomatous eyes contains an increased level of TGF-β2. Exp Eye Res. 59, 723-727.

Ubeda, A., Trillo, M.A., House, D.E., Blackman, C.F., 1995. Melatonin enhances junctional transfer in normal C3H/10T1/2 cells. Cancer Lett. 91, 241-245.

Usukura, J., Fain, G.L., Bok, D., 1988. [^{3}H]ouabain localization of Na-K ATPase in the epithelium of rabbit ciliary body pars plicata. Invest Ophthalmol Vis Sci. 29, 606-614.

Viggiano, S.R., Koskela, T.K., Klee, G.G., Samples, J.R., Arnce, R., Brubaker, R.F., 1994. The effect of melatonin on aqueous humor flow in humans during the day. Ophthalmology. 101, 326-331.

Voets, T., Droogmans, G., Wissenbach, U., Janssens, A., Flockerzi, V., Nilius, B., 2004. The principle of temperature-dependent gating in cold- and heat-sensitive TRP channels. Nature. 430, 748-754.

Voets, T., Nilius, B., 2003. TRPs make sense. J Membr Biol. 192, 1-8.

von Gall, C., Stehle, J.H., Weaver, D.R., 2002. Mammalian melatonin receptors: molecular biology and signal transduction. Cell Tissue Res. 309, 151-162.

Waitzman, M.B., Jackson, R.T., 1965. Effects of topically administered ouabain on aqueous humor dynamics. Exp Eye Res. 4, 135-145.

Wang, Z., Do, C.W., Valiunas, V., Leung, C.T., Cheng, A.K., Clark, A.F., Wax, M.B., Chatterton, J.E., Civan, M.M., 2010. Regulation of gap junction coupling in bovine ciliary epithelium. Am J Physiol Cell Physiol. 298, C798-806.

Waterhouse, J.M., DeCoursey, P.J., 2004. The Relevance of CIrcadian Rhythms for Human Welfare, in: Dunlap, J.C., Loros, J.J., DeCoursey, P.J. (Eds.), Chronobiology: Biological Timekeeper. Sinauer Associates, Inc, Sunderland, Massachusetts.

Wiechmann, A.F., Summers, J.A., 2008. Circadian rhythms in the eye: the physiological significance of melatonin receptors in ocular tissues. Prog Retin Eye Res. 27, 137-160.

Wiechmann, A.F., Wirsig-Wiechmann, C.R., 2001. Melatonin receptor mRNA and protein expression in Xenopus laevis nonpigmented ciliary epithelial cells. Exp Eye Res. 73, 617-623.

Wolosin, J.M., Candia, O.A., Peterson-Yantorno, K., Civan, M.M., Shi, X.P., 1997a. Effect of heptanol on the short circuit currents of cornea and ciliary body demonstrates rate limiting role of heterocellular gap junctions in active ciliary body transport. Exp Eye Res. 64, 945-952.

Wolosin, J.M., Chen, M., Gordon, R.E., Stegman, Z., Butler, G.A., 1993. Separation of the rabbit ciliary body epithelial layers in viable form: identification of differences in bicarbonate transport. Exp Eye Res. 56, 401-409.

Wolosin, J.M., Schutte, M., Chen, S., 1997b. Connexin distribution in the rabbit and rat ciliary body. A case for heterotypic epithelial gap junctions. Invest Ophthalmol Vis Sci. 38, 341-348.

World Health Organization, 2014. Visual impairment and blindness. http://www.who.int/mediacentre/factsheets/fs282/en/. (assessed 15.08.20)

Wu, R.Y., Ma, N., Hu, Q.Q., 2013. Effect of cAMP on short-circuit current in isolated human ciliary body. Chin Med J (Engl). 126, 2694-2698.

Yokota, S., Kitahara, M., Nagata, K., 2000. Benzylidene lactam compound, KNK437, a novel inhibitor of acquisition of thermotolerance and heat shock protein induction in human colon carcinoma cells. Cancer Res. 60, 2942-2948.

Yoshida, J., Oshikata-Miyazaki, A., Yokoo, S., Yamagami, S., Takezawa, T., Amano, S., 2014. Development and evaluation of porcine atelocollagen vitrigel membrane with a spherical curve and transplantable artificial corneal endothelial grafts. Invest Ophthalmol Vis Sci. 55, 4975-4981.

Zhai, J., Wang, Q., Tao, L., 2014. Connexin expression patterns in diseased human corneas. Exp Ther Med. 7, 791-798.

Zhang, J., Chen, F.Z., Gao, Q., Sun, J.H., Tian, G.P., Gao, Y.M., 2012. Hyperthermia induces upregulation of connexin43 in the golden hamster neural tube. Birth Defects Res A Clin Mol Teratol. 94, 16-21.

Zhang, L., An, X., Wang, Q., He, M., 2016. Activation of Cold-Sensitive Channels TRPM8 and TRPA1 Inhibits the Proliferative Airway Smooth Muscle Cell Phenotype. Lung. 194, 595-603.

Zhang, X., Cheng, M., Chintala, S.K., 2004. Kainic acid-mediated upregulation of matrix metalloproteinase-9 promotes retinal degeneration. Invest Ophthalmol Vis Sci. 45, 2374-2383.

Zhao, J.K., Guan, F.L., Duan, S.R., Zhao, J.W., Sun, R.H., Zhang, L.M., Wang, D.S., 2013. Effect of focal mild hypothermia on expression of MMP-9, TIMP-1, Tau-1 and β-APP in rats with cerebral ischaemia/reperfusion injury. Brain Inj. 27, 1190-1198.

Zhou, L., Li, Y., Yue, B.Y., 1999. Oxidative stress affects cytoskeletal structure and cell-matrix interactions in cells from an ocular tissue: the trabecular meshwork. J Cell Physiol. 180, 182-189.